ON THE USE OF LIGHT FOR THE CHARACTERIZATION AND TREATMENT OF MALIGNANT TUMOURS

Claes af Klinteberg

Lund Reports on Atomic Physics
LRAP-245

Doctoral Thesis
Department of Physics
Lund Institute of Technology
April 1999

ISBN 91-628-3511-4

To Carola

Contents

Abstract

Some aspects on the use of light for tissue characterization and treatment of malignant tumours are discussed within this thesis. The work presented aims at improving optical techniques for tissue characterization, especially to detect malignant and pre-malignant lesions. A knowledge on the interaction between light and tissue is of utmost importance to understand and improve the various techniques. A relatively thorough discussion on the light propagation in scattering media is given. A commonly used mathematical model, the diffusion approximation of the transport equation, is derived. Moreover, knowledge of the optical properties of tissue, *i.e.*, the absorption and scattering coefficients, the scattering anisotropy, and the refractive index, is needed to use the mathematical models. Various techniques for *in vivo* measurements of the tissue optical properties are presented. Furthermore, some of these techniques have been developed into prototype equipment to be used for breast cancer detection, as an alternative to the ordinary mammography based on ionizing X-rays.

A therapeutic modality, photodynamic therapy (PDT), presently being introduced into clinical practice has also been investigated. This technique relies on the selective uptake of a photosensitizing agent, and the subsequent irradiation using light. The light absorbed by the photosensitizer triggers a photochemical reaction, leading to local cell death. In the work presented here, δ-aminolevulinic acid (ALA) induced protoporphyrin IX (PpIX) has been used as a photosensitizer. A randomized Phase III clinical trial has been conducted to compare PDT with cryosurgery for the treatment of basal cell carcinomas of the skin. The influence on the treatment of various parameters have been investigated and are discussed.

Laser-induced fluorescence studies were performed to detect and demarcate superficial malignant and pre-malignant lesions. Both the tissue autofluorescence and the characteristic emission of fluorescent tumour markers were employed. Fluorescence was also used to monitor the selective buildup and the photodegradation of the photosensitizer in connection to PDT, using a point-monitoring technique. Two fluorescence imaging systems have also been used to outline skin lesions.

Laser-Doppler perfusion imaging is a non-contact optical technique used to monitor the superficial blood perfusion, and was here used to evaluate the healing time following cryosurgery and PDT.

List of papers

This thesis is based on the following papers:

Paper I. R. Berg, S. Andersson-Engels, C. af Klinteberg, S. Svanberg and O. Jarlman, Optical imaging for medical diagnostics using femtosecond white light, in *Advances in Optical Imaging and Photon Migration*, ed. R.R. Alfano, Proc. OSA vol. **21**, 126-128 (1994).

Paper II. C. af Klinteberg, R. Berg, S. Andersson-Engels and S. Svanberg, Diffusely scattered femtosecond white light examination of breast tissue *in vitro* and *in vivo*, in *Photon Propagation in Tissues*, eds. B. Chance, D.T. Delpy and G.J. Müller, Proc. SPIE vol. **2626**, 149-157 (1995).

Paper III. C. af Klinteberg, C. Lindquist, A. Pifferi, R. Berg, S. Andersson-Engels and S. Svanberg, Diffusely scattered femtosecond white light examination of breast tissue, in *Medical and Biological Applications*, ed. R. Cubeddu, OSA Trends in Optics and Photonics vol. **6**, 30-35 (1996).

Paper IV. C. af Klinteberg, A. Pifferi, S. Andersson-Engels, R. Cubeddu and S. Svanberg, In vivo absorption spectrum of disulphonated aluminium phthalocyanine (AlS_2Pc) using femtosecond white light, Manuscript for *Photochem. Photobiol.* (1999).

Paper V. C. af Klinteberg, C. Lindquist, I. Wang-Nordman, A. Vaitkuviene and K. Svanberg, Laser-induced fluorescence studies of premalignant and benign lesions in the female genital tract, in *Optical Biopsies and Microscopic Techniques II*, eds. I.J. Bigio, K. Svanberg, H. Schneckenburger, J. Slavik and P.M. Viallet, Proc. SPIE **3197**, 34-40 (1997).

Paper VI. C. af Klinteberg, M. Andreasson, O. Sandström, S. Andersson-Engels and S. Svanberg, Compact medical fluorosensor for minimally invasive tissue characterisation, Manuscript (1999).

Paper VII. C. af Klinteberg, I. Wang, I. Karu, T. Johansson, N. Bendsoe, K. Svanberg, S. Andersson-Engels, S. Svanberg, G. Canti, R. Cubeddu, A. Pifferi, P. Taroni and G. Valentini, Diode laser-mediated ALA-PDT guided by laser-induced fluorescence imaging, Submitted to *Lasers Med. Sci.* (1999).

Paper VIII. S. Andersson-Engels, G. Canti, R. Cubeddu, C. Eker, C. af Klinteberg, A. Pifferi, K. Svanberg, S. Svanberg, P. Taroni, G. Valentini and I. Wang, Spectroscopic characterisation of basal cell carcinomas of the skin with multi-colour and lifetime fluorescence imaging, Submitted to *Lasers Surg. Med.* (1999).

Paper IX. I. Karu, S. Pålsson, I. Wang, C. af Klinteberg, N. Bendsoe, S. Andersson-Engels, S. Svanberg and K. Svanberg, Photodynamic therapy using δ-amino levulinic acid and intensity modulated diode laser light, Submitted to *Lasers Med. Sci.* (1999).

Paper X. I. Karu, I. Wang, C. af Klinteberg, S. Andersson-Engels, S. Svanberg and K. Svanberg, Evaluation of pain and dysesthesia in connection with diode laser mediated ALA-PDT, Submitted to *Br. J. Dermatol.* (1999).

Paper XI. I. Wang, N. Bendsoe, C. af Klinteberg, A.M.K. Enejder, S. Andersson-Engels, S. Svanberg and K. Svanberg, Photodynamic therapy versus cryosurgery of basal cell carcinomas; results of a Phase III clinical trial, Manuscript for *Cancer* (1999).

Paper XII. C. af Klinteberg, A.M.K. Enejder, I. Wang, S. Andersson-Engels, S. Svanberg and K. Svanberg, Kinetic fluorescence studies of 5-aminolaevulinic acid-induced protoporphyrin IX in basal cell carcinomas, *J. Photochem. Photobiol. B*, In press (1999).

Paper XIII. C. af Klinteberg, I. Wang, A.M.K. Enejder, S. Andersson-Engels, S. Svanberg and K. Svanberg, 5-Aminolevulinic acid-induced protoporphyrin IX fluorescence in basal cell carcinomas of the skin, Manuscript for *Photochem. Photobiol.* (1999).

Paper XIV. A.M.K. Enejder, C. af Klinteberg, I. Wang, S. Andersson-Engels, N. Bendsoe, S. Svanberg and K. Svanberg, Blood perfusion studies on basal cell carcinomas in conjunction with photodynamic- and cryotherapy employing laser-Doppler imaging, Submitted to *Acta Derm. Venereol.* (1999).

In addition to the papers above, material is also presented in:

C. af Klinteberg, A.M.K. Nilsson, I. Wang, S. Andersson-Engels, S. Svanberg and K. Svanberg, Laser-induced fluorescence diagnostics of basal cell carcinomas of the skin following topical ALA application, in *Optical Biopsies and Microscopic Techniques*, eds. I.J. Bigio, W.S. Grundfest, H. Schneckenburger, K. Svanberg, and P.M. Viallet, Proc. SPIE vol. **2926**, 32-40 (1996).

C. af Klinteberg, A.M.K. Nilsson, I. Wang, S. Andersson-Engels, S. Svanberg and K. Svanberg, Laser-induced fluorescence diagnostics of basal cell carcinomas of the skin following topical ALA application, *Biomedical Optics Newsletter* **5**, 1-6, 1996.

S. Andersson-Engels, C. af Klinteberg, K. Svanberg, and S. Svanberg, *In vivo* fluorescence imaging for tissue diagnostics, *Phys. Med. Biol.* **42** 815-824, 1997.

K. Svanberg, C. af Klinteberg, A. Nilsson, I. Wang, S. Andersson-Engels, and S. Svanberg, Laser-based spectroscopic methods in tissue characterization, *in Advances in Optical Biopsy and Optical Mammography*, ed. R.R. Alfano, pp. 123-129 (The New York Academy of Sciences, NY, 1998).

1. Introduction

The work presented in this thesis aims at improving optical techniques for tissue characterization, especially for localization and demarcation of malignant and pre-malignant lesions. A therapeutic modality, photodynamic therapy, presently being introduced into clinical practice has also been investigated. The technique has been compared to standard procedures of today in the treatment of non-melanoma malignant skin tumours. The selective buildup and retention of the tumour seeking agent used in the treatment was studied employing laser-induced fluorescence. Finally, the healing time following these treatments has been monitored with a non-contact optical technique, laser-Doppler perfusion imaging.

The thesis consists of two parts; a summary and fourteen papers presenting original scientific material. In the summary a number of areas are covered, that are not explicitly apparent in the papers, but form a basis needed to interpret data and to understand the background for various phenomena studied. Moreover, the different techniques used in the research within this field are discussed. The summary starts with a theoretical discussion of the interaction between light and mammalian tissue, and the propagation of light in strongly scattering media in general (Chapter 2). A commonly used analytical model, the diffusion approximation of the transport equation, is derived and discussed. This model is used in several papers included in this thesis, and thus a relatively comprehensive presentation is given. A short introduction to Monte Carlo simulations, extensively used to simulate the migration of photons in an absorbing and scattering medium, is also given. The use of mathematical models is vital for all applications of biomedical optics. When lasers are used for therapy, *e.g.*, as "bloodless" knives in surgery, to reshape the cornea, or to induce photochemical reactions in photodynamic therapy, it is important to have models of the light distribution to plan the treatment. Models are also essential to correctly interpret the detected signal when light is used for tissue characterization.

To use the mathematical models, knowledge on the tissue optical properties are imperative. These properties, *i.e.*, the refractive index, the absorption and scattering coefficients, and the scattering anisotropy, can be determined in a number of ways. Direct measurements are possible in some situations, but are more or less restricted to tissue samples. For most measurements on living tissue, indirect methods must be used, *i.e.*, to use a mathematical models to obtain the properties investigated. These methods, and associated experimental techniques, are discussed in Chapter 3. The last part of the chapter is devoted to an application of these techniques; optical mammography. During the last decades, the use of X-

rays in the screening for breast cancer has been debated. Being ionizing radiation, X-rays have a potential to induce cancer. It has also been shown that some persons are specially sensitive to X-rays, and should thus avoid these investigations, if possible. This has been a driving force for the development of alternative techniques, the use of light being one. Again, models of the light distribution in the breast are required to allow the detection of tumours. For tomographic reconstructions, extensive calculations are inevitable. There is also a need to find out the optimal wavelengths to use for these applications. Results from spectroscopic investigations of breast tissue, both *in vivo* and *in vitro*, are presented in Papers I-III.

Various fluorescing tumour markers can be used to increase the contrast in the fluorescence signal between normal tissue and malignant and premalignant lesions. The properties of some of the most common substances will be discussed in Chapter 4. Paper V reports on fluorescence investigations of premalignant and benign lesions in the female genital tract, following oral administration of δ-aminolevulinic acid (ALA). Here, both the fluorescence of the tissue and of the tumour marker have been employed to try to characterize the tissue.

Another property of many of the tumour markers discussed in Chapter 4, is that they can be used as photosensitizers in photodynamic therapy, PDT. This is a treatment modality mainly used for superficial lesions, for example non-melanoma skin cancers. The treatment effect relies on the simultaneous presence of a photosensitizer, light, and oxygen. A photosensitizing agent is administered to the patient some hours, or days, prior to the treatment. During this period, the compound is accumulated in the diseased tissue to a higher degree than in normal tissue. The treatment is performed by irradiating the diseased area with light of a proper wavelength, normally in the red part of the spectrum. The photosensitizer absorbs the energy of the light, which in turn is transferred to oxygen, leading to excitation into a singlet state. In this state, oxygen becomes very reactive, resulting in an oxidation of the tissue, ending in cell death. A more detailed description of PDT, together with the influence of various parameters, such as light source, wavelength, irradiance, *etc.*, is given in Chapter 5. A randomized Phase III clinical study comparing PDT and cryosurgery in the treatment of basal cell carcinomas has been performed within the scope of this thesis. In Paper XI, the treatment results from the two modalities are compared, as well as the healing time and cosmetic result. Other aspects of PDT, such as the choice of wavelength of the therapeutic light, pulsed or continuous wave light, and one of the treatment side effects – pain – have been investigated in Papers IX-X.

One important parameter in PDT is the choice of irradiation wavelength. This is especially true when lasers are used for the irradiation. The absorption bands of

the sensitizers are usually rather narrow, and a small change of wavelength can result in large variations in treatment efficacy. In order to make the proper choice, the absorption spectrum of the sensitizer in tissue must be known. Due to the microenvironment, this can be considerably different from the spectrum obtained in solution. Absorption spectroscopy in tissue is, however, not a simple task since the scattering has a major influence. With knowledge of the scattering properties and the light propagation in tissue, the absorption spectrum can be determined. Paper IV presents the results from such investigations, and discusses the implications for PDT.

A term commonly applied to optical techniques used to characterize tissue is "optical biopsy". This is a somewhat contradictory term, since the word optical implies that the investigation is performed without affecting the tissue under investigation, while biopsy means that tissue is removed for investigation. The term is used, however, for non-invasive or minimally invasive techniques to characterize tissue, or to aid the physician in finding suspicious areas, that will be biopsied. In this context, these techniques often are said to be diagnostic. This is also misleading, since the diagnosis is made by the pathologists studying the biopsy samples, while the optical techniques are used to observe variations in the detected signals, and correlated them to certain diseases. The term "diagnostic" will in this thesis occasionally be used with this wider interpretation. One of the most commonly used techniques for optical biopsy is based on fluorescence. The basic principles of fluorescence and the main fluorophores in tissue will be discussed in Chapter 6. An overview of the equipment needed for fluorescence investigations will be given. Some technical solutions will be presented in more detail, with emphasis on the different systems constructed in Lund. The influence of the tissue optical properties on the recorded signal will also be discussed.

As mentioned above, the photosensitizers can be employed as fluorescent tumour markers. Two fluorescence imaging techniques have been used for this purpose, and results are presented in Papers VII-VIII. In Paper XII, the pharmacokinetics of the accumulation of ALA-induced protoporphyrin IX (PpIX) in basal cell carcinomas of the skin have been investigated by means of laser-induced fluorescence (LIF). The photodegradation of PpIX during irradiation is studied in Paper XIII. As a result of all the experience gained from these and several other fluorescence investigations, a new compact instrument has been constructed. A presentation of this instrument can be found in Paper VI.

Laser-Doppler perfusion imaging is a non-invasive and non-contact technique to measure the superficial blood perfusion in tissue. The small frequency shift of the diffusely backscattered light from the tissue, due to the moving red blood cells, is evaluated. This yields a measure on the perfusion, defined as the product of the

local concentration of red blood cells, and their velocities. An image is created by the stepwise scanning of a laser beam over the sampling area, with a measurement at each step. The perfusion has been used as an objective means of comparing the treatment response and the healing time of two treatment modalities, PDT and cryosurgery.

2. The interaction of light with tissue

Light is essential for all forms of life. We are surrounded by light, mainly originating from the sun. Within the biosphere, light participates in many processes. In plants, the absorption of the solar radiation by chlorophyll is a requirement for the photosynthesis. Also in our bodies many photochemical and photobiological reactions take place. The most obvious is the reaction with the photoreceptors in the eye, enabling our visual perception. In the skin we can see the result of the interaction between light and tissue, *e.g.*, as a tan following sun exposure. This is part of the protection against light that also might be harmful. The optical properties of the skin restricts the penetration depth, preventing most parts of the body from being exposed to light. Moreover, the optical properties determine the appearance of the tissue, as they are responsible for the colour and intensity of the reflected and diffusely scattered light.

The beneficial properties of light for medical treatment have been known for a long time. The ancient cultures in, for example, China, India, Egypt, and Greece have been using sun-light to treat various diseases. The introduction of light into the modern Western medicine is more recent. About 100 years ago, light was used in the treatment of small-pox and skin tuberculosis (*lupus vulgaris*).[1] Experiments with illumination of fluorescent drugs were also performed for the treatment of for example skin cancer, and ultraviolet (UV) radiation was found to be beneficial for patients suffering from psoriasis. A thorough review of the history of the therapeutic use of light in medicine was given by Daniell and Hill.[2] Light was also introduced for diagnostic purposes. During the late 1920's, the light from bright lamps shining through a female breast was used in an attempt to find breast cancer tumours, a method today termed transillumination or diaphanography.[3]

The use of lasers in medicine started soon after the invention of the ruby laser in 1960. Initially, the primary applications were based on the ability of focused laser beams to coagulate blood vessels in the retina, as reviewed by Viherkoski.[4] This was not very successful, mainly due to the poor absorption of light by the blood at the wavelength used (693 nm). With the development of other laser types, operating at various wavelengths, more medical applications were introduced. There was also a need to understand the interaction between light and tissue in order to optimize the techniques. Mathematical models of light propagation in tissue were developed, and are continuously being improved.

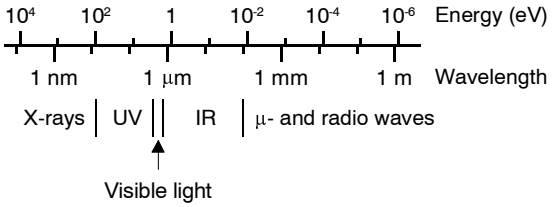

Figure 2-1 The spectrum of electromagnetic radiation.

2.1 Light propagation in tissue

Even though the interaction between light and tissue is fairly well understood on a microscopic scale, great difficulties arise when making a macroscopic description. When light, or electromagnetic radiation in general (Figure 2-1), propagates through tissue, a number of processes can occur; the light can be scattered or absorbed. These interaction processes are strongly wavelength dependent. High-energy electromagnetic radiation, such as gamma- or X-rays, is not scattered to a great extent, but rather propagates through the tissue in straight trajectories. The radiation is attenuated due to absorption, which varies with the tissue type. This kind of radiation can thus be used for imaging, such as normal X-ray images to visualize interior parts of the body. When absorbed, however, the high energy photons might lead to bond breaking and ionization of molecules, which in turn is potentially carcinogenic. Low-energy radiation such as infrared (IR) radiation or microwaves, on the other hand, induces excitations of rotational and vibrational energy levels in the molecules, leading to a temperature increase. In the following, the term light will be extended to cover not only the visible part of the wavelength spectrum, but also ultraviolet (UV) and near-infrared (NIR) radiation.

2.1.1 Reflection

When light is incident on an interface between two media with different refractive indices, a fraction will be reflected in the so-called specular reflection. Apart from the difference in refractive indices, the specular reflection is strongly dependent on the angle of incidence and polarization of the light, as well as the structure and shape of the surface. If polarization is neglected, the fraction of light reflected at the surface (r) is governed by Fresnel's law

$$r = \frac{1}{2}\left[\frac{\tan^2\left(\theta_1 - \theta_2\right)}{\tan^2\left(\theta_1 + \theta_2\right)} + \frac{\sin^2\left(\theta_1 - \theta_2\right)}{\sin^2\left(\theta_1 + \theta_2\right)}\right], \tag{2.1}$$

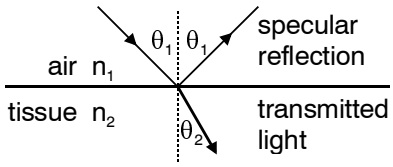

Figure 2-2 A schematic picture of the reflected and transmitted light at an air-tissue boundary, due to a mismatch of the refractive indices, *n*.

where θ_1 is the angle of incidence, and θ_2 is the angle of transmission in the second medium. The latter angle is given by Snell's law of refraction

$$n_1 \sin\theta_1 = n_2 \sin\theta_2 , \tag{2.2}$$

which depends on the refractive indices (n_1 and n_2, respectively), as depicted schematically in (Figure 2-2). For a laser beam incident perpendicularly to a tissue surface, *i.e.* when $\theta_1 = \theta_2 = 0$, Eq. (2.1) is reduced to

$$r = \left(\frac{n_2 - n_1}{n_2 + n_1} \right)^2 . \tag{2.3}$$

A typical value for the refractive index of tissue is 1.4,[5] which means that the specular reflection will be approximately 3% at an air-tissue interface. Due to the different refractive indices of tissue and air, light propagating inside the tissue will be internally reflected if it strikes the tissue surface at an angle greater than the critical angle θ_c, given by

$$\theta_c = \arcsin\left(n_1 / n_2\right) \approx 46^\circ . \tag{2.4}$$

Thus, a substantial amount of the photons migrating inside the tissue will not escape at the surface. As a result, the fluence rate just below the surface might be considerably larger than the incident irradiance.

2.1.2 Absorption

A photon can be absorbed by a molecule if its energy corresponds to the difference in energy between the electronic states of the molecule. Hence, the probability for absorption is strongly wavelength dependent. Tissue components that absorb light are called chromophores. The most important chromophores in the visible and near-infrared wavelength regions are haemoglobin and water. The absorption of light by blood depends on the oxygenation. Oxyhaemoglobin has

absorption peaks at 418, 542, and 577 nm, while deoxygenated haemoglobin has one peak at about 430 nm, one broad peak at about 450 nm, and a smaller one at about 750 nm.[6] Water, which is present to a large extent in most tissue types, is a strong absorber in the IR region, above 1300 nm, but also at very short wavelengths (below 200 nm).[7] Another important chromophore in tissue is melanin, small pigment granules in the skin and eye. Melanin exhibits a monotonically decreasing absorption with increasing wavelength. A typical absorption spectrum of tissue is shown in Figure 2-3. The spectrum represents a total haemoglobin tissue concentration of 1% (2/3 oxygenated, 1/3 deoxygenated), and a water content of 70%. As can be seen in the figure, the absorption is rather low in the red and near-infrared wavelength region, the absorption coefficient drops by almost two orders of magnitude. At about 1.3 μm, the absorption increases again due to water. The low-absorbing region between approximately 650 nm and 1300 nm is usually referred to as the tissue optical, or therapeutical, window and is used for many diagnostic and therapeutic applications. In the UV region, major absorbers are proteins and amino acids.

The physical parameter used to describe the absorption is the absorption coefficient, μ_a, which is defined as the probability for absorption per unit length, and is often given in inverse centimetres, cm^{-1}.

The energy gained by the tissue due to the absorption of light is involved in several processes. It might be re-emitted as fluorescence, contribute to photochemical reactions, or be redistributed among the molecules as heat, inducing a temperature increase.

2.1.3 Scattering

The different scattering processes can be divided into two main groups; elastic and inelastic processes. In elastic scattering there is no change of the photon energy, while inelastic scattering results in emission of a photon with an energy different from that of the incident photon. Elastic scattering that occurs when light is scattered by particles with a size much smaller than the wavelength of the light (λ), for example an atom or a molecule, is called Rayleigh scattering (unless it is a resonant process). If the scattering object is too large to be considered as a Rayleigh scatterer, the more complex Mie theory is required to describe the result of a scattering event. Rayleigh scattering theory can be considered as a simplification of the Mie theory in the limit where the size of the particle is negligible to the wavelength of the light. The wavelength dependence of the scattering varies from λ^{-4} in the Rayleigh limit to approximately λ^{-2} for large

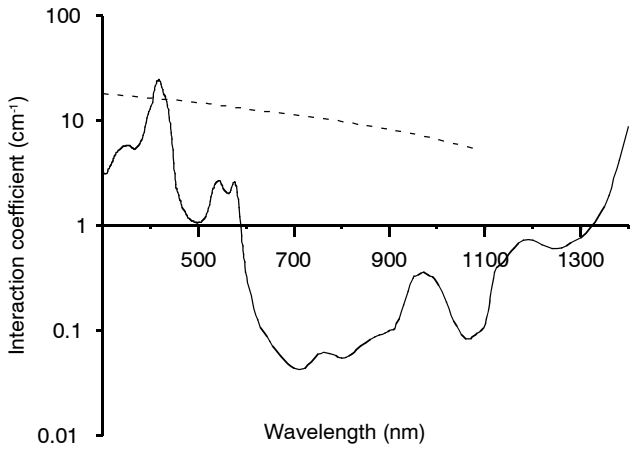

Figure 2-3 Typical interaction coefficients for tissue. The solid line represents the absorption coefficient, and is the sum of the absorption from oxygenated and deoxygenated haemoglobin (2/3 HbO_2 and 1/3 Hb), and water. A total haemoglobin concentration of 1% and a water content of 70% have been assumed. The spectra for HbO_2, Hb are adopted from Prahl,[6] and the water absorption from Hale and Querry.[7] The dashed line indicates the reduced scattering coefficient (see section. 2.1.4), corresponding to a linear extrapolation of the data presented in Paper III and unpublished data.

particles. This means that blue light is more scattered than red light, since the latter has a longer wavelength.

If the photon is scattered by a moving particle, such as a blood cell, there will be small change in energy due to the Doppler shift. This energy shift is, however, small relative to the original energy of the photon, and the scattering process will be thus described as quasi elastic. Laser Doppler perfusion imaging, described in Chapter 7, is a technique based on quasi elastic scattering for studies of the superficial tissue blood perfusion.

In Raman scattering, the scattering molecule is excited to a virtual energy level, from which is immediately relaxes to the ground state. The molecule will now be in a vibrational state with a higher, a lower, or equal energy compared to the initial state. The emitted light will thus have a longer, a shorter, or the same wavelength as the incident. Due to the change in energy, the two former processes are called inelastic scattering. The latter event is the Rayleigh scattering, and is much stronger than the inelastic Raman scattering.

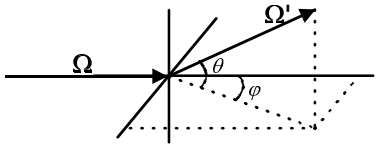

Figure 2-4 Definitions of the geometrical parameters for transport theory. The directions of the incident and scattered light are represented by the unity vectors **Ω** and **Ω'**, respectively. The zenith deflection angle θ is governed by the phase function, while the scattering is assumed to be isotropic around the azimuthal angle φ.

In the following, the term scattering will be used only for elastic scattering processes. In analogy to absorption, scattering is described by the probability of a scattering event per unit length, called the scattering coefficient, μ_s, having the same unit as the absorption coefficient. The sum of these two coefficients yields the total attenuation coefficient,

$$\mu_t = \mu_a + \mu_s, \tag{2.5}$$

which describes the probability of all light-tissue interactions per unit path length of a migrating photon.

2.1.4 Scattering anisotropy

The scattering in tissue is generally not isotropic, but strongly forward directed.[8-10] The scattering angle from a single scattering event has a probability distribution called the phase function. The phase function, generally denoted $p(\mathbf{\Omega'}\cdot\mathbf{\Omega})$, describes the probability that light travelling in the direction **Ω'** in a single event will be scattered into the direction **Ω**. For most tissue types, the scattering is symmetric about the direction of incidence. Hence, the phase function can be expressed as a function of the angle between the incident and the scattered, denoted θ (Figure 2-4). This assumption might not be valid for tissue structures with long, aligned cells. When describing light transport in tissue with various theoretical models, the phase function is usually empirically chosen. Within tissue optics, the Henyey-Greenstein phase function, originally used to describe scattering of starlight by interstellar dust,[11] has been widely used. It has also been shown to agree reasonably well with the angular distributions measured from skin[8] and aorta.[9] The Henyey-Greenstein phase function is expressed as

$$p(\mathbf{\Omega}'\cdot\mathbf{\Omega}) = p(\cos\theta) = \frac{1}{4\pi}\frac{1-g^2}{\left(1+g^2-2g\cos\theta\right)^{3/2}}. \tag{2.6}$$

Here, g is the so-called anisotropy factor, commonly referred to as the g-factor, which is defined as the mean cosine of the scattering angle, according to

$$g = \int_{4\pi}\cos\theta\cdot p(\cos\theta)\,d\mathbf{\Omega}. \tag{2.7}$$

The value of g ranges from -1 to +1, where -1 and +1 corresponds to total backscattering and total forward scattering, respectively. Isotropic scattering is represented by $g = 0$. Most mammalian tissue is, as mentioned above, strongly forward scattering with g-values between 0.7 and 0.95.[12] Human whole blood is even more forward scattering, with g-values between 0.995 and 0.999. Since the phase function is a probability distribution, a unity value is obtained when integrated over all directions,

$$\int_{4\pi} p(\cos\theta)\,d\mathbf{\Omega} = 1. \tag{2.8}$$

In order to treat light propagation problems, it is often of interest to expand the phase function into a series of well-known functions. A commonly used expansion method is to use the Legendre polynomials, $P_n(\mathbf{\Omega}'\cdot\mathbf{\Omega})$, for the expansion of the phase function as[13]

$$p(\mathbf{\Omega}'\cdot\mathbf{\Omega}) = \frac{1}{4\pi}\sum_{n=0}^{\infty}(2n+1)b_n P_n(\mathbf{\Omega}'\cdot\mathbf{\Omega}). \tag{2.9}$$

The expansion coefficients b_n follow from the fact that the Legendre polynomials form a complete orthogonal set, and are obtained as

$$b_n = \int_{4\pi} p(\mathbf{\Omega}'\cdot\mathbf{\Omega})P_n(\mathbf{\Omega}'\cdot\mathbf{\Omega})\,d\mathbf{\Omega}'. \tag{2.10}$$

The lowest order Legendre polynomials are given by

$$P_0(x) = 1,\ P_1(x) = x,\ P_2(x) = \frac{3x^2-1}{2},\ \text{and}\ P_3(x) = \frac{5x^3-3x}{2}. \tag{2.11}$$

Together, Eqs. (2.10), (2.11), (2.8), and (2.7) will give the two first expansion coefficients as

$$b_0 = 1 \text{ and } b_1 = g, \tag{2.12}$$

which in turn yields an expression for the expanded phase function

$$p\left(\boldsymbol{\Omega}'\cdot\boldsymbol{\Omega}\right)=\frac{1}{4\pi}\left(1+3g\boldsymbol{\Omega}'\cdot\boldsymbol{\Omega}\right). \tag{2.13}$$

The first term represents isotropic scattering, while the second term describes the diffuse light, also taking the forward scattering into account. Using the scheme outlined above for an expansion of the Henyey-Greenstein phase function, the expansion coefficients will simply be a power series of the g-factor, *i.e.*, $b_n = g^n$. This might not be an exact representation of the true phase function of biological tissue, but experiments have shown it to give a good approximation.[8,9] Moreover, it is practical in model calculations. It does not, however, fully account for highly forward scattering media. An improvement can be made through the inclusion of a δ-function,

$$p_{\delta-E}\left(\boldsymbol{\Omega}'\cdot\boldsymbol{\Omega}\right)=\frac{1}{4\pi}\left[2f\delta\left(1-\boldsymbol{\Omega}'\cdot\boldsymbol{\Omega}\right)+\left(1-f\right)\left(1+3g'\,\boldsymbol{\Omega}'\cdot\boldsymbol{\Omega}\right)\right], \tag{2.14}$$

where f is the fraction of light scattered directly forward, and g' governs the asymmetry of the phase function. This procedure was introduced by Joseph *et al.*,[14] and is called the δ-Eddington approximation. When integrated over all directions, a unity value is obtained, as required by Eq. (2.8):

$$\begin{aligned}&\frac{1}{4\pi}\int_{4\pi}\left[2f\delta\left(1-\boldsymbol{\Omega}'\cdot\boldsymbol{\Omega}\right)+\left(1-f\right)\left(1+3g'\,\boldsymbol{\Omega}'\cdot\boldsymbol{\Omega}\right)\right]d\boldsymbol{\Omega} \\ &\quad=\frac{1}{4\pi}\int_0^{2\pi}d\varphi\int_0^{\pi}\left[2f\delta\left(1-\cos\theta\right)+\left(1-f\right)\left(1+3g'\cos\theta\right)\right]\sin\theta\,d\theta \\ &\quad=\frac{1}{2}\int_{-1}^{1}\left[2f\delta\left(1-\mu\right)+\left(1-f\right)\left(1+3g'\,\mu\right)\right]d\mu=f+\left(1-f\right)=1\end{aligned} \tag{2.15}$$

The first moment of Eq. (2.14) yields the relation between the g-factor and the δ-Eddington parameters, which is[14]

$$g=f+\left(1-f\right)g'. \tag{2.16}$$

Since the Henyey-Greenstein phase function has been shown to give a good description of the scattering in tissues,[8] the second moment of the δ-Eddington and the Henyey-Greenstein phase functions are required to be equal. This results in the following expressions[14] for f and g'

$$f = g^2, \text{ and } g' = \frac{g}{g+1}. \tag{2.17}$$

The use of the δ-Eddington phase function has been shown to better describe the light distribution near boundaries[15] and close to the source, also when the scattering coefficient is relatively small.[16]

A useful quantity in tissue optics is the reduced scattering coefficient, μ_s', which is defined as

$$\mu_s' = (1-g)\mu_s. \tag{2.18}$$

The inverse of the reduced scattering coefficient is a measure of the effective mean free path between artificial isotropic scattering events in a multiple-scattering environment, *i.e.* the average distance a photon travels before the scattering can be regarded as isotropic. This is schematically illustrated in Figure 2-5.

Finally, the linear transport coefficient, μ_{tr}, is used to describe the inverse of the effective mean free path between interaction events in a strongly scattering medium, and is given by

$$\mu_{tr} = \mu_a + (1-g)\mu_s = \mu_a + \mu_s'. \tag{2.19}$$

The previous sections have been discussing the fundamental interactions between light and tissue. These properties will now be applied in a theoretical framework to derive a mathematical model, that can be used to study the interactions.

2.2 Theoretical models

The light distribution in tissue during illumination can be modelled using either analytical theory or transport theory.[17] In analytical theory, the light propagation is described as a continuous transfer of energy by electromagnetic waves. This model starts from basic differential equations, such as Maxwell's equations or the wave equation. The dielectric property for all positions in the medium is required, and differential or integral equations are obtained. This approach is mathematically rigorous, since it in principle includes all the multiple scattering, diffraction, and interference effects. In tissue optics, however, it is generally impossible to have a complete knowledge of the dielectric property matrix. Moreover, it would be virtually impossible to solve the equations even with this knowledge.

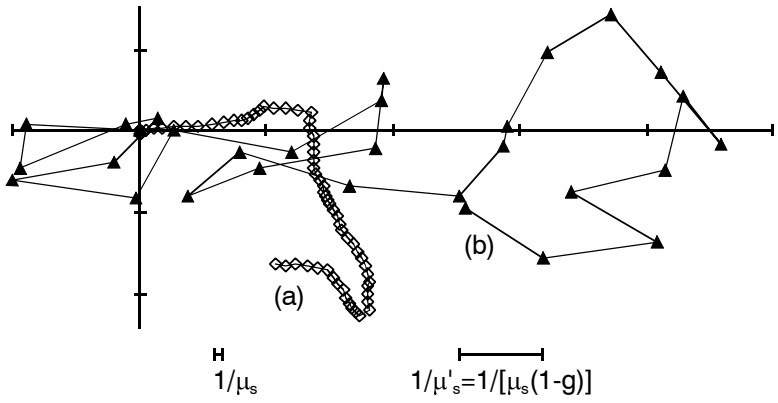

Figure 2-5 The significance of the reduced scattering coefficient μ'_s. Two simulated photon paths are illustrated. Path (a) represents forward scattering with a scattering coefficient μ_s and an anisotropy factor $g = 0.9$. This can also be seen as isotropic scattering on the scale of μ'_s. This is illustrated with path (b).

In transport theory, on the other hand, the light propagation is treated as a stream of particles, photons. Each photon has an assigned energy quantum. The mathematical description is not based on Maxwell's equations, but describes a statistical approximation of the energy transport through a turbid medium. The theory has been heuristically derived, and thus lacks the rigor of an analytical theory. Furthermore, since only the transport of power is considered, typical wave phenomena like polarization, interference and diffraction are neglected. Using transport theory, the light fluence can be calculated in two different ways; either by solving the transport equation, or by Monte Carlo simulations of the light distribution.

2.2.1 Transport theory

Transport theory has been successfully used in a large number of physical applications, such as neutron diffusion, radiative transfer, theory of plasmas, theory of sound propagation, and propagation of light in turbid media. The fundamental idea of transport theory is to describe an energy balance of the incoming, outgoing, absorbed and emitted energy of an infinitesimal volume element in the medium. This is mathematically described by a differential equation called the transport equation, which is equivalent to Boltzmann's equation, used in the kinetic theory of gases.

Since the particles of interest are photons, an assumption is made that there are no forces and therefore no collisions between them. Hence, they behave much as an ideal gas. A single-particle distribution function, $N(\mathbf{r},\boldsymbol{\Omega},t)$, with the unit $\mathrm{m^{-3}\ sr^{-1}}$, is used to describe the light distribution as a function of the position in space, $\mathbf{r}$, direction of propagation, $\boldsymbol{\Omega}$, and time, t.[18] The expected number of photons in a volume element $d\mathbf{r}$ about the position $\mathbf{r}$ with a direction $\boldsymbol{\Omega}$ within the solid angle $d\boldsymbol{\Omega}$ at time t can now be written as $N(\mathbf{r},\boldsymbol{\Omega},t)d\mathbf{r}d\boldsymbol{\Omega}$. Since all photons travel with the same speed, $v = c/n$, where c is the speed of light in vacuum and n is the refractive index of the medium, only the so-called one-speed case will be considered in the following.

The photon distribution function $N(\mathbf{r},\boldsymbol{\Omega},t)$ can easily be related to other optical entities of interest. The radiance, $L(\mathbf{r},\boldsymbol{\Omega},t)$ [$\mathrm{W\ m^{-2}\ sr^{-1}}$], which is the quantity used to describe the propagation of photon power, is obtained by multiplying the distribution function with the speed and the energy of the photons. The photon density $\rho(\mathbf{r},t)$ [$\mathrm{m^{-3}}$], *i.e.* the number of photons per unit volume, is given by the integration of N over all possible directions,

$$\rho(\mathbf{r},t) = \int_{4\pi} N(\mathbf{r},\boldsymbol{\Omega},t)\,d\boldsymbol{\Omega}\,. \tag{2.20}$$

The net number of photons crossing the area dS in time dt is given by $\mathbf{J}(\mathbf{r},t)\cdot\mathbf{n}\ dS\ dt$, where $\mathbf{n}$ is a unity vector normal to dS. Here, $\mathbf{J}(\mathbf{r},t)$ [$\mathrm{m^{-2}\ s^{-1}}$] is the photon current density, given by

$$\mathbf{J}(\mathbf{r},t) = v\int_{4\pi} N(\mathbf{r},\boldsymbol{\Omega},t)\boldsymbol{\Omega}\,d\boldsymbol{\Omega}\,. \tag{2.21}$$

The photon density and the photon current density will be of interest for the following calculations, but are not measurable quantities. For practical use, the fluence rate, $\phi(\mathbf{r},t)$ [$\mathrm{W\ m^{-2}}$] and the photon flux, $\mathbf{F}(\mathbf{r},t)$ [$\mathrm{W\ m^{-2}}$], are of more interest. The fluence rate is defined as the radiant power incident on a small sphere, divided by the cross-sectional area of that sphere, which is expressed as

$$\phi(\mathbf{r},t) = \int_{4\pi} L(\mathbf{r},\boldsymbol{\Omega},t)\,d\boldsymbol{\Omega}\,. \tag{2.22}$$

In analogy with the photon current density, the photon flux is defined as

$$\mathbf{F}(\mathbf{r},t) = \int_{4\pi} L(\mathbf{r},\boldsymbol{\Omega},t)\boldsymbol{\Omega}\,d\boldsymbol{\Omega}\,. \tag{2.23}$$

The photon flux multiplied by a unit vector, $\mathbf{F}\cdot\mathbf{n}$, represents the net flux per unit area over an area dS orthogonal to $\mathbf{n}$.

There has been some controversy about which of the above mentioned quantities are being measured. For measurements of the diffusely reflected and transmitted light using a detector on the tissue surface, most researchers have used the model presented by Patterson *et al.*,[19] where the photon current density (or rather the related photon flux, following the definitions above) is considered to be measured. Other work has been presented, where the photon density (or the related fluence rate) has been used to describe the signal obtained. Experimental time-resolved studies by Liu *et al.* verified that the fluence rate is measured when the detector is placed within the medium.[20] With a detector on the surface, both the fluence rate and the photon density were found to correctly describe the data, provided that the diffusion approximation is valid. Kaltenbach and Kaschke stated, through theoretical discussions, that the signal from a detector on the surface of the medium is proportional to the photon current density, and thus the photon flux is being measured.[21]

A simple derivation of the transport equation may start from a balance equation based on conservation of particles within a small volume element of phase space.[18] The change in the total number of photons dN in time dt travelling within a small solid angle $d\mathbf{\Omega}$ within a volume V, located around the point $\mathbf{r}$, can be written as

$$dN = d\mathbf{\Omega}\, dt \int_V \frac{\partial N(\mathbf{r},\mathbf{\Omega},t)}{\partial t} d\mathbf{r}\,. \tag{2.24}$$

This change is also given by a balance equation, where

$dN =$
- (a) photons lost through flow over the surface S of the V
- (b) photons lost due to absorption within V
- (c) photons scattered from $\mathbf{\Omega}$ into other directions $\mathbf{\Omega'}$
- (d) photons scattered into direction $\mathbf{\Omega}$ from other directions $\mathbf{\Omega'}$
- (e) photons with direction, produced from sources within V.

This balance is schematically depicted in Figure 2-6. Photons entering and leaving the volume with no change in direction are included in term (a), while photons scattered from or into the direction studied without change in position are included in terms (c) and (d), respectively. The five terms of the balance equation must now be expressed mathematically. First, the photon flow over the boundary surface is described by

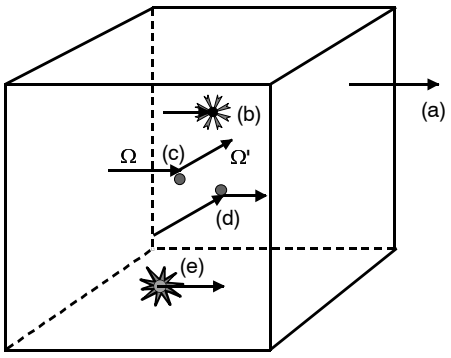

Figure 2-6 A schematic representation of the balance equation used to derive the transport equation. The (a) boundary losses, (b) losses due to absorption, (c) losses due to scattering into other directions, (d) gain due to scattering into the direction studied, and (e) gain due to sources in the volume element are considered.

$$\text{(a)} = v\,d\boldsymbol{\Omega}\,dt \oint_S \boldsymbol{\Omega} N(\mathbf{r},\boldsymbol{\Omega},t)\cdot\mathbf{n}\,dS = v\,d\boldsymbol{\Omega}\,dt \int_V \boldsymbol{\Omega}\cdot\nabla N(\mathbf{r},\boldsymbol{\Omega},t)\,dV, \tag{2.25a}$$

where **n** is the outward normal to the surface element dS. The second equality is obtained, in order to get a volume integral, by applying Gauss' theorem. The other terms are given by the following equations,

$$\text{(b)} = v\,d\boldsymbol{\Omega}\,dt \int_V \mu_a(\mathbf{r}) N(\mathbf{r},\boldsymbol{\Omega},t)\,dV, \tag{2.25b}$$

$$\text{(c)} = v\,d\boldsymbol{\Omega}\,dt \int_V \mu_s(\mathbf{r}) N(\mathbf{r},\boldsymbol{\Omega},t)\,dV, \tag{2.25c}$$

$$\text{(d)} = v\,dt \int_V \mu_s(\mathbf{r}) \int_{4\pi} p(\boldsymbol{\Omega}'\cdot\boldsymbol{\Omega}) N(\mathbf{r},\boldsymbol{\Omega}',t)\,dV d\boldsymbol{\Omega}', \text{ and} \tag{2.25d}$$

$$\text{(e)} = d\boldsymbol{\Omega}\,dt \int_V q(\mathbf{r},\boldsymbol{\Omega},t)\,dV. \tag{2.25e}$$

In the latter equation, $q(\mathbf{r},\boldsymbol{\Omega},t)$ [m^{-3} sr^{-1} s^{-1}] is a source term. As all terms in the balance equation, obtained by setting Eqs. (2.24) and (2.25) equal, are integrated over an arbitrary volume V, the balance must also apply for the integrands, according to

$$\frac{\partial L(\mathbf{r},\mathbf{\Omega},t)}{\partial t} = -v\mathbf{\Omega}\cdot\nabla L(\mathbf{r},\mathbf{\Omega},t) - v\mu_t L(\mathbf{r},\mathbf{\Omega},t) + v\mu_s(\mathbf{r})\int_{4\pi} p(\mathbf{\Omega}'\cdot\mathbf{\Omega})L(\mathbf{r},\mathbf{\Omega}',t)d\mathbf{\Omega}' + Q(\mathbf{r},\mathbf{\Omega},t) \tag{2.26}$$

In this equation, the distribution of photons $N(\mathbf{r},\mathbf{\Omega},t)$, can be substituted with the radiance $L(\mathbf{r},\mathbf{\Omega},t)$. The source term then has to be replaced by $Q(\mathbf{r},\mathbf{\Omega},t)$ [W m^{-2} s^{-1} sr^{-1}], in order to have the right dimensions.

Now, the transport equation, Eq. (2.26), used to model the light propagation in tissue has been formulated. The next step is to find its solution.

2.2.2 Expansion in spherical harmonics

The traditional way to solve integro-differential equations in mathematical physics is to use an expansion of the problem into a series of eigenfunctions in order to obtain a separation of variables. Case and Zweifel[18] applied this method on the transport equation using spherical harmonics. Thus, the position and directional variables can be treated separately. First, the radiance $L(\mathbf{r},\mathbf{\Omega},t)$ is expanded into

$$L(\mathbf{r},\mathbf{\Omega},t) = \sum_{l=0}^{\infty}\sum_{m=-l}^{l}\sqrt{\frac{2l+1}{4\pi}}L_{lm}(\mathbf{r},t)Y_{lm}(\mathbf{\Omega}). \tag{2.27}$$

The same procedure is applied to the source function $Q(\mathbf{r},\mathbf{\Omega},t)$. To fully describe the problem, also the phase function can be expanded into spherical harmonics. These expansion series are then inserted into the transport equation. The result is an infinite series of coupled differential equations. To reach the solution, this series must be truncated at some l. The general equations will still be complex. The lowest-order approximation, keeping only the terms for which $l = 0$ and $l = 1$, can be derived quite simply for an arbitrary geometry, however. This approximation is commonly known as the diffusion approximation, or the P_1-approximation, and is widely used in tissue optics. Truncation of Eq. (2.27) yields

$$L(\mathbf{r},\mathbf{\Omega},t) = \sqrt{\frac{1}{4\pi}}L_{00}(\mathbf{r})Y_{00}(\mathbf{\Omega}) + \sqrt{\frac{3}{4\pi}}\sum_{m=-1}^{1}L_{1m}(\mathbf{r})Y_{1m}(\mathbf{\Omega}). \tag{2.28}$$

This expression could now be inserted into the transport equation, which after integration over $\mathbf{\Omega}$ would give four equations and four unknowns. Another approach is to observe that Y_{00} is a scalar and that Y_{1m} ($m = 0, \pm 1$) represent the three components of a vector. The expression in Eq. (2.28) can thus be substituted by[18]

$$L(\mathbf{r},\Omega,t) = A + \Omega \cdot \mathbf{B}\,. \tag{2.29}$$

Through integration of this expression over the angular space, we obtain

$$\int_{4\pi} L(\mathbf{r},\Omega,t)\,d\Omega = \int_{4\pi} \left(A + \Omega \cdot \mathbf{B}\right) d\Omega\,. \tag{2.30}$$

The left-hand side is identified as the definition of the photon density, Eq. (2.20). On the right-hand side, the last term is zero (see appendix to this section), and thus

$$A = \frac{1}{4\pi}\phi(\mathbf{r},t)\,. \tag{2.31}$$

Similarly, if Eq. (2.28) is multiplied by Ω before the integration, we find that

$$\int_{4\pi} \Omega L(\mathbf{r},\Omega,t)\,d\Omega = \int_{4\pi} \Omega\left(A + \Omega \cdot \mathbf{B}\right) d\Omega\,. \tag{2.32}$$

Here, the left-hand side is the definition of the photon flux divided by the speed. The first term of the left-hand side cancels out during the integration, while the second term results in $(4\pi/3)\mathbf{B}$. Thus,

$$\mathbf{B} = \frac{3}{4\pi}\mathbf{F}(\mathbf{r},t)\,. \tag{2.33}$$

With the expressions for A and $\mathbf{B}$, the radiance in this approximation becomes

$$L(\mathbf{r},\Omega,t) = \frac{1}{4\pi}\left[\phi(\mathbf{r},t) + 3\mathbf{F}(\mathbf{r},t)\cdot\Omega\right]. \tag{2.34}$$

In a similar way, the source function is expanded and truncated, yielding

$$Q(\mathbf{r},\Omega,t) = \frac{1}{4\pi}\left(Q_0(\mathbf{r},t) + 3\mathbf{Q}_1(\mathbf{r},t)\cdot\Omega\right). \tag{2.35}$$

These two simplified expansions are now inserted into the transport equation, Eq. (2.26), which, after multiplication with a factor 4π, will result in

$$\begin{aligned}\frac{\partial}{\partial t}\left[\phi + 3\mathbf{F}\cdot\Omega\right] &= -v\Omega\cdot\nabla\left[\phi + 3\mathbf{F}\cdot\Omega\right] - v\mu_t(\mathbf{r})\left[\phi + \mathbf{F}\cdot\Omega\right] \\ &\quad + v\mu_s(\mathbf{r})\int p(\Omega'\cdot\Omega)\left[\phi + \mathbf{F}\cdot\Omega'\right]d\Omega' + \left[Q_0 + 3\mathbf{Q}_1\cdot\Omega\right]\end{aligned} \tag{2.36}$$

The integral can be solved using the properties of the phase function, expressed in Eqs. (2.7) and (2.8), reducing Eq. (2.36) to

$$\frac{\partial \phi}{\partial t} + 3\frac{\partial(\mathbf{F}\cdot\boldsymbol{\Omega})}{\partial t} = v\left(-\boldsymbol{\Omega}\cdot\nabla - \mu_t + \mu_s\right)\phi \qquad (2.37)$$
$$+ 3v\left(-\boldsymbol{\Omega}\cdot\nabla - \mu_t + g\mu_s\right)\mathbf{F}\cdot\boldsymbol{\Omega} + \left[Q_0 + 3\mathbf{Q}_1\cdot\boldsymbol{\Omega}\right]$$

A slight rearrangement of the terms, together with the introduction of Eqs. (2.5) and (2.19) yields

$$\frac{1}{v}\left[\frac{\partial \phi}{\partial t} + 3\frac{\partial(\mathbf{F}\cdot\boldsymbol{\Omega})}{\partial t}\right] = \left(-\boldsymbol{\Omega}\cdot\nabla - \mu_a\right)\phi \qquad (2.38)$$
$$+ 3\left(-\boldsymbol{\Omega}\cdot\nabla - \mu_{tr}\right)\mathbf{F}\cdot\boldsymbol{\Omega} + \frac{1}{v}\left[Q_0 + 3\mathbf{Q}_1\cdot\boldsymbol{\Omega}\right]$$

An integration of this expression over $\boldsymbol{\Omega}$ will, with the help of Eqs. (2.46) and (2.49), result in

$$\frac{1}{v}\frac{\partial \phi}{\partial t} = -\mu_a\phi - \nabla\cdot\mathbf{F} + \frac{1}{v}Q_0 . \qquad (2.39)$$

If, on the other hand, the expression in Eq. (2.38) multiplied with $\boldsymbol{\Omega}$ before the integration is carried out, Eqs. (2.47), (2.48) and (2.50) will help us to get

$$\frac{1}{v}\frac{\partial \mathbf{F}}{\partial t} = -\frac{1}{3}\nabla\phi - \mu_{tr}\mathbf{F} + \frac{1}{v}\mathbf{Q}_1 \qquad (2.40)$$

The last two expressions are the basic equations of diffusion theory, and can be reduced to a single equation by elimination of the dependent variable $\mathbf{F}$. For an isotropic source ($\mathbf{Q}_1 = 0$), the steady-state solution of Eq. (2.40) will be Fick's law

$$\mathbf{F} = -D\nabla\phi , \qquad (2.41)$$

where the diffusion coefficient D [m] is introduced as

$$D = \frac{1}{3\mu_{tr}} = \frac{1}{3\left[\mu_a + (1-g)\mu_s\right]} . \qquad (2.42)$$

Using Fick's law and the diffusion coefficient, the final expression for the diffusion equation can be obtained as

$$\frac{1}{v}\frac{\partial \phi}{\partial t} - \nabla \cdot \left(D \nabla \phi \right) + \mu_a \phi = \frac{1}{v} Q_0 \,. \tag{2.43}$$

This is the rather simple expression for the light distribution in tissue. To be valid, some requirements must be fulfilled, though. First, the reduced scattering coefficient must be much larger than the absorption coefficient, *i.e.* $(1\text{-}g)\mu_s >> \mu_a$, to allow a diffuse light fluence. This restriction is given by the P_1-approximation of Eq. (2.27), which only allows a diffuse fluence with a small anisotropy. Furthermore, the separation between the light source and the location where the fluence rate is monitored must be large, again to ascertain a diffuse propagation.

Since most of the work in tissue optics is performed with a collimated laser beam, or light from an optical fibre, perhaps with a spherical or cylindrical diffusing tip, the radiance is often separated into one collimated part (denoted by subscript *p*, from primary) and one scattered part (denoted by subscript *s*):

$$L\left(\mathbf{r}, \Omega, t\right) = L_s\left(\mathbf{r}, \Omega, t\right) + L_p\left(\mathbf{r}, \Omega, t\right) \tag{2.44}$$

By definition, the fluence rate then also consists of a primary and a scattered part:

$$\begin{aligned} \phi\left(\mathbf{r}, t\right) &= \int_{4\pi} L\left(\mathbf{r}, \Omega, t\right) d\Omega \\ &= \int_{4\pi} L_s\left(\mathbf{r}, \Omega, t\right) d\Omega + \int_{4\pi} L_p\left(\mathbf{r}, \Omega, t\right) d\Omega = \phi_s\left(\mathbf{r}, t\right) + \phi_p\left(\mathbf{r}, t\right) \end{aligned} \tag{2.45}$$

The primary beam, or collimated beam, consists of the light that has not interacted with the tissue. This part is attenuated according to the Beer-Lambert law; $\exp(-\mu_t z)$. At the first scattering event, photons are moved from the primary to the scattered part. The separation into primary and scattered light is particularly useful when the δ-Eddington phase function is applied, as that function consists of two terms, each handling one of these parts.

Appendix to section 2.2.2

To solve some of the integral expressions in the previous section, the following identities have been used. Here, **A** and **B** are arbitrary vectors, while C is a scalar, all independent on $\boldsymbol{\Omega}$.

$$\int_{4\pi} \mathbf{A}\cdot\boldsymbol{\Omega}\, d\boldsymbol{\Omega} = 0 \tag{2.46}$$

$$\int_{4\pi} \boldsymbol{\Omega}\left(\boldsymbol{\Omega}\cdot\mathbf{A}\right) d\boldsymbol{\Omega} = \frac{4\pi}{3}\mathbf{A} \tag{2.47}$$

$$\int_{4\pi} C\boldsymbol{\Omega}\, d\boldsymbol{\Omega} = 0 \tag{2.48}$$

$$\int_{4\pi} \left(\mathbf{A}\cdot\boldsymbol{\Omega}\right)\left(\mathbf{B}\cdot\boldsymbol{\Omega}\right) d\boldsymbol{\Omega} = \frac{4\pi}{3}\left(\mathbf{A}\cdot\mathbf{B}\right) \tag{2.49}$$

$$\int_{4\pi} \boldsymbol{\Omega}\left(\mathbf{A}\cdot\boldsymbol{\Omega}\right)\left(\mathbf{B}\cdot\boldsymbol{\Omega}\right) d\boldsymbol{\Omega} = 0 \tag{2.50}$$

2.2.3 Solutions in the time-domain

Solutions to the time-dependent diffusion equation can be obtained for some elementary geometries, such as an infinite medium or a medium with simple boundary conditions. Moreover, if the medium is considered to be homogeneous, and thus the diffusion coefficient D has a constant value, the second term in Eq. (2.41) can be substituted with

$$\nabla\cdot\left(D\nabla\phi\right) = D\nabla^2\phi\,. \tag{2.51}$$

Consider an isotropic light source, emitting an infinitely short pulse of unity strength at time $t = 0$ and at the position $\mathbf{r} = \mathbf{r}_0$, mathematically described by

$$Q = \delta\left(\mathbf{r}-\mathbf{r}_0\right)\delta\left(t\right). \tag{2.52}$$

It can be shown,[22] that the solution to the diffusion equation then becomes

$$\phi\left(\mathbf{r},t\right) = v\left(4\pi Dct\right)^{-3/2}\exp\left(-\mu_a vt - \frac{\left(\mathbf{r}-\mathbf{r}_0\right)^2}{4Dvt}\right). \tag{2.53}$$

This function is called the Green's function for free diffusion, and will be used to solve the problem for other simple geometries, such as a semi-infinite

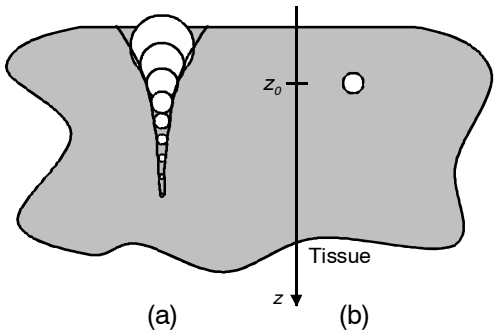

Figure 2-7 Two possible representations of the source. In (a) a continuous line of sources with an exponential decay is used. In (b), the source is represented by a delta-function at a depth of $z_0 = 1/\mu'_s$.

homogeneous scattering medium, or a slab with finite thickness and infinite extensions in the two other dimensions. When illuminating a small spot on the tissue surface, the source function cannot be described by an isotropic point source. A stringent model would be to use a line source, consisting of isotropic point sources, with an exponentially decaying strength, proportional to $\exp(-\mu_{tr} z)$, where z is the distance from the boundary. Thus, the fluence can be calculated from an integration of the Green's function for sources at all depths. A simplification, proposed by Patterson *et al.*,[19] is to assume that all the incident photons are initially scattered at a depth equal to the mean free path for effective isotropic scattering,

$$z_0 = \frac{1}{\mu'_s}. \tag{2.54}$$

At this depth, the source can be approximated with the simple delta-function described above. The two source-models are shown in Figure 2-7.

Next, the problem requires a specification of the boundary condition at the tissue surface. If the tissue and the surrounding medium have the same refractive index, the boundary condition is simply that there should be no photon flux back into the tissue from the surrounding medium, and can be mathematically expressed as[23]

$$\phi(\mathbf{r}) - 2D\mathbf{n}\cdot\nabla\phi(\mathbf{r}) = 0, \tag{2.55}$$

where $\mathbf{r}$ is a point on the interface and $\mathbf{n}$ is a unit normal vector directed into the tissue. Setting the fluence to zero at an extrapolated boundary at $z_e \approx 2D$, or $z_e = 3\cdot 0.7104\cdot D$ as presented by Ishimaru,[17] will approximately satisfy this

boundary condition. If, on the other hand, there is a mismatch between the media, such as at an air-tissue interface, the boundary condition must be changed to allow internal reflection at the surface, according to[24]

$$\phi(\mathbf{r}) - 2AD\mathbf{n}\cdot\nabla\phi(\mathbf{r}) = 0\,. \tag{2.56}$$

Here A can be derived from the Fresnel reflection coefficients as

$$A = \frac{2/(1-R_0) - 1 + |\cos\theta_c|^3}{1 - |\cos\theta_c|^2}, \text{ with} \tag{2.57}$$

$$R_0 = \frac{(n_{rel}-1)^2}{(n_{rel}+1)^2}, \tag{2.58}$$

$$n_{rel} = n_{tissue}/n_{air}\,, \text{ and} \tag{2.59}$$

$$\theta_c = \arcsin n_{rel}\,. \tag{2.60}$$

An extrapolated boundary with zero fluence at $z_e = 2AD \approx 5.5D \approx 2/\mu_{tr}$ will roughly satisfy the boundary condition for an air-tissue interface ($n_{tissue} = 1.4$).

The most commonly used approach to set the fluence to zero at the extrapolated boundary is to introduce negative mirror sources.[25] The point source at $z = z_0$ is mirrored in $z = -z_e$, resulting in a negative source at $z = -(2z_e + z_0)$. This source geometry is represented in Figure 2-8. For a slab, an infinite series of sources and sinks will be needed to fully cancel out the fluence rate over the extrapolated boundaries at both sides. These source term can thus be expressed as

$$Q(\mathbf{r},t) = Q_0\delta(t)\sum_{k=-\infty}^{+\infty}\left[\delta(\mathbf{r}-\mathbf{r}_{k,pos}) - \delta(\mathbf{r}-\mathbf{r}_{k,neg})\right] \text{ with} \tag{2.61}$$

$$\mathbf{r}_{k,pos} = \left[2k(d+2z_e) + z_0\right]\mathbf{e}_z \text{ and } \mathbf{r}_{k,neg} = \left[2k(d+2z_e) - (2z_e + z_0)\right]\mathbf{e}_z\,. \tag{2.62}$$

For the diffuse reflectance from a semi-infinite geometry, only the source term corresponding to $k = 0$ is used, while for the diffuse transmittance through a slab, only the terms for which $k = -1$, 0, +1, +2 will significantly contribute to the result. Furthermore, when the light propagation is studied at distances from the source much larger than z_e, Patterson *et al.* have shown that the pulse shape is insensitive to the exact location of the extrapolated boundary, and thus it could be placed on the physical border of the tissue.[19]

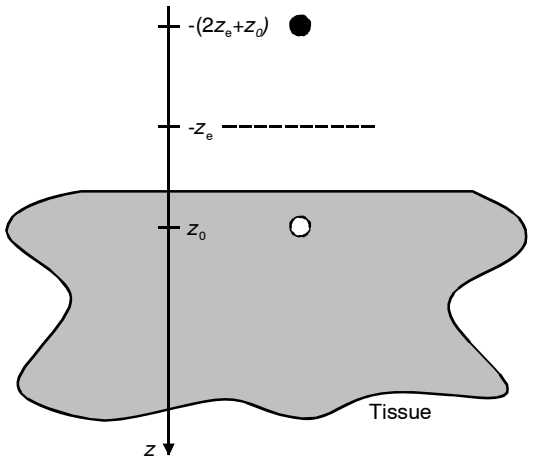

Figure 2-8 A schematic representation of a commonly used approach to meet the boundary conditions. A dipole source is placed symmetrically around an extrapolated boundary, over which the light fluence is zero. A positive source is placed at $z = -z_0$, and a negative at $z = -(2z_e+z_0)$.

The detected signal on the tissue surface is, as discussed earlier, proportional to the photon flux, which is related to the fluence rate through Fick's law, Eq. (2.41). The diffuse reflectance per incident photon can now be expressed in cylindrical co-ordinates as

$$R(r,t) = \left| -D\nabla\phi(r,z,t)\right|_{z=0} \tag{2.63}$$
$$= Q_0 (4\pi Dc)^{-3/2} z_0 t^{-5/2} \exp(-\mu_a v t) \exp\left(-\frac{z_0^2 + \rho^2}{4Dvt}\right).$$

The light transmitted through a slab, detected on the side opposite to the source, will then similarly be

$$T(r,d,t) = Q_0 (4\pi Dc)^{-3/2} t^{-5/2} \exp(-\mu_a v t) \exp\left(-\frac{\rho^2}{4Dvt}\right) \tag{2.64}$$
$$\times \left\{ (d - z_0) \exp\left[-\frac{(d - z_0)^2}{4Dvt}\right] - (d + z_0) \exp\left[-\frac{(d + z_0)^2}{4Dvt}\right] \right.$$
$$\left. + (3d - z_0) \exp\left[-\frac{(3d - z_0)^2}{4Dvt}\right] - (3d + z_0) \exp\left[-\frac{(3d + z_0)^2}{4Dvt}\right] \right\}.$$

These two functions can be used to estimate the optical properties in a highly scattering medium by fitting the appropriate analytical expression to the measured diffuse reflectance or transmittance, as was done in Papers II-IV.

2.2.4 Solutions in the frequency domain

In the previous section the diffusion equation was solved for some geometries using a very short light pulse. This description of light diffusion in the time domain can be complemented by an equivalent description in the frequency domain, a technique well established in spectroscopy.[26] The solution to the problem can then formally be obtained through the Fourier transform of the time-domain equation.[27,28] Alternatively, a more intuitive approach is to introduce a sinusoidally amplitude-modulated point source, expressed as[29,30]

$$Q = \delta(\mathbf{r})Q_0\left(1 + A\exp\left[-i(\omega t + \varepsilon)\right]\right), \tag{2.65}$$

where Q_0 is the source strength, A is the modulation of the source, ω is the angular modulation frequency, and ε is an arbitrary phase. The fluence rate and the photon flux are assumed to have the same form as the source, *i.e.*, a DC part and an harmonically oscillating AC part. The diffusion equation can now be separated into two equations, one steady state and one frequency dependent equation, which can be treated individually. The final result will then be[30]

$$\begin{aligned}\phi(\mathbf{r},t) = {} & \frac{Q_0}{4\pi v D r}\exp\left(-r\sqrt{\mu_a/D}\right) \\ & + \frac{AQ_0}{4\pi v D r}\exp\left\{-r\left(\frac{v^2\mu_a^2+\omega^2}{v^2D^2}\right)^{1/4}\cos\left[\frac{1}{2}\tan^{-1}\left(\frac{\omega}{v\mu_a}\right)\right]\right\} \\ & \times\exp\left\{ir\left(\frac{v^2\mu_a^2+\omega^2}{v^2D^2}\right)^{1/4}\sin\left[\frac{1}{2}\tan^{-1}\left(\frac{\omega}{v\mu_a}\right)\right]-i(\omega t+\varepsilon)\right\},\end{aligned} \tag{2.66}$$

where r is the distance between the source and the detector. For a non-absorbing medium, this is reduced to

$$\phi(\mathbf{r},t) = \frac{Q_0}{4\pi v D r} + \frac{AQ_0}{4\pi v D r}\exp\left(-r\sqrt{\frac{\omega}{2vD}}\right)\exp\left(ir\sqrt{\frac{\omega}{2vD}} - i(\omega t+\varepsilon)\right) \tag{2.67}$$

From measurements of the phase and the modulation, the optical properties can be derived. A closer examination of this expression reveals that the fluence rate, or photon density, from an harmonically intensity-modulated point source in a

strongly scattering, infinite medium is given by a spherical wave that is attenuated as $\exp(-\alpha r)/r$ as it propagates. The AC component is more attenuated at higher frequencies. Further, the photon density propagates with a constant phase velocity, in contrast short pulses that are being dispersed owing to the different phase velocities of each frequency component. The wavelength of the photon density wave in a non-absorbing medium is

$$\Lambda = 2\pi\sqrt{\frac{2vD}{\omega}} \tag{2.68}$$

and its wave front advances at constant speed

$$V = \sqrt{2vD\omega}\,. \tag{2.69}$$

For a modulation frequency of 1 GHz, and a diffusion length of the order of 1 mm, the wavelength of the photon density wave will be approximately 50 mm, and the speed of the wave front about 10^{10} mm s^{-1}. It can be noted that the wavelength decreases for decreasing diffusion lengths and increasing modulation frequencies. As a result, the spatial resolving power improves with increased scattering. Unfortunately, increased scattering and modulation frequency also increases the attenuation of the diffuse wave.

In the frequency domain, all the restrictions from the time-domain remain. Thus, it is possible to solve the diffusion equation for a homogeneous medium and for a limited number of simple geometries. The boundary conditions can be handled in the same way as in the time domain, by introducing extrapolated boundaries and mirror sources.[31]

The wave properties of the photon density waves have been studied by several groups. Fishkin and Gratton[32] investigated the diffraction of the photon density by a straight edge, while O'Leary *et al.* investigated refraction and found that the photon density waves obey simple relations such as Snell's law.[33] Photon density waves of opposite phase were shown to interfere with each other, a phenomenon that was studied and exploited by Knüttel *et al.*,[34] Schmitt *et al.*,[35] and Chance *et al.*[36] Lindquist *et al.* showed that the interference phenomenon is not dependent on the simultaneous existence of two photon density waves, as classical interference of light, but could also be obtained by adding the detected signal from consecutive measurements.[37] These measurements were performed in the time domain and Fourier transformed to reach the frequency domain. By introducing a time delay before the Fourier transform was performed, one of the curves could be shifted 180° for a chosen modulation frequency. Thus, the same set of measurements could be used to study the interference at virtually any frequency.

The applications of diffuse light measured in the time- or frequency domain will be further discussed in Chapter 3.

2.3 Monte Carlo modelling

A frequently used technique to describe photon propagation in tissue is to perform Monte Carlo simulations. This technique is based on random walk of photons in an absorbing and scattering medium, and is a flexible, yet rigorous, tool for investigations of photon transport. A photon package is injected into the tissue model, and is traced until it exits the tissue or is terminated through absorption. During the simulation, any physical parameter such as the path, absorption position, time-of-flight, *etc.*, can be logged. This tracking is made for a large number of photon packages to yield a statistical distribution of the parameter studied. There are no limitations in tissue geometry or homogeneity. Different layers and inhomogeneities can be included in the simulation. Further, it is not required that the diffusion approximation is valid. The drawback is that substantial computation time is needed to have good statistics, especially if the point of interest is far from the source, and the scattering and absorption is high.

A public domain computer code by Wang and Jacques treats the steady state case for a multi-layered medium,[38] and has been used as is or in a modified version for many investigations. With the original code, it is possible to specify an arbitrary number of layers with different scattering and absorption coefficients, as well as refractive index. The result from the computation includes the specular reflection of the incident light, the distribution of light absorbed within the tissue, and the distribution of the exiting diffuse light.

Initially, a photon package with the weight W enters the tissue. The step size to the next point of interaction, s, is calculated as

$$s = \frac{-\ln(1-\zeta)}{\mu_t}, \tag{2.70}$$

where ζ is a random number between 0 and 1. Once the photon package has taken a step, a fraction of the photon weight is deposited due to absorption. This fraction is calculated by

$$\Delta W = \frac{\mu_a}{\mu_t}. \tag{2.71}$$

The weight of the photon package is reduced by ΔW, and the scattering angle is calculated. The deflection angle is calculated from the Henyey-Greenstein phase function, while the azimuthal angle is given by a new random number. The whole process is now repeated until the photon package leaves the tissue, or the weight is reduced below a threshold. In the latter case, a new random number decides whether the photon package is considered to be totally absorbed, or, in order to conserve energy, if the weight is to be multiplied with a certain factor to continue the random walk.

3. Measurements of tissue optical properties

Several techniques can be used to determine one or more of the optical properties in a scattering medium. Some methods can be used only on tissue samples *in vitro*, while other techniques are applicable to bulk tissue *in vivo*, either with invasive probes, or non-invasively. For thin tissue samples, the amount of absorbed or scattered light can be determined by direct measurements, while for thicker samples indirect measurements are made and the optical properties are calculated by solving the inverse problem. In the following sections, techniques used for non-invasive measurements of the *in vivo* optical properties are presented. The methods are divided into steady-state, time-resolved, and frequency-domain measurements. Some of these techniques have been used in Papers I-IV to determine, *e.g.*, the scattering and absorption coefficient of breast tissue, and to assess the *in vivo* absorption spectrum of di-sulphonated aluminium phthalocyanine, a tumour-seeking photosensitizing agent.

3.1 Steady-state techniques

In steady-state measurements, the light irradiation and detection are either continuous or, if chopped or pulsed, the pulse length is long compared to the propagation time of the photons, which is typically of the order of nanoseconds. The reflected light will, as discussed in Chapter 2, consist of two parts; the specular reflection and the diffuse reflectance. The specular reflection, due to differences in the refractive indices between the tissue and the surrounding medium and on the surface texture, will not be considered in the applications discussed here.

There are two possible entities that can be measured, either the total diffuse reflectance, R_d, or the local diffuse reflectance, $R_d(r)$. The total diffuse reflectance is the fraction of the incident flux that is remitted through the tissue surface. This parameter can be measured by placing an optical integrating sphere on the tissue surface, or by using a distant detector, see Figure 3-1. When $\mu_s > \mu_a$, the similarity principle applies, and there is no significant differences in R_d for tissues with different μ_s and g, but the same value of μ'_s. The diffuse reflectance will then depend only on the reduced albedo, defined as[39]

$$a' = \frac{\mu'_s}{\mu'_s + \mu_a}, \tag{3.1}$$

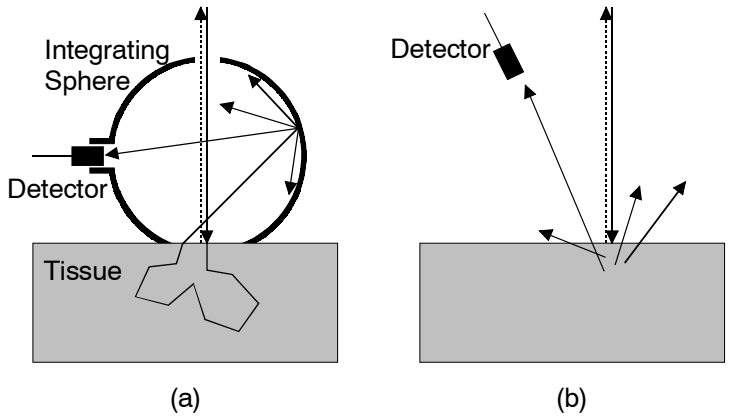

Figure 3-1 Techniques for measuring total diffuse reflectance from tissue. (a) An integrating sphere is used to collect the diffusely reflected light, while the specular reflection (dashed line) exits through the input port. (b) A detector placed at a distance, avoiding the specular reflection, is used to measure a fraction of the total diffuse reflectance over an area of the surface.

and the refractive index, *n*. Therefore, it is not possible to separate the scattering and absorbing properties of the tissue. This limits the usefulness of the technique. Assuming that the reduced scattering is constant, it is, however, possible to measure relative changes in absorption coefficient at two wavelengths or dynamically at the same location.

In order to separate the scattering and absorbing properties, another dimension has to be added to the measurement. This can be accomplished by resolving the measurements spatially, *i.e.*, by measuring the local reflectance at a number of distances from a pencil-beam or point source. When the intensity is plotted *versus* the radial distance *r*, the terminal logarithmic slope *S*,

$$S = \lim_{r\to\infty} \frac{\partial\left[\ln\left(r^m R_d(r)\right)\right]}{\partial r}, \tag{3.2}$$

can be shown[40,41] to be proportional to the effective attenuation coefficient μ_{eff}, defined as

$$\mu_{eff} = \sqrt{3\mu_a\left(\mu_a + \mu_s'\right)}\,. \tag{3.3}$$

In Eq. (3.2), *m* is a constant which has been variously cited as ½, 1, or 2, depending on the model used and the distances covered. If the distance is

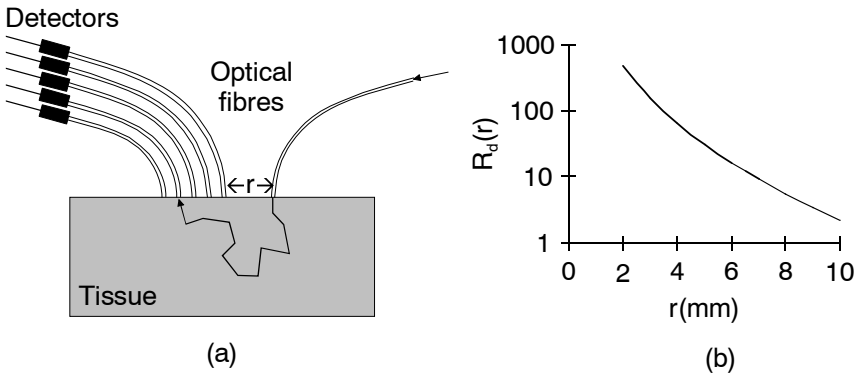

Figure 3-2 Measurements of the local diffuse reflectance. (a) A schematic drawing of a system based on optical fibres. (b) A typical reflectance curve, calculated with the diffusion equation.

considerably larger than the mean free path for scattering ($r >> 1/\mu'_s$), diffusion theory predicts $m = 2$. When the reduced albedo, obtained from the measurements of the total diffuse reflectance, and the effective attenuation coefficient are determined, it is possible to calculate the absorption and reduced scattering coefficients.

The optical properties can also be derived from measurements of the shape of the whole curve.[40,41] Here, a correct handling of the boundary conditions in the model of the reflectance is critical, as discussed in section 2.2.3. The mathematical model, based on the diffusion approximation, is fitted to the recorded data, using the optical properties as free parameters. The advantage of this method is that no absolute reflectance measurements are needed. The accuracy of the optical properties derived from measurements on tissue phantoms has been reported to be of the order of 5-10%.[23,42] A schematic drawing of a fibre-based set-up for the measurement of local diffuse reflectance and a typical signal are shown in Figure 3-2. This type of set-up is relatively inexpensive. Filtered lamps or diode lasers can be used as light sources. If a white light source is used for illumination, and the detected light is spectrally dispersed in an imaging spectrometer, the diffuse reflectance can be obtained for a large spectral region in a single measurement.[43,44] The detection fibres are typically distributed to cover distances up to 10 to 15 mm from the source fibre, and can be placed on a line, on the perimeter of a circle, or as concentric rings around the source fibre. Since the measurement is based on light detection at several distances, this technique is sensitive to variations in the optical properties over the sampling volume. The use of detection fibres in concentric rings averages the diffuse reflectance at each distance, making this probe geometry less sensitive to local variations. To have a more homogeneous

probe volume, distance between the source and detector fibres should be small. For short distances, however, the diffusion approximation is not valid. For better accuracy, Monte Carlo simulations or calibration measurements on samples with known optical properties, can be used for the evaluation. The evaluation can be performed using neural networks[45] or multivariate calibration.[46] Using the latter approach, root-mean-square errors of less than 1% for both the absorption and the reduced scattering coefficient has been reported for simulated reflectance curves.[46]

3.2 Time-resolved techniques

If the transmitted, or diffusely reflected, light from a femto- or picosecond laser pulse is recorded as a function of time, a mathematical model can be used to assess the optical properties. For some applications, such as neonatal brain transmission spectroscopy,[47,48] it might be sufficient to measure the effective optical path length of the detected photons at each wavelength, to be used in the Beer-Lambert law. The average path length can be estimated by determining the average time-of-flight of the photons. In the diffusion approximation, the absorption coefficient can be estimated by the final slope of the time-dependent local reflectance curve, described by Eq. (2.57), as

$$\mu_a = \frac{-1}{v} \lim_{t\to\infty} \frac{\partial}{\partial t} \ln R(r,t). \tag{3.4}$$

The transport scattering coefficient can then be calculated from the time-to-maximum of the reflectance curve.[19] Alternatively, the entire analytical expression can be fitted to the acquired temporal dispersion curve, with the absorption and reduced scattering coefficients as free parameters. This has been proven in a phantom to predict the optical properties with an accuracy of better than 10%.[49] As mentioned earlier, a requirement is that the detection point is located a large distance from the source, and that the scattering dominates over the absorption, *i.e.*, that near infrared light is used. If this is not the case, other evaluation approaches must be considered. Interpolation in a library of curves generated with Monte Carlo simulations have been shown to give accurate results.[50,51]

Several groups have investigated the probing depth for measurements in the backscattering geometry. Bonner *et al.* used a random walk model to show that the maximum depth probed by a photon is approximately proportional to $r^{2/3}$, while the mean depth varies as $r^{1/2}$, for sufficiently large distances, r, between the injection and detection points.[52] These theoretical investigations were confirmed with experiments by Cui *et al.*[53] Feng *et al.* theoretically found that, in the weak

absorption limit, the average probing depth is approximately $\sqrt{2}r/4$.[54,55] Experimental work by Patterson *et al.*[56] gave an average probing depth of $\sqrt{r\delta}/2$, where δ is the light penetration depth, defined as $(D/\mu_a)^{1/2}$. These studies all show that a rather shallow tissue volume is probed when the diffusely reflected light is measured.

We have used the fitting procedure on the data obtained in time- and wavelength-resolved images, using a spectrometer and a streak camera. As a light source very short white-light pulses were used, as described in section 3.4. False colour images of the intensity as a function of both time and wavelength were obtained. Time-dispersion curves were obtained by summing the intensity in a number of wavelength channels; see Figure 3-3. The theoretical reflectance, or transmittance, curve was fitted to the data. In this way the optical properties of breast tissue *in vivo* and *in vitro* were studied (Papers II-III).[57,58] In a single measurement, a wavelength region of approximately 250 nm was covered with a spectral resolution of 3 nm, and a temporal resolution of 30-50 ps. The same technique was also utilized to determine the *in vivo* absorption spectrum of a photosensitizer (AlS_2Pc) in rodent muscle and tumour tissue (Paper IV). Measurements of the diffusely backscattered white light were made in animals with and without injection of the photosensitizer. The scattering and absorption spectra were determined by fitting solutions to the diffusion equation to the data in two ways. In the first evaluation, both the absorption and the reduced scattering coefficients were varied to obtain the best fit. Then, a second evaluation was made by varying a free time-shift and the absorption coefficient, while the reduced scattering coefficient was set to the value obtained in the first evaluation. This latter fitting procedure has been shown to be rather insensitive to variations in the scattering properties, while it significantly improves the precision and accuracy of the absorption coefficient.[59]

The technique described here can, of course, be applied to other objects than tissue. Time-resolved transmittance has been used, *e.g.*, for studies of the optical properties of plant material[60] and paper.[61] For thin samples, such as a leaf, the diffusion approximation is not valid, and it is thus not possible to use the fitting procedure described above. Instead, a library of Monte Carlo simulations was generated and fitted to the data. This approach has given good accuracy in phantom studies.[50,51]

In the following two sections, two detection techniques for time-resolved measurements, time-correlated single-photon counting and the streak-camera recording, are described.

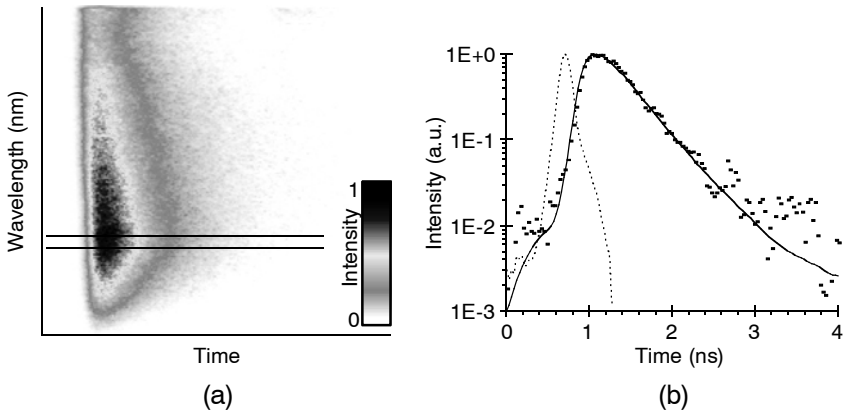

Figure 3-3 A time- and wavelength resolved measurement of light propagation in tissue using femtosecond white light. (a) The intensity as a function of time and wavelength. (b) A time-dispersion curve obtained from an image by summing the intensity in a wavelength band, as indicated in (a). The dashed line corresponds to the impulse response of the system, while the solid line is the model curve fitted to the measured data. (From Paper III).

3.2.1 Time-correlated single photon-counting

Time-correlated single-photon counting (TCSPC) is a commonly used technique for time-resolved measurements of light, for example to determine the life-time of excited states of free atoms and for fluorescence life-time measurements of molecules. It is closely related to the delayed coincidence technique used in nuclear physics for measurements of the decay time of radioactive material. It is a very sensitive technique, as it is based on the detection of single photons. Moreover, it is possible to increase the signal-to-noise ratio by increasing the acquisition time. The idea of the method is to measure the delay between two events, *e.g.*, an excitation laser pulse and the detection of a fluorescence photon, and to repeat this procedure a large number of times. In this way, a statistical distribution of the time delay is obtained. For time-resolved measurements of photon propagation, short (pico- or femtosecond) laser pulses from high-repetition-rate lasers are used to illuminate the scattering medium. A frequently used laser today is the Ti:Sapphire laser, emitting femtosecond pulses at typically 75 MHz. This laser is tuneable in the near infrared wavelength region. Pulsed diode lasers have become available lately, and have been applied to this kind of measurements.[62-64] The detection of the light is performed using a photon counting detector, *i.e.*, a detector that generates one electric pulse for every photon it detects. This pulse and a reference pulse, generated for each laser pulse, are fed to a time-to-amplitude converter

(TAC). The output from the TAC is a voltage pulse with an amplitude proportional to the time between the two input pulses. This voltage is sent to a multi-channel analyser (MCA), which converts the analogue signal to a digital one and adds one count to the channel corresponding to the voltage, *i.e.* the time difference. By repeating this procedure a large number of times, a distribution of the time between a laser pulse and a detected photon is obtained. To obtain a correct statistical representation of the time differences, it is important that the probability of detecting more than one photon per laser pulse is negligible. Otherwise, only the first will be handled by the electronics, leading to a distortion of the distribution. This pile-up effect can be avoided if the probability of detecting one photon per pulse is low, usually less than 1%.

Due to amplitude fluctuations in the signal from the detector, a constant fraction discriminator (CFD) is often used. The CFD is a device that improves the timing by compensating for the amplitude variations. Furthermore, a threshold can be set to reject noise.

A major difference between the TCSPC method and analogue signal processing, is that the temporal resolution is not limited to the width of the detector impulse response, but rather to the transit time spread of the single photon pulses in the detector. The triggering accuracy of the electronic system is another limiting factor. The resulting width of the impulse response of the system is of the order of 30-100 ps. Recently, all the electronics (CFD, TAC, and MCA) have become commercially available on a single computer board, making it realistic to use several detectors simultaneously.

A drawback of this technique is the long acquisition time needed to get a good signal-to-noise ratio. The relatively low count rate can make the sampling time considerable, especially when photon propagation in thick multiple-scattering objects is studied. Moreover, the equipment needed is rather expensive.

3.2.2 Streak camera measurement

Another detection technique allowing measurements in the picosecond range is the use of a streak camera. The streak camera has a better time resolution compared to TCSPC, but is a very expensive device and has a limited dynamic range. It can only be used to detect very weak signals. The technical principle behind the streak camera is similar to that of an oscilloscope, only that it displays the temporal variations of optical, rather than electronic, signals. The light pulse to be measured is focused onto the adjustable entrance slit of the streak camera. This slit is then imaged onto a photo cathode. When a photon hits the photo cathode,

an electron is emitted and accelerated by a high voltage towards a phosphorus screen. A rapidly rising voltage, synchronized with the incident light pulse, is applied transversely across the direction of acceleration to deflect the electrons. The deflected electron beam is amplified in a microchannel plate before hitting the screen. An image is created on the screen, where one axis corresponds to the entrance slit and the other to time. Finally, this image is captured by a CCD camera, controlled by a computer. The streak camera can be used in two different modes; single shot or synchroscan. In the single-shot mode, signal is collected from one laser pulse. This results in a high temporal resolution, of the order of 1 ps, but low dynamic width. To achieve a better signal-to-noise ratio, it is possible to accumulate light from several laser pulses. This will, however, result in a worse temporal resolution (20-50 ps) due to internal jitter in the camera. Furthermore, this is possible only for lasers having a repetition rate of less than 1 kHz. For high repetition rate lasers, the synchroscan mode can be used. An internal oscillator in the camera is phase locked to a reference signal from the laser. The deflection sweep is then driven by the sinusoidal signal from the oscillator. The signal is accumulated from several laser pulses. Due to the synchronization of the light source and the detector, a better temporal resolution (approximately 10 ps) is obtained, compared to the accumulation of single shots.

The streak camera has, like the TCSPC system, been widely used for investigations of tissue and tissue-like phantoms.[48,65-67] The output from a streak camera is an image of the entrance slit, a one-dimensional image, as a function of time. This dimension can be used as a wavelength axis for simultaneous time-resolved measurements over a large wavelength region, as described in section 3.2. Another possibility is to use this axis to study the spatial variations over a line, and through a single scan in the transverse direction a full image can be obtained.[68] One major disadvantage of streak cameras compared to other time-resolved techniques is the high cost.

3.3 Frequency-domain techniques

The measurements previously described in the time domain have their equivalents in the frequency domain, which can be reached through the Fourier transform; see section 2.2.4.

From measurements of the phase shift and demodulation of the detected light, the optical properties can be determined. Patterson *et al.* applied the Fourier transform on the expression in Eq. (2.63), resulting in analytical expressions for the phase and modulation.[27] From measurements of these two parameters, the absorption and reduced scattering coefficients can be determined. Fishkin *et al.* derived

expressions for the phase, and AC and DC amplitudes versus the distance in an infinite medium, and confirmed them experimentally.[29] Similar expressions were also presented by Tromberg *et al.*[69]

For frequency-domain measurements, instrumentation is available at a lower cost than for time-resolved systems. The modulation is made in the frequency range (MHz to GHz) where equipment has been developed for radio applications. Diode lasers, available at low cost, are easily amplitude modulated. For the detection, relatively cheap photo diodes or photomultiplier tubes can be used.

3.4 White light generation

For time-resolved absorption or scattering spectroscopy, a tuneable light source, such as a dye laser, is usually used. This requires sequential recordings as the wavelength of the light is scanned. An alternative possibility, that we have used in Lund, is to create sub-picosecond white light pulses through self-phase modulation of the refractive index in water. Self-phase modulation is the frequency broadening of an optical pulse due to the non-linear part of the refractive index of the medium.[70] Consider an optical pulse

$$\begin{aligned}\tilde{E}(z,t) &= \tilde{A}(z,t)\exp\left(i\left(\omega_0 t - kz\right)\right) + \text{c.c.} \\ &= \tilde{A}(z,t)\exp\left(i\left(\omega_0 t - \frac{n\omega_0}{c}z\right)\right) + \text{c.c.}\end{aligned} \tag{3.5}$$

that propagates through a medium. Here, c.c. denotes the complex conjugate. A non-linear refractive index can be expressed as

$$n(z,t) = n_0 + n_2 I(z,t), \tag{3.6}$$

where

$$I(z,t) = \frac{n_0 c}{2\pi}\left|\tilde{A}(z,t)\right|^2, \tag{3.7}$$

is the intensity of the electromagnetic field. Further, assume that the medium can respond instantaneously to the pulse intensity, and that the non-linear medium is sufficiently short that no reshaping of the pulse occur within the medium. The electromagnetic field at the end of the medium ($z = L$) will then be

$$\tilde{E}(L,t) = \tilde{A}(L,t)\exp\left(i\left(\omega_0 t - \frac{n\omega_0}{c}L\right)\right) + \text{c. c.} \tag{3.8}$$

$$\tilde{A}(L,t)\exp\left(i\left(\omega_0 t - \frac{n_0\omega_0}{c}L - \frac{n_2 I(L,t)\omega_0}{c}L\right)\right) + \text{c. c.}$$

If the slowly varying envelope approximation is assumed to be valid, *i.e.*, that the amplitude does not change considerably during one optical period, the phase of the transmitted pulse will be

$$\varphi = \varphi_L + \varphi_{NL} = \omega_0 t - \frac{n_0\omega}{c}L - \frac{n_2 I\omega_0}{c}L, \tag{3.9}$$

where the indices L and NL represent the linear and non-linear parts, respectively. The frequency is of the field is obtained as the time-derivative of the phase, and will consequently vary during the pulse as

$$\omega(t) = \frac{d\varphi}{dt} = \omega_0 - \frac{n_2\omega_0 L}{c}\frac{dI}{dt}. \tag{3.10}$$

The rapid change in intensity will lead to a spectral broadening of the transmitted pulse. Figure 3-4 illustrates a Gaussian pulse, and its variation in instantaneous frequency, assuming that n_2 is positive. It can be seen that the leading edge of the pulse is shifted to lower frequencies, while the trailing edge is shifted to higher frequencies. This effect was first studied in the late 1960's by several groups,[71-74] and a more extensive presentation of theoretical and experimental work can be found elsewhere.[75]

To produce white light pulses, we have used the high-power laser facility in Lund.[76] Near-infrared light pulses (792 nm, 150 fs, 10 Hz) with a pulse energy of

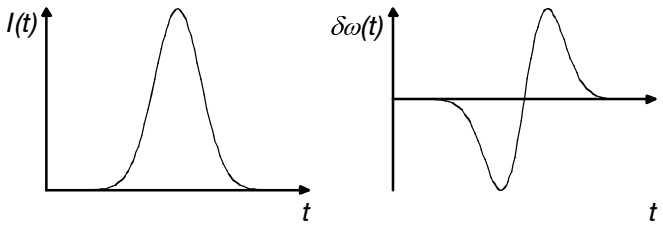

Figure 3-4 (a) Time dependence of the incident pulse. (b) Change in instantaneous frequency of the transmitted pulse.

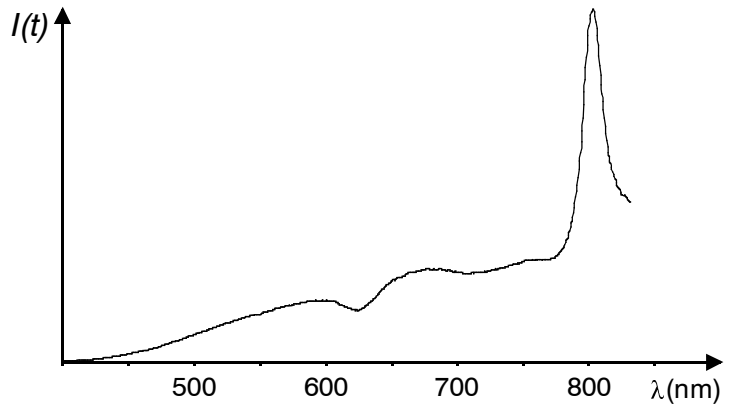

Figure 3-5 A spectrum obtained from self-phase modulation of a near-infrared high-power laser pulse focused into water. The dip at about 630 nm is due to the inverse Raman effect.

2-5 mJ were focused into a cuvette filled with water. According to the theory of self-phase modulation, outlined above, the transmitted pulses were spectrally broadened to cover the whole visible and near-infrared part of the spectrum. The anti-Stokes part of a typical supercontinuum spectrum can be seen in Figure 3-5. The dip in the spectrum around 630 nm is due to inverse Raman effect,[77] that will appear at approximately 3400 cm^{-1} in pure water.

3.5 Breast cancer

Breast cancer is the most frequent malignant tumour in women in the Western part of the world today. It is also the most common cause of death among women aged 40 to 54. In 1996, breast cancer accounted for 27% of all cancers in women in Sweden.[78] About 8% of the female population in Sweden will suffer from the disease during their lifetime. The earlier the tumour is detected, the better are the chances for a successful treatment. Most tumours are detected by the women themselves by palpation. In order to find more tumours at an early stage, various screening programs are employed. The most commonly used diagnostic technique for breast tumour detection today is mammography, which has proved to be efficient for the detection of breast cancer. There are, however, problems in interpreting the images produced, due to the variability of the structure and density in both tumours and healthy tissue. The skill of the interpreting physician is an important factor in finding tumours. Anyway, about 7% of all tumours in all women are not seen on a mammogram. The corresponding number for women aged below 50 is 22%.[79]

Conventional mammography is based on differences in the absorbance of X-rays transmitted through the breast. Being ionizing radiation, X-rays are associated with a risk of inducing cancer. This risk must be considered, especially in regular screening of large populations, such as mammography. It has been shown, that persons heterozygous for the ataxia-telangiectasia (AT) gene, who make up about 1% of the U.S. caucasian population, have an excess risk of cancer.[80] The risk is specially high for female breast cancer, and heterozygotes may constitute 9 to 18% of all persons with breast cancer in the same population. Moreover, the AT-gene is associated with unusual sensitivity to ionizing radiation. Persons homozygous to for the AT-gene, with an world-wide incidence of about 1 to 3 in 100 000, suffer from balance disorders, a depressed immune system, a high risk of blood cancer, and acute sensitivity to ionizing radiation.[81,82] Another potential risk with mammography is caused by the compression of the examined breast. Some physicians claim that this might lead to a spreading of the cancer cells, which might induce metastatic tumour growth.

A number of other techniques have thus been developed to improve the possibility to detect breast cancer without using ionizing radiation. Thermography has been proposed to detect the increased temperature due to the higher metabolism in tumours. This method is, however, not specific for cancer, but also detects acute inflammatory diseases. Ultrasonography can be used to detect differences in the acoustic impedance between tissues. With this technique, it has been shown to be difficult to differentiate between benign and malignant tumours. The difference in acoustic properties between fat and connective tissue also makes the interpretation difficult.[79] Measurements of the skin-surface electropotentials have been used in a European multi-centre study to distinguish between benign and malignant tumours with some success.[83] The best result was obtained in women with palpable lesions.

The use of low energy photons, especially in the near-infrared wavelength region, is another field of research that has attracted much interest. This field will be presented in the next section.

3.6 Diaphanography, transillumination, and optical mammography

3.6.1 Continuous wave techniques

The use of visible light for transillumination of the breast was first suggested in 1928 by Ewing and Adair of the Breast Clinic Memorial Hospital in New York. One year later, the first clinical results using light transmitted through the breast was reported by Cutler at the same hospital.[3] He used a strong lamp for

illumination, and made direct observation of the breast in a darkened room. Blood and solid tumours appeared opaque, while fat was found to be highly translucent. The technique was, however, impractical and the diagnostic value was limited. Some improvements of the light source were performed from 1950 through the 1970's, and photographic recordings using ordinary colour film were added to the detection. Filtered lamps permitted the use of higher intensities at the useful wavelengths. The trechnique was termed diaphanography or diaphanoscopy. Ohlsson *et al.*[84] introduced highly IR-sensitive film for the detection. They reported good screening results with this technique, but this was not verified by others. The photographic film was replaced by IR-sensitive vidicon tubes for detection, and false-colour images were generated from the light detected in the different wavelength bands. This technique was termed telediaphanography or lightscanning.[85-87] Some major limitations to this technique was, however, the difficulty to distinguish between malignant and benign lesions and a poor spatial resolution, especially if the lesions were located more than 2 cm below the surface.[85] The lightscanning technique has in several studies been shown to be inferior to ordinary X-ray mammography for tumour detection.[79,88,89]

Recently, a prototype for CW optical transillumination has been developed at Philips Research Laboratories, Eindhoven, the Netherlands.[90] The person investigated is lying on a table with the breast freely pending in a 130 mm diameter cup. The cup is filled with a fluid to be able to use a fixed geometry without inducing mismatches in the refractive index. In the wall of the cup, 255 source fibres and 255 detectors are mounted. Laser diodes at three wavelengths (670, 780, and 920 nm) are sequentially switched into the source fibres. The light is detected for all combinations of sources and detectors, a procedure that takes less than two minutes per wavelength. Tomographic calculations are then performed to get an image of the light attenuation coefficient in the breast.

3.6.1.1 Time-resolved techniques

Various techniques to improve tumour detection using light have become feasible with the rapid development within optics and electronics during the last decades. One possibility to perform enhanced imaging in tissue is to use a technique called time-gated viewing, in which only the first photons arriving in a short time window are detected. These early photons are the least scattered, and thus had a shorter and straighter path through the tissue. As a result, more information about the spatial localization of an embedded optical inhomogeneity can be obtained. Time-gated viewing was first theoretically proposed by Maarek *et al.*, who used Monte Carlo simulations to show an improved contrast.[91] The first *in vivo* results using time-gated transillumination were presented by Berg *et al.*[92,93] In this work a linear scan over a hand showed a clear demarcation of the bones in the hand.

Photons that are not scattered in the tissue are sometimes referred to as ballistic photons.[94] These photons are attenuated according to Beer-Lambert's law and would thus give a good resolution in a transillumination image. Ballistic photon detection is, however, not possible in thick biological tissues, such as the breast or the brain. For a 5 cm thick tissue with a typical scattering coefficient of 100 cm^{-1}, the fraction of true ballistic photons would be $e^{-500} \approx 10^{-217}$. In the visible wavelength region, 1 J corresponds to approximately 10^{18} photons. Thus, 10^{199} J are needed to detect one ballistic photon, which is unrealistic. Consequently, time-gated imaging must rely on scattered photons, and the idea of the gate is to only record the quasi-ballistic photons. The number of quasi-ballistic photons in an early time-gate is largely influenced by the scattering properties of the tissue, while the late arriving photons are more sensitive to absorption.[62,95,96] Thus, the use of early time gates for optical mammography would mostly be based on the detection of variations in the scattering. Experimental work has shown differences in the reduced scattering coefficient between normal breast tissue and tumour tissue[62,97] (Paper II).

In time-gated viewing, only a very small fraction of the photons arriving at the area of detection are detected, as most of them arrive too late to fall inside the time gate. However, in many experimental set-ups used for time-gated viewing, all photons are recorded anyway. Thus, it is possible to use all the information obtained from the temporal distribution. One approach would be to map the absorption and transport scattering coefficients, obtained by fitting solutions of the diffusion equation to the data, for different points in a scan. This is feasible, *e.g.*, for a breast compressed between two plates. Cubeddu *et al.* have proposed the use of this method to map out differences in scattering properties, while integrating the late-arriving photons to evaluate the variations in absorption.[98] For imaging purposes, some kind of tomographic reconstruction of the diffuse light for a number of light sources and detectors is needed. Arridge and Hebden recently reviewed different image reconstruction approaches.[99]

Some tomographic systems based on time-resolved detection have been constructed. Delpy and collaborators at the University College, London, have constructed a system for imaging of the female breast or neonatal head.[100] The system, known as MONSTIR (Multi-channel Opto-electronic Near-infrared System for Time-resolved Image Reconstruction), uses pulses (1 ps) from a Ti:Sapphire-laser that are sequentially switched into 32 different optical source fibres. The diffusely transmitted light is simultaneously collected with 32 other fibres, and detected by microchannel-plate photomultiplier tubes, using time-correlated single photon counting. This results in a data set consisting of 1024 time-dispersion curves, that are processed using an diffusion approximation model based on the

Finite Element Method (FEM). More information on this system and the image reconstruction algorithms used can be found on the Internet.[101]

Another TCSPC system has been constructed by Chance and collaborators at the University of Pennsylvania. Here, the light sources used are two pulsed laser diodes (780 and 830 nm, 50 ps, 5 MHz) that are multiplexed into the same fibre. The excitation light can then be switched into any of 24 source fibres. The detection side consists of eight parallel TCSPC-channels. This instrument has been used to monitor changes in blood oxygenation in the primary motor cortex area of the brain for functional imaging,[63] and together with magnetic resonance imaging (MRI) for breast imaging.[64]

One commercial system, not much presented in the literature, has been constructed by Imaging Diagnostic Systems, Inc., Plantation, Florida. It is based on what they call computed tomography laser mammography (CTLM), using time-gated viewing. Clinical studies have been approved by FDA, and are ongoing.[102]

3.6.1.2 Frequency domain

The first *in vivo* images using a frequency domain system were recorded by Gratton *et al.* in 1993.[103] Laser pulses from a cavity dumped dye laser (690 nm) were incident on a hand. The diffusely transmitted light was detected with a cross-correlation, or heterodyne, technique. This means that the gain of the detector is modulated at a slightly different frequency, with a beat frequency of 40 Hz. A two-dimensional scan of the source and the detector was performed. The data were presented in three images, representing maps of the intensity, phase, and modulation in each pixel. The authors claimed that the bones and blood vessels could be imaged with a spatial resolution of the order of a millimetre.

In 1994, Madsen *et al.* presented a portable, high-bandwidth frequency-domain instrument for photon migration studies.[104] A vector network analyser, usually used to measure reflection and transmission characteristics of devices and networks, was used to sweep the modulation of laser diodes from 300 kHz to 1 GHz. This instrument has been used to investigate the optical properties of breast tissue *in vivo*. Several investigations have been performed using four different wavelengths, 674, 811, 849, and 956 nm.[105-107] The absorption coefficients obtained for the different wavelengths can then be used to calculate the haemoglobin concentration (total, oxy-, and deoxy- forms), oxygen saturation, and water content. By the addition of another laser diode (915 nm), the fat content can also be estimated.[108]

Some industrial companies have constructed frequency-domain breast imaging devices. Clinical trials have been performed using prototypes developed at Carl

Zeiss and Siemens, both in Germany. The system developed at Carl Zeiss is briefly described by Kaschke *et al.*,[109] and is based on frequency-modulated (>100 MHz) laser diodes at about 690 and 810 nm. The light is detected by a photomultiplier tube. As in a conventional X-ray mammograph, the breast is compressed between two plates, to a maximum thickness of 6 cm. Data are obtained through a collinear scan of the source and the detector over two dimensions, leading to a measurement time of 3-5 minutes. Images acquired with this system were also presented by Fantini *et al.*[110] The specifications of the system built at Siemens, and the results from clinical trials have not been widely published.

A review of the instrumentation and techniques involved in various systems for phase measurements of absorption and scattering in human tissues was recently published.[111] Apart from those described above, a large variety of other detection schemes have been proposed for imaging of scattering media, such as tissue. Reviews of these techniques can, for example, be found in Refs. (112-113).

4. Tumour-selective photosensitizing compounds

Tumour selective agents can be used both as an aid for localization and characterization of various diseases, and for treatment. For tissue characterization, fluorescent tumour markers have been used, mainly in oncologic applications. A fluorescing agent is administered, usually by intravenous injection. During a certain time, the substance will selectively accumulate in malignancies. The fluorescence of the agent, often in the red wavelength region, can be detected following low-power irradiation in the UV or near-UV part of the spectrum. For therapy, the agent is administered and irradiated with higher energies and, frequently, at longer wavelengths than is the case for fluorescence measurements. The light will then trigger a photochemical reaction, leading to a selective cell death. This is the principle of photodynamic therapy, and in this context the tumour-selective compound is known as a photosensitizer. The most commonly investigated photosensitizers also have fluorescing properties. This allows convenient *in vivo* monitoring of the accumulation of the photosensitizer and the progress of the therapy. On the other hand, not all photosensitizers are suitable for purely diagnostic purposes due to an induced long-term photosensitivity. Work has also been performed to develop fluorescent tumour markers without any photosensitizing properties. Within the literature, the term photosensitizer is often used also when only the properties of a fluorescent tumour marker is of concern. In the following, the discussion will mostly concern photosensitizers, all also having fluorescent properties. The term fluorescent tumour marker is used when the compound is used for fluorescence-based diagnostic purposes only.

4.1 Commonly used photosensitizers

A variety of compounds have been investigated in the search for the ideal photosensitizer. There are several properties that are of interest. A high degree of selective accumulation of the photosensitizer to malignant tissue is desirable, in order to only destroy tumour tissue. Next, a high quantum yield for singlet oxygen generation is favourable for an efficient treatment. This also requires a good tissue penetration of the treatment light, which preferably should be in the near infrared wavelength region. A destruction of the photosensitizer through photobleaching is also advantageous. This helps saving the normal tissue, where the available photosensitizer concentration is low. The PDT effects may thus be below the damage threshold, also for high light doses. Another important aspect is that the accumulation and clearance times are short, to minimize a general skin photosensitivity. This can also be accomplished by local application of the

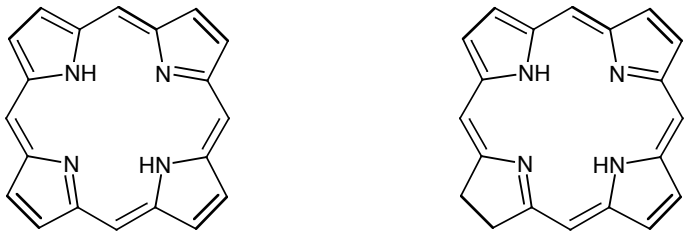

Figure 4-1 The main cores of the porphyrin and chlorin structures, respectively. The difference between is that for chlorins at least one double bond in the pyrrole rings is reduced to a single bond.

photosensitizer, *e.g.*, by topical application on skin tumours. For topical applications, a good tissue penetration of the compound is needed.

4.1.1 Porphyrins

Porphyrins make up a group of molecules based on the chemical structure shown to the left in Figure 4-1. The photosensitizing properties and tumour selective accumulation of haematoporphyrin were investigated in the first half of this century (see section 5.1). Porphyrins have a strong absorption peak at about 400 nm (the Soret band), and a number of minor peaks at longer wavelengths, up to about 630 nm. The fluorescence is characterized by a dual-peaked emission in the red wavelength region, at about 630 and 700 nm. Substantial pre-clinical and clinical investigations have been performed with Photofrin. Photofrin is a partially purified form of haematoporphyrin derivative (HpD), which in turn is obtained from preparations of haematoporphyrin with acetic and sulphuric acid. It consists of a mixture of several porphyrins, monomers as well as dimers and oligomers. The first health agency approval for PDT with Photofrin was obtained in Canada in 1993 for prophylactic treatment of bladder cancer. Since then, further approvals have been obtained in the United States, Japan, and some countries in Europe.[114] Photofrin is, however, associated with a long-lasting skin phototoxicity, making it less attractive for clinical use.

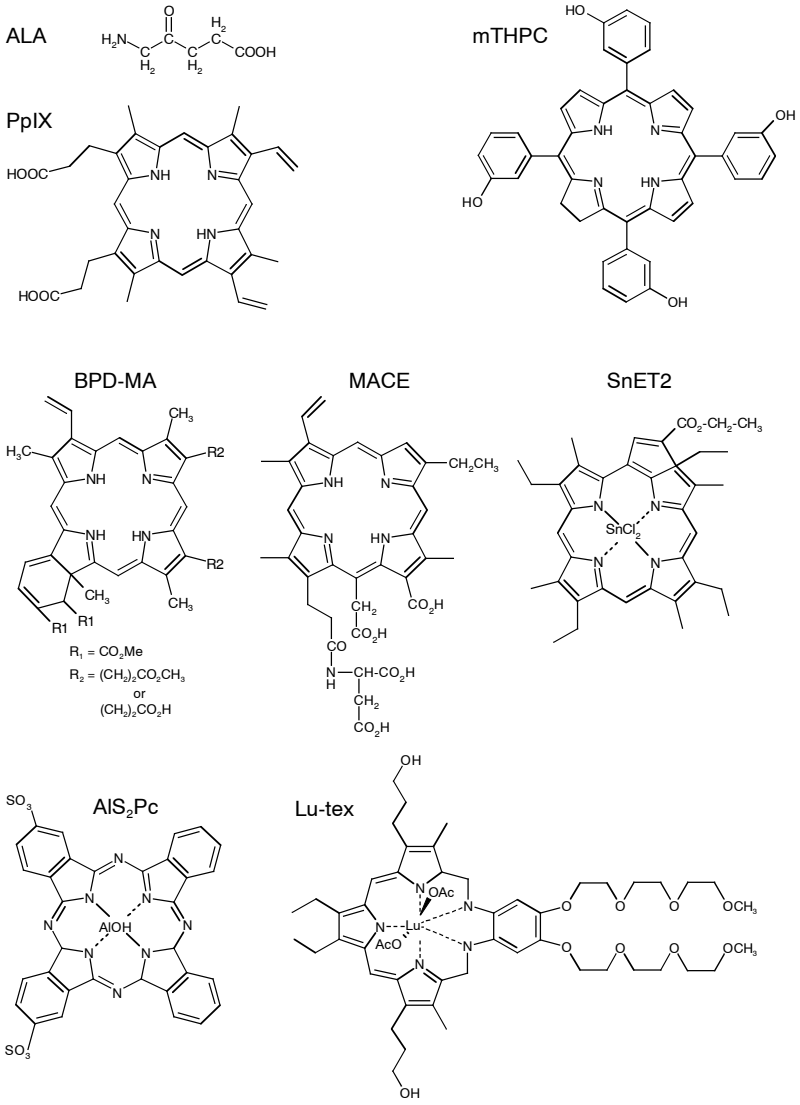

Figure 4-2 The chemical structures of some molecules used for photodynamic therapy and fluorescence investigations. The molecules are ALA, δ-aminolevulinic acid; PpIX: protoporphyrin IX; mTHPC: meso-tetra hydroxyphenyl chlorin; BPD-MA: benzoporphyrin derivative-monoacid ring A; MACE: mono-aspartyl chlorin e_6; SnET2: tin etiopurpurin; AlS_2Pc: di-sulphonated aluminium phthalocyanine; Lu-tex: lutetium texaphyrin.

During the last decade, δ-aminolevulinic acid (ALA) induced protoporphyrin IX (PpIX) has become a widely used photosensitizer. In contrast to other photosensitizers, PpIX is synthesized within the cells following administration ALA. The properties of ALA and PpIX will be discussed in more detail in section 4.2.

4.1.2 Chlorins

Chlorins are reduced porphyrins, *i.e.* one or more double bonds in the pyrrole rings are reduced to a single bond (Figure 4-1). One major difference between the two groups is that chlorins have the strongest absorption peak in the red part of the spectrum (640-700 nm), which gives the compound a green colour.[115] One well-known member of this group of molecules is chlorophyll. Several chlorins have been investigated as possible photosensitizers for PDT. One of the most active of all photosensitizers studied so far is *meso*-tetra hydroxyphenyl chlorin (mTHPC, Foscan). Both the drug and light doses needed for a successful treatment is one order of magnitude lower than for Photofrin.[114] Presently, mTHPC is undergoing clinical trials for head and neck cancer.

Benzoporphyrin derivative-monoacid ring A (BPD-MA) is, despite the name, a photodynamically active chlorin, synthesized from protoporphyrin.[116] It has a strong absorption maximum at 690 nm, and a single fluorescence peak at 700 nm.[117] The accumulation is rapid, peak levels are reached at 3 hours post injection, and 50-60% remains after 48 hours.[118] BPD-MA has gained most interest in the treatment of age-related macula degeneration, which is a common cause of blindness in elderly people. With PDT, the leaky vessels of the retina can be closed without damage to the overlying retinal tissue.

Chlorin e_6 is a compound derived from chlorophyll-a. The absorption spectrum is similar to that of haematoporphyrin, with a Soret band at 400 nm and three or four Q-bands ranging from 500 to 670 nm. The fluorescence spectrum contains only one peak, which is centred at about 670 nm. Various derivatives, including mono-L-aspartyl chlorin e_6 (MACE, NPe6) and di-aspartyl chlorin e_6 (DACE), have been used for PDT, *in vitro* as well as *in vivo*. NPe6 is undergoing clinical trials in Japan for treatment of endobronchial lung cancer.[114]

Yet another chlorin sensitizer is tin etiopurpurin (SnET2, Purlytin). This agent is in phase II clinical trial for cutaneous metastatic breast cancer and Kaposi's sarcoma.[114] The wavelength used for PDT with SnET2 is around 660 nm. Some problems with photosensitization one or more months after treatment have been reported.

4.1.3 Phthalocyanines

Phthalocyanines have been subject for much research, being photosensitizers with some attractive qualities. The absorption spectrum reveals a single peak in the red wavelength region (670-690 nm). The absorption in the UV and blue part of the spectrum is low, resulting in a lower cutaneous photosensitivity. The fluorescence spectrum exhibits a single peak at about 700 nm.

The properties of phthalocyanines can be altered in two ways. Firstly, various metal ions can be chelated into the centre position of the ring structure. The choice of metal ion affects the fluorescence quantum yield, the triplet yield, and the triplet lifetime. The use of aluminium results in a highly fluorescent compound (AlPc) with high photosensitizing ability, while a substitution by a copper ion (CuPc) will eliminate these properties. Secondly, the water solubility can be enhanced by increasing the degree of sulphonation. Crude phthalocyanine is insoluble in water, while the substitution of four sulphonic groups (SO_3) results in a water-soluble tetrasulphonated phthalocyanine.

4.1.4 Texaphyrins

Texaphyrins are a new class of porphyrin-like photosensitizers, consisting of an expanded aromatic macromolecule with complex large metal cations. These compounds have a high absorbance peak in the near-infrared, 730-770 nm. One dye belonging to this group is lutetium texaphyrin (Lu-tex, LUTRIN). The absorption spectrum of Lu-tex exhibits a major peak at 470-480 nm, depending on the solvent, and also a strong peak at about 730 nm.[119] The long-wavelength absorption peak allows the treatment of thicker lesions, due to the increased penetration of light at these wavelengths. Potentially, it could also be used in the treatment of pigmented lesions, such as melanomas. Furthermore, the drug has been reported to be highly selective for malignant tumours versus normal tissue.[119]

4.1.5 Comparison of different sensitizers

As mentioned above, several factor must be taken into account when comparing different photosensitizers for PDT. The intrinsic efficiency of a photodynamic process can be quantified by a parameter (α) defined as the singlet oxygen generation rate [M s^{-1}] per unit incident power [mW cm^{-2}] at the irradiation wavelength λ [nm], per unit sensitizer concentration [M]. An expression for α in terms of measurable quantities is

$$\alpha = 1.925 \times 10^{-5} \lambda \Phi_{\Delta} \varepsilon_s , \qquad (4.1)$$

where ε_s [M^{-1} cm^{-1}] is the sensitizer extinction coefficient. The photodynamic and fluorescent properties of some photosensitizers are given in Table 4-1.

4.2 δ-Aminolevulinic acid

During the last decade, much research activity within the field of PDT and fluorescence investigations have been performed with the photosensitizer pro-drug δ-aminolevulinic acid (ALA). When ALA is administered to living tissue, it takes part in a chain of biochemical reactions, called the haem-cycle, where it will be converted to the fluorescent and photodynamically active compound protoporphyrin IX (PpIX). Studies on the porphyrin biochemistry have earlier been performed in relation to porphyric diseases, and is thus rather well-known. Already in 1956, Berlin *et al.* investigated the pharmacokinetics of radio-labelled ALA in humans and rats.[123,124] In 1987, Malik and Lugaci used ALA-induced PpIX

	PDT			Fluorescence			
Sensitizer	**Φ_Δ (%)[a]**	**λ_{PDT} (nm)[a]**	**α (cm^2 J^{-1})[a]**	**λ_{exc} (nm)[b]**	**λ_{em} (nm)[b]**	**τ (ns)[b]**	**Φ_F (%)[b]**
HP	73	630	30	405	610	13.5	9
HpD				400	610	15.5, 2.5	2-7
PpIX	56	630	110				
PF	89	630	30				<10[c]
Chl-e6	64	662	220	410*	664*	3.7	
BPD-MA	84	687	320	400	690	5.5	10-20[c]
AlS_4Pc	38	673	760	350	675	5.3	30~50[c]

[a]Ref.(120); [b]Ref. (121); [c]Ref. (122)
*MACE

Table 4-1 Photophysical and photochemical properties of some photosensitizers. Φ_Δ: singlet oxygen yield; λ_{PDT}: wavelength used for PDT; α: singlet oxygen generation rate at λ_{PDT}; λ_{exc}, λ_{em}: main fluorescence excitation and emission wavelengths, respectively; Φ_F: fluorescence quantum yield, Hp: haematoporphyrin; HpD: haemato-porphyrin derivative; PpIX: protoporphyrin IX; PF: Photofrin; Chl-e6: chlorin e_6; MACE: mono-aspartyl chlorin e_6; BPD-MA: benzoporphyrin derivative monoacid ring A; AlS_4Pc: tetra-sulphonated aluminium phthalocyanine.

for PDT of cells *in vitro*.[125] The same year, Peng *et al.* studied the uptake of nine different potential sensitizers in tumours and normal tissue of rats and mice.[126] They also tested ALA, and found that porphyrin fluorescence was induced, and that the levels in several normal tissue types was rather low. They concluded that the possibility to use porphyrin precursors in PDT needed to be further investigated. Kennedy and Pottier pioneered the use of topically applied ALA in the treatment of human malignant skin tumours, and published their initial results in 1990 and 1992.[127,128] Since then, the experimental and clinical work of PDT has grown exponentially, evaluated as the number of papers published in the scientific press. In Lund, the first treatments with ALA-PDT took place in 1991, and is now performed on a regular basis at the University hospital.

As mentioned above, ALA is a naturally occurring compound. It is a small straight amino-acid that is neither fluorescent nor photodynamically active. In the first step of the haem biosynthetic pathway ALA is naturally formed from glycine and succinyl coenzyme A. The last step is the formation of haem through the incorporation of iron into PpIX under the action of the enzyme ferrochelatase. All nucleated mammalian cells can produce haem, but cells in a proliferative state are more active in this production. It has been shown that porphobilinogen deaminase, an enzyme catalyzing one of the early steps in the pathway, is more active in some malignant tumours.[129-131] Moreover, ferrochelatase is reported to have a reduced activity in malignancies.[129,130,132-134] As a result, a selective accumulation of PpIX takes place in malignant cells.[135,136] ALA is a hydrophilic molecule that does not easily penetrate intact skin.[127] The keratin layer of the skin is the main barrier for ALA when topically applied. For cutaneous lesions, however, this layer is usually damaged, resulting in an increased penetration of ALA and thus an enhanced selective accumulation of PpIX. PpIX exhibits a strong red fluorescence when excited at its Soret band (approximately 410 nm). The fluorescence spectrum is dual-peaked, with a major peak at about 635 nm, and a smaller peak at approximately 705 nm, see *e.g.*, Papers XII-XIII. The absorption peak in the red wavelength region is at about 635 nm when dissolved in human serum.[137]

Most of the work in fluorescence diagnostics and photodynamic therapy presented in this thesis will be based on topical application of ALA for investigations and treatment of non-melanoma skin malignancies. ALA has several advantages over other photosensitizers. First of all, it is an endogenous substance, associated with low toxicity also when given in excess. It can be delivered intravenously, orally, or topically. The topical application reduces the systemic photosensitivity. For fluorescence investigations, it is possible to give the drug in a low dose, not inducing any detectable fluorescence signal in the normal skin. The accumulation time is rather short, and most of the photosensitizer is cleared within onr or two

days. The main drawback is the small penetration depth of the light at the excitation wavelength (635 nm). For topical application, the drug penetration is also rather low.

4.2.1 Pharmacokinetics and selectivity

The fast clearance is one of the main advantages of ALA-induced PpIX. This also restricts the timing for PDT or fluorescence investigations following the administration. Several investigations have been performed to find the optimal time schedule after systemic or local administration. We have used laser-induced fluorescence to investigate the pharmacokinetics of PpIX in basal cell carcinomas of the skin following topical application of ALA (Paper XII). The first measurements were performed prior to the application, to be used as a reference. New fluorescence recordings were performed two, four, and six hours after the application. The therapeutic irradiation took place immediately after the last investigation. At each occasion, the fluorescence was recorded in scans over the lesion and the adjacent normal skin. It was found that the PpIX fluorescence reached maximum levels earlier for nodular lesions as compared to superficial ones. In the head and neck area, the fluorescence intensities were higher for both lesion and normal skin, compared to other sites on the body. This resulted in a lower tumour-to-normal ratio for facial lesions. Furthermore, the buildup in the normal skin of the face was much quicker than on other parts of the body. These findings are in agreement with the results presented by Tope *et al.*, who studied the pharmacokinetics of PpIX following systemic administration.[138]

Two hours after the treatment, a new set of measurements was acquired. At this time, the PpIX fluorescence had again increased. Both the lesions and the normal tissue demonstrated approximately the same intensity. This phenomenon has been observed earlier[128,139] and it has been suggested to use the newly synthesized PpIX for another illumination period.

On a larger group of patients, the selective buildup of PpIX was investigated (Paper XIII). For these patients, the fluorescence recordings were performed only prior to the application of ALA, and immediately before and after PDT (six hours after the accumulation). Before PDT, a certain level of PpIX could be found also in normal epidermis. The average tumour-to-normal ratio was found to be approximately 2.3:1. Furthermore, the results of the fluorescence investigations were correlated with the treatment outcome. The conclusion was that neither the level of PpIX prior to the irradiation nor the amount of photobleaching during treatment could be used to predict the clinical result. There was, however, a tendency that superficial lesions not completely responding to the treatment

exhibited a higher PpIX-fluorescence prior to the irradiation, compared to the successfully treated ones.

5. Photodynamic therapy

A photodynamic reaction is a chemical reaction involving oxygen which is facilitated by light irradiation. This type of reaction is taken advantage of in photodynamic therapy (PDT). PDT is a modality for local treatment, that has mostly been applied to malignant tumours. The technique relies on the coexistence of three components; a photosensitizer, oxygen, and light. A photosensitizer is a chromophore that is administered to the body, and that accumulates to a higher degree in diseased tissue. After a certain time, depending on the photosensitizing agent being used, the area is irradiated with non-ionizing radiation, usually light in the red wavelength region. A cytotoxic reaction is photochemically induced in the presence of oxygen and photosensitizer, leading to local cell destruction.

Photodynamic therapy offers a number of advantages compared to other oncological treatment modalities. Since photosensitizers that are selectively accumulated in malignant tissue can be utilized, the treatment will also be selective even if a margin of the adjacent normal tissue is irradiated. The healing is relatively fast, and the scar formation minimal, if any. The treatment does not generally require any anaesthesia, provided that the treatment area is easily accessible, and PDT can be repeated an unlimited number of times. Moreover, the cost is moderate and it has minimal hazardous effects on patients or medical personnel. The major disadvantage is the limited penetration of the treatment light and of topically applied photosensitizers, restricting this modality to superficial lesions. For thicker lesions, interstitial light delivery is possible, however. Another drawback is the relatively long elevation in skin photosensitivity associated with several photosensitizers.

Various aspects of PDT is presented in this thesis. The most important work is presented in Paper XI, which reports on a Phase III clinical trial, comparing this treatment modality with cryosurgery for the treatment of basal cell carcinomas of the skin. Laser-induced fluorescence measurements and laser-Doppler perfusion imaging were performed in connection with this study in order to monitor the buildup of the sensitizer and the course of healing (Papers XII-XIV). Pain has been reported to be one of the side effects associated with PDT, and was investigated in Paper X. Furthermore, a comparison was made between a continuous wave light delivery, and various pulse modulated schemes, using two irradiation wavelengths (Paper IX). Paper VII reports on, probably, the first ALA-PDT treatment using a clinically adapted diode laser, emitting light at 633 nm.

5.1 History

Light has been used in the treatment of various diseases since ancient times. In Egypt, China, and India, the beneficial action of the sun on skin diseases without any special photosensitizer was known. Sun exposure was used to treat vitiligo, rickets, psoriasis, and skin cancer.[140,141] About 3000 years ago, the Greeks introduced heliotherapy, a whole-body exposure to the sun, which they claimed to be useful for the restoration of health. In the late 18th century, these ancient forms of phototherapy were rediscovered, and the sun exposure was re-established as an effective therapy for rickets.[142] During the 19th century, phototherapy developed into a science, with the Danish physician Niels Finsen as one of the most important researchers. In 1893 he found that the use of red light in the treatment of smallpox prevented suppuration of pustules. Later he also used ultraviolet radiation from a carbon arc in the treatment of *lupus vulgaris* (skin tuberculosis),[1] a work for which he was awarded the Nobel prize in 1903.

The use of exogenous photosensitizers to improve the efficacy of phototherapy was described already in India's sacred book *Atharva-veda* (1400 BC).[143] Here, detailed descriptions on the use of psoralens (furocoumarins) obtained from the seeds of *Psoralea corvlifolia* were used for the repigmentation of vitiligenous skin. The Egyptians used psoralens from another plant, *Amni majus*, which they used in the treatment of vitiligo around the 12th century AD. In 1974, psoralen dyes activated by UV-A radiation (320-400 nm), were found to be effective in the treatment of psoriasis. Further development has made this treatment modality (PUVA) practical for the treatment of psoriasis, vitiligo, and as a part of immunotherapy.

By the end of the 19th century, the first scientific investigations were performed on photosensitized reactions. An important finding was made by Oscar Raab, a student of Herman von Tappeiner in Munich, when investigating the toxic properties of acridine, a coal tar derivative, to the paramecium.[144] He found that the toxicity varied significantly with the ambient light level. Further experiments confirmed that acridine and light increased the toxicity, while acridine or light alone were not toxic. Raab concluded that the "optical property" of the fluorescence was responsible for the toxicity, and realized that it was not the light itself, but some product of the fluorescence that was active. He also predicted the use of fluorescent substances as therapeutic agents in dermatology.[145] The work of Raab was later taken over by von Tappeiner. He found that oxygen was required for photosensitization, and coined the term photodynamic therapy to describe this phenomenon.[146] Moreover, von Tappeiner was the first scientist to use PDT on patients. He treated nine patients with skin tumours using eosin as a

photosensitizer, and the sun or an arc lamp as a light source.[147] The tumour area was irradiated during a period of several weeks, and improvement was reported.

The photosensitizing properties of haematoporphyrin were discovered in 1908 by Hausman,[148] who reported on destruction of red blood cells, and observed symptoms of sensitized mice. Five years later, Meyer-Betz proved the photosensitizing properties of haematoporphyrin, after injecting himself with the agent.[149] After a few minutes of irradiation, he noticed severe pain and swelling of the light exposed areas, and remained photosensitive for more than two months. In the period between the two world wars, there were two major advances in PDT. Firstly, Policard observed spontaneous fluorescence in experimental tumours illuminated with a Wood's lamp, and concluded that porphyrins selectively accumulate in tumours.[150] Secondly, Auler and Banzer made the first report on photodynamic action involving haematoporphyrin on tumours.[151] They investigated the selective uptake in animal tumours, and initiated some studies on humans, that were interrupted by the Second World War. This work, however, stimulated further studies on accumulation and retention of porphyrins. Figge *et al.*[152] investigated the selective retention *in vivo*, and proposed the use of haematoporphyrin for cancer diagnosis. Further studies confirmed the tumour-localizing properties of haematoporphyrin in a variety of tumours.[153] The therapeutic effect of crude haematoporphyrin was poor. In an attempt to purify this mixture, Schwartz *et al.* found that another porphyrin preparation, haematoporphyrin derivative (HpD), had superior tissue-localizing properties. The first use of HpD in the treatment of a malignant tumour in a patient was reported in 1966 by Lipson *et al.*, who treated a recurrent breast carcinoma with moderate success.[154] In 1972, Diamond *et al.* reported on effective destruction on HpD-sensitized experimental glioma,[155] and three years later Dougherty *et al.* were the first to show long term cures of various tumours in HpD-sensitized rats and mice.[156] Kelly *et al.* studied the selective HpD uptake in malignant and pre-malignant bladder lesions, and reported on one case treated with PDT.[157] The first systematic human trials were performed in 1978 by Dougherty *et al.*[158] They reported on complete or partial response in 111 of 113 cutaneous or subcutaneous malignant lesions in 25 patients, using HpD and a filtered xenon arc lamp. The next major step within clinical PDT, was the introduction of ALA. Kennedy *et al.* reported on the first clinical use of topical ALA in the treatment of skin malignancies in 1990 and 1992.[127,128] Since then, ALA-PDT has been used in a large number of clinical specialities at various places. A review of the clinical research using this treatment modality can be found in Ref. (137). More detailed reviews of the history of PDT can be found elsewhere.[2,159]

5.2 Mechanisms of PDT

The treatment of tumours with photodynamic therapy involves a photosensitizer that is selectively accumulated in the tumour, the subsequent exposure of the tumour to light, and the presence of oxygen. The following presentation will relate to the use of ALA-induced PpIX as a photosensitizer. Most of the discussion will, however, also be applicable to other photosensitizers. When light with a wavelength of about 635 nm is absorbed by PpIX, the molecules will be excited to the first excited singlet state (S_1), also called the Q-band. From here, the molecules can be transferred to the lowest triplet state (T_1). This inter-system crossing is spin-forbidden, but still has a high quantum yield due to the small energy separation. The energy of T_1 is lower than that of S_1, inhibiting the reverse process. The relaxation to the singlet ground state (S_0) is again a spin-forbidden inter-system crossing. The probability for this relaxation is low, leading to a relatively long lifetime (of the order of milliseconds) and thus a high probability for the interaction with surrounding molecules. The reactions involved in PDT are divided into two groups depending on the nature of the reaction. In Type I reactions, the energy of the excited sensitizer is transferred to another molecule via electron transfer or hydrogen abstraction. A Type II reaction is a process where the excess energy of the sensitizer is transferred to oxygen molecules, exciting them from the triplet ground state ($^3\Sigma_g^-$) to one of the first excited singlet state $^1\Delta_g$. Singlet oxygen is very reactive, and acts as an aggressive oxidant on many target molecules, such as proteins, nucleic acids, and phospholipids. The diffusion distance of singlet oxygen in biological tissue has been estimated to be of the order of 0.01 μm, corresponding to a lifetime of about 0.01-0.04 μs.[160] Thus, not only the concentration, but also the subcellular localization of the sensitizer is important for the cell killing efficacy. The amount of oxygen available is, of course, also of great importance. This is further discussed in section 5.5.3.

5.3 Photobleaching and photoproduct formation

When the excited photosensitizer molecule transfers its excess energy in the reactions discussed above, it relaxes to the ground state and can again be excited through light absorption. The photosensitizer might also be oxidized by the singlet oxygen,[161,162] that by definition is generated in the immediate surrounding. This process is called photobleaching or photodegradation. When PpIX is photodegraded during PDT, a new fluorescence peak can be observed at about 670 nm[163] (Papers XII-XIII). The photoproducts responsible for this fluorescence are believed to by of a chlorin type,[162,164] and are also believed to be photodegraded in the same way as the porphyrins.[162,165] One of the major products is photoprotoporphyrin, which is a good photosensitizer, but also a photolabile molecule.[163,166,167] Being a chlorin, it has a relatively strong absorption at about 670 nm.[137,167] Thus, it could be of interest to include irradiation at this wavelength

in the treatment. We investigated the fluorescence of the photoproducts in connection with ALA-PDT (Papers XII,XIII). It was found that the fluorescence intensity of the photoproducts (at 670 nm) after the treatment was only about 2% of the fluorescence intensity of PpIX (at 635 nm) prior to the irradiation. We also found a correlation between the amount of photoproducts and PpIX at the end of the treatment. Thus, probably most of the photoproducts are efficiently bleached away using only light at 635 nm.

5.4 Light sources

The first light source used for phototherapy was, as described above, the sun. During the latter part of the 19th century, the bactericidal effect of the so called "chemical rays" (UV and blue light) was discovered. It was also shown that these chemical rays, and not the heat from the sun, were responsible for the erythema induced by sun light. Finsen realized, from own and others' experiments, that chemical rays also caused scar formation in phototherapy of small-pox. Consequently, he suggested the use of red glass or thick red cloth to exclude this part of the solar spectrum.[1] He, and several other researchers, reported on minimal scarring when using red treatment light. The first PDT treatments, however, continued to use either sunlight, or the white light spectrum of an arc lamp. It was not until 1966 that filtered lamps were being used for PDT in humans. Since then, a number of different light sources have been used in clinical and experimental PDT. Both lasers and non-laser light sources (including light-emitting diode arrays, fluorescent tubes, and arc or incandescent lamps), emitting pulsed or continuous wave light, are being used.

5.4.1 Lasers

Lasers have been considered to be ideal PDT light sources, because of their beam and spectral qualities. The monochromaticity of laser light enables the output to be confined to an absorption band of the photosensitizer at a wavelength with good tissue penetration. Thus, the hyperthermic effects, induced by tissue absorption of the light, can be minimized. Due to the coherent properties, laser light can efficiently be focused into optical fibres. This permits the access to body cavities by guiding the fibre through endoscopes, or interstitial illumination, if the fibre is inserted into the tissue through the lumen of a needle. Much work in PDT, both clinical and experimental, has been performed using industrial or scientific lasers, such as dye lasers pumped by argon-ion or copper-vapour lasers. The advantage of dye laser systems is the possibility to work with different photosensitizers, since the emission wavelength can be virtually arbitrary chosen by selecting the appropriate dye. The drawback is that the dye has to be exchanged on a regular basis to maintain a high output power. Furthermore, the continuous wave argon-

ion laser and the pulsed copper-vapour laser, used to pump the dye laser, need delicate adjustments and frequent service. Moreover, they consume several kilowatts of electrical power, and need extensive water cooling. For work with Photofrin or HpD, the pulsed gold-vapour laser can be an alternative. It operates at 628 nm, and no dye laser is thus needed. Unfortunately, the other drawbacks mentioned above apply also here.

During the last decade, the use of pulsed Nd:YAG (neodymium-doped yttrium-aluminium-garnet) lasers for PDT has increased. By frequency-doubling the infrared light (1064 nm) to green (532 nm), it can be used to pump a dye laser. This configuration is often called a KTP (potassium titanyl phosphate) laser in medical applications, from the name of the crystal used for frequency-doubling. To obtain a good conversion efficiency, the laser is pulsed (approximately 100 ns pulses at a repetition rate of a few kilohertz) and the KTP crystal is usually placed inside the laser cavity. A KTP-dye laser system (Multilase Dye, Technomed International, Bron, France) was installed in Lund in 1991. This system generates green light at a power of up to 20 W that is used to pump a dye laser, emitting up to 2 W of red light (635 nm). A 400 V, 16 A three-phase power outlet is needed, as well as tap water for cooling. The system is mobile, but still large and heavy, and quite expensive. This laser was used for most of our clinical[168,169] (Paper XI) and experimental[170-172] work with ALA-PDT until 1998. Although the KTP-laser is clinically adapted, it is usually rather sophisticated, resulting in high cost, large size, and more or less complex operation. A general opinion is that smaller and less expensive light sources are needed for PDT to be widely accepted. In recent years, compact diode-pumped Nd:YAG and Nd:YLF lasers have become available. These lasers can provide a high output power at the second harmonic, which can be used to pump, *e.g.*, a dye laser.

A diode laser is a very efficient light source, compared to many other laser systems. Usually, it only requires a standard electric outlet. Moreover, the need of cooling water can often be eliminated. It is also possible to make small and easily operated systems, that are considerably less expensive than conventional lasers. This makes diode laser systems suitable for clinical use. Diode laser arrays having up to 100 W of output power at, *e.g.*, 820 nm (GaAs) have been available for some time now. Unfortunately, these wavelengths are not useful for PDT, since most photosensitizers only absorb at shorter wavelengths. Great efforts have been made, both in the development of high power diode lasers at wavelengths matching the absorption band of porphyrin-based photosensitizers (HpD and ALA-induced PpIX) at about 630 nm, and in the development of new photosensitizing agents, that absorb light at longer wavelengths where diode lasers are available. The latter attempt will also increase the treatment depth, since light with longer wavelengths penetrates tissue better. Commercial diode laser systems,

emitting up to 2 W at 635 nm, have been available since early 1998. The Lund University Medical Laser Centre purchased probably the first commercial unit for ALA-PDT (CeraLas PDT635, CeramOptec, Bonn, Germany), which was delivered in January 1998 (Figure 5-1). The maximum power of this system was 1.5 W at a wavelength of 633 nm, emitted from the distal end of a 400 μm core diameter microlensed optical fibre (NA 0.37). The small size and weight of this unit (size: 19×43×38 cm^3, weight: 15 kg), significantly facilitates treatment at different clinics, and even at bed-side. The system is also available with an onboard integrating sphere for calibration, to assure that the correct light dose is delivered. The first patients treated using a diode laser at 635 nm for ALA-PDT are reported in (Paper VII). As could be expected, the clinical result were not significantly different from similar lesions treated with the KTP/dye-laser system used in earlier studies[168] (Paper XI). Similar diode laser systems are now also available from Diomed Inc. (Boston, MA). Various wavelengths are available to match different sensitizers, including 630 nm (for Photofrin), 635 nm (for ALA), 652 nm (for mTHPC), and 730 nm (for Lu-tex).

Another advantage with diode lasers is that they are easily modulated. Thus, different light delivery modes can easily be achieved. Recent cell experiments using pulse-modulated diode lasers have shown both increased[173] and unchanged cell killing.[174] Busetti *et al.* stress the necessity for standardized protocols in these kinds of studies,[174] which is facilitated by the possibility to computer controlled modulation of the light output from diode lasers. In Lund, we have made the first *in vivo* ALA-PDT using a modulated diode laser system (Photo Dynamic Therapy HGesmbH, Vienna, Austria) operating at 652 nm (Papers IX-X).

Other types of laser-based sources are currently under development. Laserpaint™ (Spectrascience Corp., USA) uses a short-wavelength pulsed laser to pump a mixture of a fluorescent dye and a light-scattering material included in disposable discs or optical fibre tips[175] for specific wavelengths. By choosing different fluorescent dyes, it is possible to change the wavelength of the treatment light. Another tuneable light source, now available in a clinical configuration, is the pulsed optical parametric oscillator (OPO).[176]

5.4.2 Incoherent light sources

Different kinds of filtered lamps are commonly used in PDT, and have been shown to be useful for ALA-PDT of skin lesions.[127,128,177-180] These light sources have the advantage of low costs, simple operation, and reasonably small size. On the other hand, their use is limited to superficial illumination. In early ALA-PDT, filtered tungsten filament lamps, such as modified slide-projectors, were used.[127,128,178] These lamps were equipped with filters transmitting light with a

wavelength typically longer than 600 nm. High-pressure lamps, such as xenon-lamps, are now available with a total power of some kilowatts. With appropriate filters adequate amounts of useful light can be obtained. There is, however, a trade-off between spectral bandwidth and output power. Whitehurst *et al.*[181,182] have constructed a tuneable light source, emitting 1 W directly or 0.5 W via a light guide within a 30 nm band, centred at any wavelength between 300 and 1100 nm. The limited bandwidth was chosen to be slightly narrower than the red absorption band of HpD. Other lamps have been presented with a width of the wavelength band ranging from 50 to 130 nm.[177,179,183] The light not matching the absorption band of the photosensitizer will, in general, contribute to an increase of the tissue temperature. In the case of ALA-PDT, some of the light might be therapeutically useful, since one of the photodegradation products of PpIX, photoprotoporphyrin, has an absorption peak around 670 nm and has also been shown to have photodynamic properties.[163,166,167,184]

The output from high-power lamps contains a significant amount of infrared radiation.[185] Peng *et al.* propose that this should be filtered out in order to avoid hyperthermia,[137] although some groups claim that mild hyperthermia (40-42°C) acts additively or synergistically with PDT.[186,187] If hyperthermic effects are to be avoided, fluence rates lower than 150 mW cm^{-2} should be used.[188] Some commercially available filtered lamps for PDT include the infrared light to take advantage of the effect. One such system (VersaLight, Medic Lightech Ltd., Nesher, Israel) has been available in Lund since 1994. This lamp has three different filters, permitting the use of either red (580-720 nm) or green light (520-

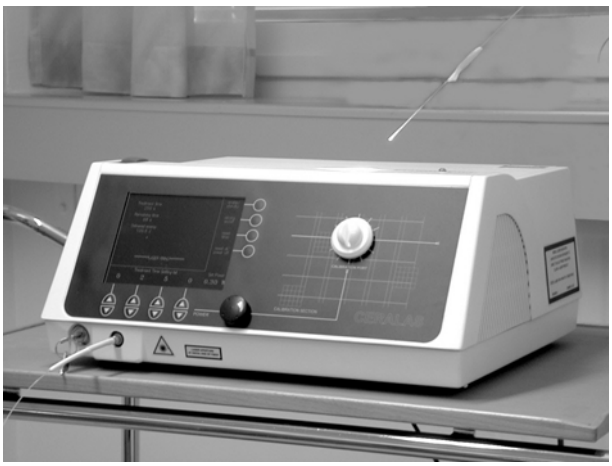

Figure 5-1 A photo of the diode laser used for ALA-PDT in Lund.

590 nm) for PDT, or blue light (380-450 nm) for fluorescence diagnostics. When using the green or red light, additional irradiation is obtained in the IR region (1200-1700 nm). The light is delivered from a light guide in a Gaussian profile. A hand-piece, held in contact with the tissue, defines the 3-cm-diameter illumination spot. The average fluence rate is of the order of 120 mW cm^{-2}. Due to the significant amount of heat generated from the IR light, this occasionally has to be filtered out, *e.g.*, by using a cuvette filled with water. The red light from this lamp has been used for clinical ALA-PDT in Lund, but we have not performed any controlled comparison of the results from laser- and lamp-induced PDT. Recently, progress in lamp design permitted the introduction of light sources based on high-pressure lithium-iodide or neon large-arc lamps.[189] These low-cost units provide very high continuous power levels in a narrow wavelength band.

An alternative light source with a relatively narrow spectral bandwidth, but still possible to make small and inexpensive equipment can be based on light-emitting diodes (LEDs). With LEDs the bandwidth of the light source is typically some ten nanometers, centred around a fix wavelength. The output power is low, but it is possible to construct arrays consisting of a large number of LEDs that can be configured in different shapes for particular applications.[190,191] Applicators have been developed for superficial treatments, such as treatment of skin lesion, interoperative applications, and even for interstitial use. With the general development of solid-state components, LEDs are constantly being developed to give higher output powers at various wavelengths.

Until recently, most PDT sources were designed to be general purpose, allowing the treatment of lesions at various locations, and often with the possibility of using different sensitizers. Lately, systems dedicated to a specific treatment have been developed. One example is a turn-key system with pre-set light dose and built-in calibration, based on blue fluorescent-lamps, designed specially for the treatment of actinic keratosis of the face and scalp using topical ALA-PDT (DUSA Pharmaceuticals, Inc., Toronto, Canada).

5.5 Light delivery

The clinical efficacy of PDT is dependent on a number of parameters, such as the total light dose, the fluence rate, the illumination geometry, *etc.* In the following sections, some of these parameters and their effects on the treatment result will be discussed.

5.5.1 Light dosimetry

The most simple form of light dosimetry in PDT is when superficial lesions, such as skin lesions, are treated. The total light dose is then given as the total light energy density [J cm^{-2}], delivered to the irradiated area. This is calculated as the product of the irradiance, or fluence rate [W cm^{-2}], and the treatment time [s]. This parameter is easily interpreted for monochromatic, or narrow-band, light sources. When comparing the results from treatments with lasers and filtered lamps, equal light dose does probably not give the same response, due to variations in the output from the lamp and the activation spectrum of the sensitizer as functions of the wavelength. Whitehurst *et al.* suggested that the relative biological efficiency (RBE) has to be calculated for evaluating different light sources.[181] The RBE was defined as

$$\mathrm{RBE} = \frac{\int I(\lambda)E(\lambda)d\lambda}{\int I(\lambda)d\lambda}, \tag{5.1}$$

where $I(\lambda)$ is the lamp intensity as a function of wavelength, and $E(\lambda)$ is the action spectrum of the photosensitizer.

For the treatment of non-melanoma malignant skin cancers with ALA-PDT, light doses between 40 and 250 J cm^{-2} for laser irradiation, and between 30 and 540 J cm^{-2} for filtered lamp, have been used.[137] In Lund, the standard procedure has been to use a light dose of 60 J cm^{-2}, delivered at a fluence rate of approximately 100 mW cm^{-2} (Paper XI).[168] Thus, the treatment time is about 10 minutes, which is reasonable for clinical use. The idea behind the choice of the light dose is to illuminate until most photosensitizer molecules are photobleached. This can be monitored on-line by studying the fluorescence, *e.g.*, at the second peak of PpIX (around 700 nm) when ALA is used. We have used point-monitoring LIF spectroscopy to assess the PpIX fluorescence before and after the therapeutic irradiation of basal cell carcinomas. After the full light dose (60 J cm^{-2}), approximately 8-10% of the initial fluorescence intensity remained (Paper XIII). This would thus suggest that further illumination might be beneficial for the treatment outcome.

Several mathematical models for light and drug dosimetry have been presented in order to calculate the depth of necrosis. These models need to include light distribution in the tissue for the illumination geometry used, the concentration of the photosensitizer, and the yield of cytotoxic oxygen. The dynamic behaviour of the optical properties during PDT should also be considered. Finally, the photobleaching and clearance of the photosensitizer from the treated region must be taken into account. Grossweiner published a model where all the quantities

above, except for any changes of the optical properties, were included to determine the depth of necrosis for different illumination geometries.[192]

When topically applied ALA is used, the dosimetry gets even more complicated. The penetration of ALA into the tissue and the subsequent formation of PpIX must then be included in the model. Svaasand *et al.* presented a mathematical expression for the *in situ* cytotoxic dose, as a function of depth.[193,194] The depth at which the dose was reduced by 50%, after an ALA-application time of two hours, was estimated to 3 mm for BCCs. The model does not, however, indicate if this is enough to achieve tissue necrosis.

5.5.2 Wavelength dependence of PDT

When using ALA for PDT, light at 635 nm is often used. This wavelength matches the absorption peak furthest to the red, which allows maximum penetration of the therapeutic light. The absorption is, on the other hand, much higher at the Soret band at approximately 410 nm, where the penetration depth is of the order of 100 μm. Light at this wavelength could thus be used for efficient treatment of very thin superficial lesions. Moan *et al.* found that light at 410 nm could be efficiently used for cell inactivation to a depth of 2 mm in human skin, muscle tissues and BCC lesions, while 635 nm was optimal for larger depths.[184]

To optimize the treatment response, it is important to gain knowledge of the absorption spectrum of the photosensitizing agent. The position of the absorption peak used for PDT is, however, not always the same for the *in vivo* situation as in aqueous solution. When a laser is used for irradiation, it is thus important to choose the right wavelength to get a high photodynamic yield and a maximum tumour-to-normal contrast. With other light sources, such as filtered lamps, it is easier to cover the absorption peak, although much light will not be efficiently absorbed by the photosensitizer, but by the tissue, leading to a temperature increase. Using a laser tuned to the right wavelength, the temperature increase could be kept at a minimum.

The absorption spectrum *in vivo* can be shifted due to the functional state, metabolism, blood perfusion, *etc.* Several researchers have demonstrated that for HpD and Photofrin, the absorption spectrum,[195] the action spectrum,[196,197] and the fluorescence excitation spectrum[198] all have a maximum at 625 nm *in vivo*, as compared to 630 nm for the action spectrum *in vitro*.[199] In contrast to porphyrin-based sensitizers, sulphonated metallo-phthalocyanines exhibit a red-shift of the above mentioned *in vivo* spectra. Griffiths *et al.* have reported an increased PDT-effect when the wavelength of the activating light was increased from 680 to

692 nm, using zinc phthalocyanine tetrasulphonic acid.[200] Similar results have also been reported by Cubeddu *et al.*[201] for AlS_2Pc, where the *in vivo* absorption spectrum peaked at 685 nm, compared to 672 nm for absorption in aqueous solution[202] and cell cultures.[203] Furthermore, Weersink *et al.*[204] found a red-shift to about 680 nm of the absorption peak of AlS_4Pc in rabbit skin. In Paper IV, we have studied the *in vivo* absorption spectrum of AlS_2Pc using time-resolved diffuse reflectance, as described in section 3.2. These measurements also confirmed the red-shift of the absorption peak. This shift was larger in tumour tissue than in normal muscle. We also found that the contrast in the sensitizer absorption between tumour and normal tissue is dependent on both the wavelength and the administered drug dose. Thus, to enhance the selectivity in the treatment, these findings ought to be taken into consideration.

In another study, we have investigated the difference in treatment response of skin lesions using light at 652 nm compared to the standard treatment at 635 nm (Paper IX). The PpIX absorption at 652 nm was estimated to be 63% of that at 635 nm,[137] and the total light dose was increased to compensate for this difference. In spite of that, the response rate was lower when the longer wavelength was used. In connection to the treatments, the sensations experienced by the patients were studied (Paper X). It was found that the more effective treatment using light at 635 nm was accompanied by increased sensations of pain and dysesthesia. The pain can, however, be efficiently reduced by spraying the treated area with water.

5.5.3 Fluence rate effects

A large number of studies have been published on the relationship between the fluence rate and the efficacy of PDT, and were reviewed by Veenhuizen and Stewart.[205] High fluence rates, above 200 mW cm^{-2}, are generally considered to induce a marked hyperthermic effect, and are not discussed in this section. Three studies reported on cell cultures *in vitro* that were incubated with HpD, AlS_4Pc, and Photofrin, respectively. Chinese hamster ovary cells were used in the two former studies, while human lung adenocarcinoma cells (A549) were used in the latter investigation. The fluence rates investigated varied significantly. In the HpD study, no significant differences were found between the different fluence rates (0.5-60 mW cm^{-2}), which could be due to the rather high light fluence. In the two other studies, lower fluence rates were used, and an increased cell killing was found when increasing the fluence rate.

Seven studies, in which the effect of the fluence rate was investigated, were performed on tumour models, using Photofrin (four studies), ALA, benzophenothiazine, and phthalocyanine. The fluence rates used were usually

ranging from 50 to 200 mW cm^{-2}, but in two cases only fluence rates below 100 mW cm^{-2} were considered. In five reports an inverse relation between the fluence rate and the treatments response was found, *i.e.*, a lower fluence rate resulted in a better effect. Calculations by Foster *et al.*[206] indicate that oxygen depletion could occur within 10 s in well-perfused tissues at an incident fluence rate of 50 mW cm^{-2}. In two of the tumour models, no relationship was found between fluence rate and PDT response. This was explained with a good perfusion of the tumour in the model used. In more recent studies an increased tumour response at lower fluence rates was found in experimental tumour models in rat and hamster. The animals were injected with mTHPC[207,208] or Photofrin.[209,210] Sitnik and Henderson observed, however, that lower fluence rates required longer treatment times for equivalent anti-tumour effects; 95 min for 57 J cm^{-2} at 10 mW cm^{-2} compared to 11 min for 100 J cm^{-2} at 150 mW cm^{-2}.[209] Unfortunately, the higher light dose and irradiance also caused a more severe effect in the normal foot, prolonging the healing time from 8 to 30 days, while the lower fluence rate induced longer healing time at equal light dose. Thus, if the tumour response is increased at lower fluence rates and light doses, this would also be favourable for normal tissue. For PDT to be used in the clinical setting, however, the treatment time must for most applications be kept rather short.

The effects on normal tissue were reported for rat skin sensitized with HpD and rodent liver and brain sensitized with Photofrin. No influence of the fluence rate was reported in any of the three studies. Chen *et al.* suggested that normal tissues is less sensitive to variations in irradiance due to a better vascular oxygen supply.[211] This is in concordance with the calculations of Foster *et al.*[206] Recent reports by Robinson *et al.* on the fluence rate effects on normal skin of hairless mice, sensitized with topical ALA and irradiated at 514 nm, contradicts the other reports on normal tissue.[212,213] A seven-fold increase of the PDT damage was found when the fluence rate was decreased from 150 to 5 mW cm^{-2}. At 50 mW cm^{-2} the PDT effect was 2-3 times that obtained with the higher fluence rate. The authors speculate that this could be due to that the oxygenation of the mouse epidermis is dependent on the diffusion of oxygen from the dermis, and that oxygen depletion might occur at high irradiance, reducing the PDT effect.

5.5.4 Pulsed versus continuous wave light

In clinical practice, the laser has so far been the most commonly used light source. As described in section 5.4.1, the lasers used are emitting either continuous wave (CW) or pulsed light, with pulse lengths of a few nanoseconds. The photodynamic efficacy might be affected in two ways by light with a very high peak fluence. Firstly, the photosensitizer might be saturated, leading to a poorer photodynamic

effect. Secondly, the light penetration might be increased due to saturation of the tissue chromophores. The first effect was studied by Pogue *et al.*, who found that pulsed light (10 ns pulses at 10 Hz with a peak-pulse irradiance of 3 MW cm^{-2}) could saturate the optical transitions in the photosensitizer (BPD-MA), resulting in a decrease in the absorption.[214] This effect reduces the PDT effect higher up, but may also allow a deeper treatment effect, since the penetration depth increases. The second effect was studied by LaPlant *et al.*,[215] who showed that the optical penetration depth was not changed at average fluence rates between 50 and 380 mW cm^{-2} from a gold-vapour laser. Several investigations have been performed in order to compare the efficacy of pulsed and the CW light both *in* vitro and *in vivo*. Rausch *et al.* studied the efficacy of two laser systems in the treatment of squamous cell carcinoma subcutaneously implanted in nude mice, using HpD as a photosensitizer.[216] They found that a pulsed excimer-pumped dye laser was at least as efficient as the argon-ion laser pumped dye laser. With similar laser systems, Okunaka *et al.* examined the average depth of necrosis from HpD-PDT in a mouse kidney tumour model. They observed an increase from 4 mm for CW light to 15 mm for the pulsed light for the same total light dose.[217] When HpD is used as a photosensitizer, the pulsed gold-vapour laser, operating at 628 nm, might replace the argon-ion laser pumped dye laser (see section 5.4.1). Thus, several comparisons of these systems have been made. These studies showed no significant differences between the two excitation sources in the treatment of cell cultures, transplantable mouse tumours, virally induced papillomas in rabbits, and in human tumours.[218-220] Similar results were obtained when comparing the frequency-doubled Nd:YAG-dye-laser system with the argon-ion laser pumped dye laser in normal canine oesophagus[221] and transplanted mammary carcinoma in rats.[222] Flashlamp pumped dye lasers, emitting microsecond pulses at repetition frequencies below 20 Hz have also been tested. Pope *et al.*[223] found in a cell study using HpD and green light, that a pulse fluence below 10 mJ cm^{-2} (or a fluence rate of 10^4 W cm^{-2}) probably would be needed to achieve cell death. Bellnier *et al.* treated implanted experimental tumours in mice using HpD and red light at a pulse fluence of 0.25 and 0.13 J cm^{-2} at 4 Hz (corresponding to a fluence rate on the order of 10^5 W cm^{-2}). This resulted in a significant temperature increase, but little PDT effect, which was attributed to saturation of the sensitizer.[224]

A mathematical analysis on the effect of pulsed lasers on haematoporphyrin excitation and singlet oxygen yield was presented by Sterenborg and van Gemert.[225] They concluded that the treatment efficacy for pulsed lasers is identical to that of CW lasers, provided that the peak fluence rate is less than 4×10^4 W cm^{-2}. For higher fluence rates, obtained from lasers with high-energy pulses and low pulse rate, the effectiveness drops significantly. Using 100 ns pulses at a repetition frequency of 5 kHz, *e.g.*, from a KTP-dye laser system as the one previously used

in Lund, at a time-averaged fluence rate of 100 mW cm^{-2}, the peak fluence rate is 2×10^2 W cm^{-2}, which is well below this threshold. This is also the case for the gold-vapour laser, and the dye laser pumped by a copper-vapour laser. Flashlamp pumped dye laser systems, on the other hand, are operating at or above this threshold, due to their high pulse energy and low repetition rate.[223,224]

5.5.5 Fractionated light doses

As mentioned above, the presence of oxygen is essential for the PDT process and thus a reduced fluence rate can be used to minimize the oxygen depletion. An alternative method would be to split the light dose in one or more fractions. This would allow the transport of oxygen to the treatment site during the pauses, to replace the oxygen that was consumed during the irradiation. As a result, the tumour damage might increase. By varying the duration of the light doses and pauses also mechanisms other than oxygen depletion could produce different treatment results. Such mechanisms may be transport of photosensitizer molecules to the treatment region and also redistribution of the drug within the treatment region. In structural models it has been shown that fractionation increases the dose of singlet oxygen to the cells relatively remote from the capillary walls and fractionating the light dose should result in an improved therapeutic ratio for PDT.[226] Various light fractionation schemes for PDT have been investigated, both on cell cultures and on tumours *in vivo*. The light fractions, as well as the time between the fractions, are spanning over large intervals. The dark periods between the irradiations ranges from 24 hours down to less than a minute. Additionally, different studies using millisecond light pulses have been reported as fractionated treatments. The effect of a 24-hour-long dark period between two light fractions on a mouse tumour model was shown to be poorer than that of a single delivery of the same light dose.[227] This may be explained by a decrease in drug concentration due to the long time involved. In an early cell-culture study using haematoporphyrin, Moan and Christensen found an increased cell-killing using two fractions separated by 70 seconds, instead of a single irradiation.[228] Berg *et al.*[229] studied human cervix carcinoma cells incubated with $TPPS_4$ and found that a small initial light dose increased the sensitivity of the cells several hours after the first irradiation. They also found that an optimal time between the two fractions would be between 30 and 90 minutes. For a mouse tumour model sensitized with mTHPC or Photofrin, van Geel *et al.* found that a treatment scheme employing dark periods of one hour between six fractions of light delivery was superior to a single illumination with the same light dose.[207] The use of alternating light and dark periods of 30 seconds improved the tumour response even further for mTHPC, but did not result in any change using Photofrin. During the first fraction some vasoconstriction occurs which relaxes during the first break, permitting re-

oxygenation. This suggests that even a single short interruption of the light may reduce the light dose needed to achieve extensive necrosis. The optimal time for the pause was found to be after 50 seconds of irradiation.[230] Curnow *et al.* studied the area of necrosis in rat colon using ALA and various numbers of equal light fractions, all separated with 150 seconds, and also the influence of different fraction energies. For a given energy (25 J delivered over an area of 0.03 mm^2), and an initial fraction of 5 J followed, after 150 seconds, by the remaining 20 J, the necrotic area was increased by a factor of three compared to a single fraction. To achieve the same area of necrosis, only two fractions of 5 J were needed, reducing the total energy by 60%, but the total time needed was constant.[231] Foster *et al.* also found a better treatment effect with Photofrin when using 30-second fractions separated by 30-second-long dark periods and claimed re-oxygenation being responsible for the enhanced effect.[206] Similar effects were observed for AlS_4Pc when 15-second-long fractions were used and the effect was thought to be due to the fact that the photosensitizing dye changes the localization in the tumour during the first seconds of exposure.[232] In two recent studies, irradiation fractions of 50 or 100 milliseconds, separated by a dark phase of the same length, at 652 nm were used to treat cells incubated with mTHPC. An increased cell killing, as compared to CW illumination, could be found in both cases.[173,233] The authors speculate on possible photochemical and photobiological phenomena that might be responsible for such an effect. Busetti *et al.* repeated the experiment, but did not find any increase in the cell-killing using the pulsed light.[174] In Lund, we performed a clinical comparison between this pulse-modulated modality and CW irradiation for ALA-PDT (Paper IX). A third mode, having intensity variations with frequencies up to 30 Hz according to a predetermined pattern, was used for two lesions. All modes had the same maximum fluence rate (100 mW cm^{-2}), resulting in average fluence rates of 50% and 67% for the two pulsed modes, respectively. No significant differences were found between the two former modes, while the statistical material was too small to allow direct comparison with the latter mode.

5.5.6 Light delivery techniques

Given a suitable light source with adequate power output, the major challenge is to deliver the light conveniently to achieve optimal irradiation of the tumour target volume. Ideally, the whole volume should be uniformly irradiated. For skin lesions, this can be realized with a lamp and a simple lens. Fibre-optics render flexibility when a laser is used as a light source. The output from a fibre is, however, non-uniform with a high intensity in the centre and radially decreasing. To achieve uniform illumination over the illuminated area, the distal end of the fibre can be imaged onto the tissue using a microscope objective, or by a micro-lens attached

to the fibre. The latter approach is also convenient for localized treatment of lesions in the body cavities.

To illuminate lesions in body cavities, different types of diffusing fibre tips have been developed. Spherical diffusing tips can be used to uniformly irradiate spherical organs such as the bladder. For tubular structures, such as the oesophagus or the bronchi, different cylindrical diffusing and side-illuminating fibre tips exist. Inflatable "balloons", covered on the inside with a strongly scattering material, formed to fit for example the cavity of the cervix, are commercially available.

Due to the relatively poor penetration depth of the red light used for most photosensitizers, it is not possible to treat tumours thicker than a few millimetres using surface illumination. If thicker tumours are to be treated, the light must be interstitially delivered through one or more optical fibres inserted into the tumour mass. The individual fibres do not need to have diffusing tips, since the multiple light scattering in the tissue will generate a diffuse and approximately uniform light distribution around the tip. High fluence rates might, however, induce coagulation which can lead to a destruction of the fibre tip. The light dosimetry is especially complex for this type of treatment. Knowledge on the dynamic changes of the optical properties during PDT is desirable.[171,234] An interstitial light delivery system for PDT has been developed at the Department of Physics in Lund.[235,236] The treatment light is coupled from a laser to a box, where the light is equally split into three or six optical fibres by means of beam splitters. The distal ends of these fibres are inserted into the tumour tissue, and the co-ordinates of the fibre tips are entered into the controlling computer software. The computer program can also suggest suitable positions for the fibres for certain geometries. The light in each fibre can be individually switched on and off by blocking the light just before the fibre port. When the beam path is blocked, a photo diode is placed behind the fibre to measure the light fluence at the fibre tip. The total light distribution in the tumour volume can be estimated by transmitting light in one fibre while using the others for detection, and repeating this process for all combinations. The light distribution is then calculated using FEM modelling of the diffusion equation, and a light dose distribution is presented on the computer monitor. New estimates of the illumination times for each fibre are calculated in order to reach above a threshold light dose in all parts of the tumour. The therapeutic irradiation then proceeds, with intermediate dose calculations and corrections, until the whole tumour has received the required treatment light dose.

5.5.7 Conclusions

The experimental studies reviewed in the previous sections suggest that improvements are still to be made in the drug and light dosimetry in order to optimize the treatment outcome of PDT. Today, such optimization studies require extensive investigations, since the treatment response can only be seen some time after the irradiation. It would be very valuable if an on-line tool to monitor the PDT effect could be developed. As indicated above, several factors are still partly unknown, but ongoing and future research will hopefully turn PDT into a largely accepted treatment modality. To achieve that, an inexpensive and easily handled light source with adequate output in a spectral band matching the absorption of the photosensitizer is needed. An ideal photosensitizer should have a good tumour-selectivity, and preferably absorb light in the near infrared wavelength region, to enhance the treatment depth. Moreover, it should have short accumulation and retention times, to minimize the unwanted general photosensitivity. An optimal treatment protocol must also be settled, which might include low fluence rates and light fractionation. To be convenient in a clinical setting, the treatment time must, however, be reasonably short. Preferably, some kind of on-line monitoring of the therapeutic progress should be included to allow changes of the irradiation due to differences in response from patient to patient.

6. Fluorescence diagnostics

Optical spectroscopy techniques have in recent years been investigated in the search for novel, minimally or non-invasive methods for tissue characterization and for measurements of various parameters in the tissue. The techniques developed for tissue characterization are frequently called "optical biopsy", a term that is somewhat contradictory, since the term biopsy refers to the removal of tissue, while the word optical implies that tissue is not removed. The ultimate goal for these investigations is to eliminate the need for surgical removal of tissue samples by employing real time characterization of tissue *in situ* based on optical measurements. This would reduce the cost and time needed to obtain the diagnostic information. The common basis of all optical techniques is that physiological, morphological or biochemical alterations, associated with the physical disorder, affect the interaction between light and tissue. The key problem is to find the "fingerprint" of different diseases on the optical signals. During the development of these techniques, an intermediate goal is to reduce the number of biopsies needed by guiding the physician to the suspicious tissue areas. A large variety of techniques have been proposed, based on, *e.g.*, fluorescence and Raman scattering. The work presented in this thesis will be restricted to fluorescence investigations. Fluorescence diagnostics is a natural counterpart to photodynamic therapy, since the photosensitizers used in the treatment are highly fluorescent. As a result of the growing interest of fluorescence for tissue investigations, several reviews of equipment used and results obtained have been published.[121,122,237-242] Fluorescence investigations have been performed in several of the papers presented in this thesis, to find and outline various pre-malignant and malignant lesions, and to investigate the selective buildup and pharmacokinetics of ALA-induced PpIX.

6.1 Historical overview

The phenomenon of fluorescence was discovered by Stokes in 1852, who observed this type of emission in fluorite.[243] He found that when illuminated with UV light, such samples emitted radiation at longer wavelengths. This discovery was not considered to be of any importance for a long time. It was not until the beginning of the 20th century that the potential of fluorescence for medical applications was being investigated. In 1911, Stübel reported that all animal tissues emitted fluorescent light when exposed to UV radiation.[244] The fluorescence was observed by the unaided eye, and classified according to the colour. The use of porphyrins as an aid for fluorescence diagnostics was partly covered in section 5.1.

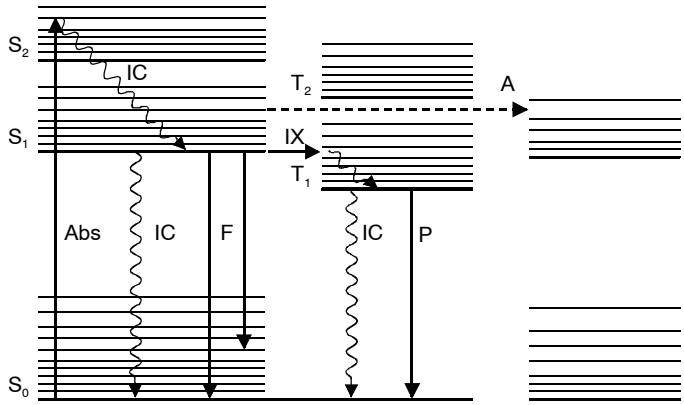

Figure 6-1 A schematic Jablonski diagram showing the various decay paths from an excited state of a molecule. The abbreviations are S_n, singlet states; T_n, triplet states; Abs, absorption; IC, internal conversion; F, fluorescence; IX, intersystem crossing; P, phosphorescence; A, energy transfer to other molecules.

6.2 Basic principles

Biological molecules are, in general, very complex with a complicated electronic configuration. Thus, the energy level diagram of such molecules becomes very elaborate. A simplified Jablonski diagram of a typical bio-molecule is shown in Figure 6-1. The electronic levels are characterized by the resulting spin vector of the electrons. If the sum of the electron spin quantum number is zero, the resulting energy level is called a singlet state, S, while one unpaired electron yields a triplet state, T. The ground state of most molecules is a singlet state. One important exception is the oxygen molecule, O_2, which has a triplet ground state. In contrast to the sharp electronic levels of an atom, the energy levels of molecules consist of a large number of vibrational states, which in turn have rotational sub-levels. The difference in energy between two electronic levels is typically of the order of a few electron volts, corresponding to light with a wavelength of 0.2-1 μm. The vibrational energy splitting is of the order of 10^{-1} eV (10 μm), and the rotational levels are typically separated by 10^{-3} eV (1 mm). For large molecules, the intervals between the levels are small and the states overlap due to molecular interactions. When a photon with sufficient energy is absorbed by a molecule in its ground state, the molecule will be excited to a higher singlet state. Electronic transitions in molecules occur so quickly that the nuclei do not change their relative positions in vibrational motion. This leads to an excitation not necessarily to the lowest vibrational level in the excited state, but often to a higher level. Since excited states are unstable, the molecule strives to loose its excess energy and to

return to the ground state. A rapid relaxation to the lowest rotational-vibrational level of the excited state will follow, a process called internal conversion (IC). The relaxation time is of the order of 1 ps, due to the high density of energy states. The energy lost in this relaxation is absorbed by neighbouring molecules, and is converted to heat.

Following relaxation, the molecule can return to the ground state through radiationless internal conversion. Alternatively, a photon can be emitted as the molecule returns to the ground state. This process is called fluorescence, and the emitted light is shifted towards red compared to the excitation wavelength (Stokes shift) due to the energy lost by internal conversion. In accordance with the excited states, the ground state also consists of a broad band of sub-levels. Thus, the fluorescence light will have a broad wavelength distribution, often without any significant structures. The shape of the fluorescence spectrum will reflect the transition probability to the lower electronic state.

The average time a molecule stays in the excited state is called the fluorescence lifetime, τ, and depends on the decay rates as

$$\frac{1}{\tau} = \frac{1}{\tau_0} + \sum k, \tag{6.1}$$

where Σk is the sum of all processes competing with fluorescence and τ_0 is the intrinsic lifetime, *i.e.*, the lifetime when fluorescence is the only decay process. The fluorescence lifetime is of the order of nanoseconds.

An excited molecule can also, although it is spin forbidden, be transferred to the triplet system. This transition is termed intersystem crossing (IX). Following internal conversion, the molecule will relax to the ground-state. Since this again is a spin-forbidden transition, it occurs at a much lower rate. This process is called phosphorescence, and has a lifetime in the range of 10^{-6} to 1 s. Phosphorescence is seldom observed at room temperature.

6.3 Tissue autofluorescence

When exposed to UV or near UV light, mammalian tissue emits fluorescence light in the blue-green wavelength region. This fluorescence is often called tissue autofluorescence, and origins from the endogenous tissue fluorophores. Much effort has been spent on investigating these fluorophores, and many of them have been identified using various spectroscopic techniques, such as excitation-emission matrices[245-247] and time-resolved fluorescence spectroscopy.[248] Fluorescence

microscopy and microspectrofluorimetry have also been used in the identification of tissue fluorophores, as well as their localization and distribution.[249,250] The fluorescence properties of most aromatic molecules present in tissue are well known in solution.[251,252] Despite that, it is difficult to get a detailed interpretation of the fluorescence signals from tissue, due to the composite, and usually unstructured, spectra and their dependence on the *in vivo* microenvironment. The wavelength-dependent optical properties of the tissue chromophores also influences the recorded spectra. The strong absorption from haemoglobin can strongly affect the measured fluorescence spectra of the tissue. Haemoglobin can absorb the excitation light and thereby drastically reduce the overall fluorescence signal, acting as an attenuation filter. Another possibility is that the emitted fluorescence is absorbed by haemoglobin, which induces distortion in the recorded spectra. Due to strong absorption at certain wavelengths, this can lead to dips or illusory peaks in the spectrum.

The most important tissue fluorophores have been found to be tryptophan,[253] collagen and elastin,[246,248] reduced nicotinamide adenine dinucleotide (NADH) and its phosphate (NADPH),[254-256] flavins and flavoproteins,[257,258] beta-carotene,[248] and porphyrins.[245,259] The wavelengths of the main excitation and emission peaks and the fluorescence lifetimes for some of the major tissue fluorophores are shown in Table 6-1.

Tryptophan is mainly located in proteins in the mitochondria and dominates the autofluorescence when the excitation wavelength is shorter than 300 nm. For longer excitation wavelengths, the contribution is smaller. Collagen and elastin are associated with the structural matrix of tissues, and are present in, *e.g.*, tendons and tissue stroma. When excited with a nitrogen laser (337 nm), the tissue fluorescence spectrum is dominated by collagen and elastin, while NADH dominates when the autofluorescence is excited at 365 nm. NADH is present in the cytoplasm and in the mitochondria of the cells, acting as a co-enzyme in the citric acid cycle. As malignant tissue is associated with an increased metabolism, the NADH fluorescence might be different as compared to normal tissue. Moreover, the pH is not the same for malignant and normal tissue, leading to a change in the redox balance between NADH and the less fluorescent NAD^+. Consequently, the blue fluorescence from malignant and pre-malignant tissue has been reported to be lower in a number of *in vivo* tumours.[255,260]

Fluorophore	λ_{exc} (nm)	λ_{em} (nm)	τ (ns)
Tryptophan	275	350	2.8, 1.5
Collagen	340	395	9.9, 5.0, 0.8
	270	395	
	285	310	
Elastin	460	520	6.7, 1.4
	360	410	7.8, 2.6, 0.5
	425	490	
	260	410	
NADH	350	460	0.6, 0.2
Beta-carotene		520	9.6, 2.0, 0.3
Endogenous porphyrins	400	610, 675	

Table 6-1 The most important fluorophores in tissue, together with their main excitation and emission wavelengths and fluorescence lifetimes.[121]

6.4 Excitation light sources

The excitation light sources used for fluorescence investigations can be divided into two main groups; lamps and lasers. The choice of light source is dependent on several factors. First of all, the appropriate wavelength for the application must be considered. Other aspects, especially for clinical work, are the detection technique used and the portability and operability of the system. In early work, Wood's lamps were used, but have later been replaced by high-pressure mercury lamps and xenon lamps. The xenon lamp has a broad spectrum in the near-UV region, and needs to be filtered with an optical filter or a monochromator to give an appropriate excitation wavelength. By changing filters, or turning the grating of the monochromator, the wavelength can be arbitrarily chosen. The mercury lamp, on the other hand, has a discrete spectrum with a number of relatively narrow emission lines. One of these lines (405 nm) coincides with the Soret band of porphyrins, and is thus of special interest for medical fluorescence applications. The line at 365 nm is suitable for excitation of the tissue autofluorescence, especially from NADH.

Lasers have several advantages over lamps for many applications. First of all, high intensity emission over a narrow wavelength region can be achieved. Moreover, a highly parallel beam, allowing efficient coupling of the light into optical fibres, is an advantage. A large variety of lasers have been used for fluorescence investigations. The continuous wave (CW) krypton-ion laser has several lines,

ranging from UV to IR. The lines at 337 nm and 407 nm are of special interest in the excitation of tissue autofluorescence and porphyrin fluorescence, respectively. The CW helium-cadmium laser has also been used for these kinds of investigations, with suitable emission lines at 325 and 442 nm.

A variety of pulsed lasers can also be used for fluorescence excitation. The high peak powers of many pulsed lasers make them suitable for frequency doubling or tripling. The near-infrared light from a Nd:YAG laser (1064 nm) can be frequency-tripled to 355 nm, a wavelength appropriate for autofluorescence excitation. Currently, there is a development of compact diode pumped solid state lasers, such as Nd:YAG and Nd:YLF lasers. The third harmonic of these lasers can be used to excite fluorescence. It is also possible to use them together with optical parametric oscillators (OPOs), instead of dye lasers, to get a tuneable light source. The Soret band of porphyrins can be approximately matched with, *e.g.*, light from a frequency-doubled Alexandrite laser (390 nm). The excimer lasers constitute a class of pulsed lasers operating in the UV region. Very high pulse energies can be obtained, and thus they can be used as excitation sources for fluorescence imaging. It is also possible to use them in combination with dye lasers to obtain a tuneable excitation light source. Because of their size and inconvenient operation, they have not been widely used. Furthermore, their use involves handling of hazardous gases.

A very convenient pulsed laser is the nitrogen laser. This is an easily operated laser, emitting light at 337 nm, in very short pulses, approximately 3 ns. Moreover, it can be made very small and only needs little electrical power, typically 12 V DC. It is possible to use this laser in combination with a compact dye laser to select other excitation wavelengths.

Presently, much research is put into the field of developing semiconductors emitting light in the blue and near-UV wavelength region. One major driving force is the possibility to use blue diode lasers to achieve higher data capacity of compact discs. Also for fluorescence investigations, these light emitting diodes, or diode lasers, would be of great interest. They would allow the construction of even more compact and easily operated systems.

6.5 Detection principles

Equipment used for fluorescence investigations are usually divided into two categories, point-monitoring and imaging systems. The first category includes systems that are used to characterize the sample in a single point from recordings of the fluorescence intensity, spectrum, or lifetime. Usually, only a small area

(typically of the order of 1 mm^2) is investigated, which makes an investigation of a larger area very time consuming. For clinical use, imaging systems are generally of more interest. For these purposes, the amount of data collected in each spot must be reduced to present an image of the investigated area. Both point-monitoring and imaging systems can be used to record the intensity as a function of wavelength, or as a function of time, on a nanosecond time-scale. These two approaches can give complementary information on the composition of fluorophores, and on changes due to the microenvironment. Most systems used for *in vivo* investigations are based on the emission spectrum obtained from one or a few excitation wavelengths. For *ex vivo* and *in vitro* studies, it is also possible to investigate the fluorescence excitation spectrum. This can be of interest to find the optimum excitation wavelength, and also to determine the composition of fluorophores in the sample.

6.5.1 Point-monitoring systems

Point-monitoring systems are usually relying on fibre-optics to guide the excitation light to the tissue, and to collect the emitted fluorescence. The simplest instrumentation only uses a single detector, such as a photomultiplier tube or a photo diode to measure the signal. In many cases, however, the spectroscopic information in the fluorescence light will improve the tissue characterization. To detect the red fluorescence from a photosensitizer, a band-pass filter can be used. In this way, also a fraction of the tissue autofluorescence will be detected. By placing several filters on a wheel in front of the detector, the fluorescence in various wavelength bands can be sequentially recorded.[261] Similarly, if a lamp is used as a light source, the excitation wavelength can be chosen by means of different filters. Lock-in techniques can be used to make the measurements less sensitive to ambient light, which otherwise might severely affect the detected signal.

To increase the spectroscopic information further, a scanning monochromator can be placed in front of the detector. This is not very practical for clinical applications, since the scanning procedure will require substantial acquisition times. A better approach is to use a linear diode array or a CCD camera attached to a spectrometer. Such a system, consisting of some optical coupling components, a spectrometer, a multichannel detector, and a computer, is usually referred to as an optical multichannel analyser (OMA) system.[262] The detector is preferably equipped with an image intensifier, which is used to amplify the faint optical signal. Another advantage of image intensifiers is that they can be used as very fast electrical shutters. Conventional image intensifiers of today can be switched on and off within a few nanoseconds, and even gating times of fractions

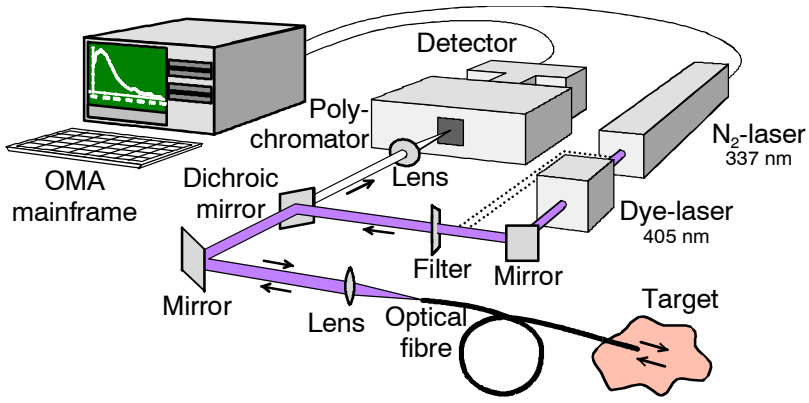

Figure 6-2 A schematic representation of the OMA-system used for *in vivo* fluorescence investigations.

of nanoseconds can be achieved. When combined with pulsed laser excitation, they can be used to efficiently suppress the influence of ambient light. A commonly used pulsed laser for fluorescence investigations is the nitrogen laser, having nanosecond pulse duration and a repetition rate of tens of hertz. Since the fluorescence lifetime is of the order of nanoseconds, there will not be any signal to detect most of the time. Immediately after the excitation light pulse, the collected light will be dominated by the fluorescence emission. If the detector is switched on only during, *e.g.*, 100 ns in connection to the excitation pulse, and the laser is operating at 10 Hz, the influence of the ambient light will be reduced by a factor of 10^6.

In Lund, the first clinically adapted OMA system was presented in 1991.[263] This system has been widely used in many pre-clinical and clinical applications, as well as for investigations of fluorescence from vegetation and oil, see *e.g.* Refs. (264-266). The system is schematically described in Figure 6-2. In short, the system uses a nitrogen laser (3 ns pulses at a rate of 10 Hz), alone or in combination with a dye laser tuned to 405 nm, as an excitation light source. The selection of wavelength is made by two flip-in mirrors. A 600-µm-diameter optical quartz fibre is used to guide this light to the sample under investigation. The emitted fluorescence light is collected with the same fibre. A dichroic mirror and an optical filter are used to separate the fluorescence from scattered excitation light. The fluorescence light is spectrally dispersed in the spectrometer, and detected with an image-intensified linear diode array. A computer controls the equipment, and also presents and stores the recorded fluorescence spectra. The entire equipment is mounted on a mobile trolley, to facilitate the use at different locations.

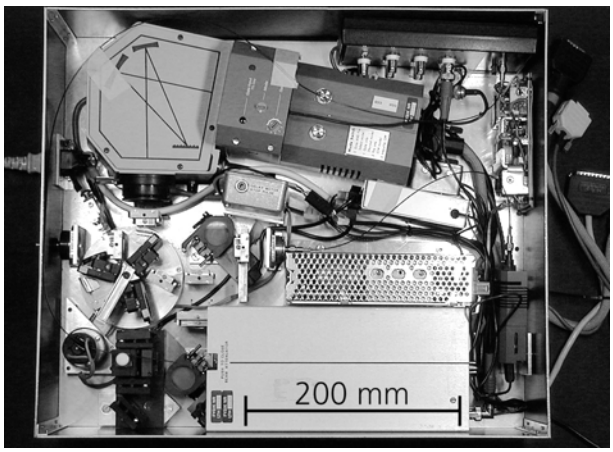

Figure 6-3 The new, portable OMA system for fluorescence investigations. A nitrogen laser, located at the bottom part of the picture, can be used alone or in combination with a dye laser module. A turn-plate is used to choose filters and beam splitters for the different wavelengths. At the top is an image-intensified CCD camera coupled to a spectrometer. As a probe, a single optical fibre is used, which is connected at the middle of the left side.

A second version of this system was presented in 1994.[267] This system is a little smaller than the previous. The sensitivity is also increased by the use of an intensified CCD camera as a detector, instead of the linear diode array. Recently, a third generation has been developed[268] (Paper VI). This system has several improvements compared to the two predecessors. The size of the system has been largely reduced, and is now of the order of a carry-on luggage (Figure 6-3). The switching between the two excitation wavelengths is made automatically to allow measurements at the same spot. A bright halogen lamp has also been incorporated in order to study the reflectance spectrum. This spectral variations of the reflected light can be taken into account when evaluating the fluorescence data. Finally, the equipment can be operated in a time-resolved mode in order to evaluate the lifetime of the recorded signal. A lap-top computer is used to control the equipment, using a software developed in LabVIEW™. The user interface can be individually designed for different operators and applications.

6.5.2 Imaging systems

The systems described in the previous section provide much information from a small area. In order to investigate larger areas of clinical relevance, and thus to avoid random sampling, an imaging technique is needed. Imaging also facilitates

the interpretation of the signal, as spatial variations are better visualized. The simplest "imaging" system is to use the eye to directly observe the emitted fluorescence. This is feasible when, *e.g.*, porphyrin-based fluorescent tumour markers are excited by violet light.[269,270] The first clinical fluorescence bronchoscope was presented in 1979.[271,272] This system was based on a mercury arc lamp, and later a CW krypton-ion laser, for excitation and an image intensifier to amplify the faint fluorescence signal. In this system, it was not possible to make normal white light bronchoscopy at the same time, an option later implemented through rapid switching between white light and fluorescence modes.[273] In general, the detection of light in a single wavelength band seriously limits the reliability of the fluorescence diagnosis.[273] A number of approaches have been used to circumvent this limitation. Hirano *et al.* incorporated a point-measuring device into the imaging system, to allow spectroscopic investigation of suspicious areas.[274] Alternatively, sequential or parallel imaging at several excitation or emission wavelengths, followed by image processing to subtract the autofluorescence contribution or to form wavelength ratios. One system, based on parallel detection of two image in different wavelength bands, has been developed into a commercial product for endoscopic applications (Light-induced fluorescence endoscopy, LIFE, Xillix Technologies Corp., BC, Canada). The excitation light source of this system is either a high-pressure mercury lamp (405 and 436 nm) or a helium-cadmium laser (442 nm). The fluorescence is detected in a red and a green wavelength region by two cameras and the signal from these cameras are fed to the red and the green channel of a colour monitor, to produce a pseudo-colour image. The system has provided useful information in various clinical specialities, such as investigations of the bronchi, and for the detection of cancers in the head and neck region and in the gastro-intestinal tract.

A more sophisticated multi-colour fluorescence imaging system, that can be used together with fibre-optical endoscopes, has been developed in Lund.[275-277] This system uses beam-splitting optics to produce four spatially identical images, individually filtered in different wavelength bands (Figure 6-4). The four images are captured on the same image-intensified CCD camera. The gating of the camera is synchronized with the excitation light source, a frequency-doubled Alexandrite laser tuned to 390 nm. This detection scheme allows the use of a colour video camera to record the ordinary white light reflection image. The multi-colour imaging system has been used in combination with a photosensitizer (HpD or ALA-induced PpIX) to investigate malignant tumours in a variety of organs.[278] Usually, three wavelength bands have been detected. The sensitizer-related fluorescence (called *A*) was detected in the red wavelength region, the autofluorescence (*B*) was detected around 470 nm, and one band (*D*) in the green-yellow part of the spectrum was used to subtract the part of the autofluorescence

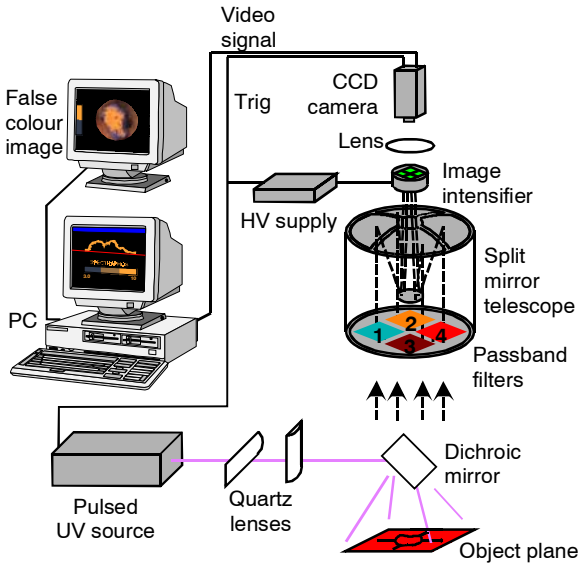

Figure 6-4 The set-up of the multi-colour fluorescence imaging system.

that overlapped the photosensitizer spectrum. For each corresponding pixels in the different sub-images, an optimized contrast function, defined as

$$F_c = \frac{A - k_1 D}{k_2 B} \tag{6.2}$$

is calculated. Here k_1 and k_2 are constants, assigned to different values for different applications. This function results in a high value for malignant tissues, as the sensitizer fluorescence increases and the tissue autofluorescence decreases. The result of the calculation is mixed with the ordinary image, and a threshold value can be set to only mark suspicious areas. The image is updated in real-time at a rate of up to eight images per second. Results from this system in connection with ALA-PDT is presented in Papers VII-VIII. An example of an image is given in Figure 6-6.

A very advanced and powerful device for multi-spectral fluorescence imaging of tissue was presented by Malik *et al.* in 1996.[279] This instrument is based on a Fourier transform spectrometer, that records the full fluorescence emission spectrum in every pixel. With such a system coupled to a microscope, local variations in the fluorescence emission due to changes in the microenvironment can be studied. There is, however, a trade-off between the spectral resolution and

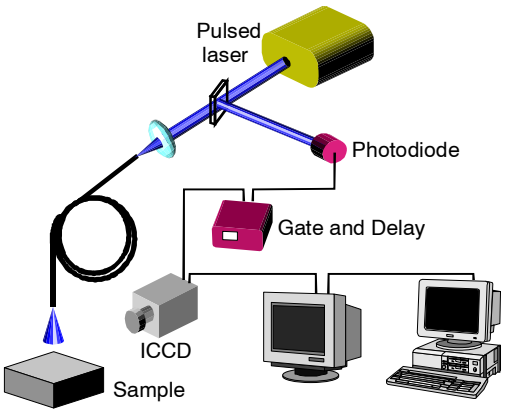

Figure 6-5 The principle of a time-resolved fluorescence imaging system. The gate of the image-intensified is opened at various delays following the excitation light pulse. The fluorescence lifetime is calculated for each pixel from the sequentially acquired images.

the acquisition time, making high-resolution investigations restricted to *in vitro* and *ex vivo* investigations.

A conceptually different approach to fluorescence imaging is to make images of the fluorescence lifetimes. Cubeddu *et al.* have constructed a system based on this technique,[280] for the detection of tumours after administration of photosensitizers at very low doses (Figure 6-5). The excitation light source is a pulsed (1 ns) nitrogen laser-pumped dye laser (405 nm). The fluorescence light is detected by a gateable image-intensified CCD camera, having a gate rise time of approximately 2 ns. The camera is equipped with a cut-off filter to suppress most of the blue-green autofluorescence, and only transmit the red fluorescence light. To form the lifetime images, sequential fluorescence images are recorded where the gate is opened at various delays with respect to the excitation pulse. For each pixel, the fluorescence lifetime is calculated from the different images by assuming a mono-exponential decay. The lifetime distribution is then presented in a pseudo-colour image. This system has been used to visualize transplanted tumours in a mouse model following administration of AlS_2Pc,[281] and to show that the fluorescence lifetime of HpD is up to 20% longer in tumours as compared to the surrounding normal skin.[282] The latter finding was believed to be induced by changes in the microenvironment of the sensitizer.

The fluorescence lifetime imaging system was used in parallel with the multi-colour imaging system developed in Lund in connection with ALA-PDT of various skin lesions (Papers VII-VIII).[283] Figure 6-6 shows a superficial basal cell

carcinoma on the neck of a 84-year-old man. A photograph of the lesion is shown in the top of the figure. Below to the left is a grey scale image from the multi-colour fluorescence imaging system, and to the right is the output from the fluorescence lifetime imaging system. The lesion is clearly outlined with both imaging techniques. For the multi-colour fluorescence image, the fluorescence intensity in the red channel is divided by that obtained in the green channel. In the centre of the fluorescence lifetime image, the lesion can be seen as having a longer effective fluorescence lifetime. The immediately adjacent normal skin also shows an increase in the fluorescence lifetime, due to a certain uptake of ALA and the subsequent synthesis of PpIX. ALA was not applied to the normal skin further away, which has the shortest lifetime in the image. The increase in the lifetime obtained in the lesion might be due to a change in the microenvironment of the sensitizer. The relative contribution of the long-lived PpIX fluorescence compared to the small amount of short-lived autofluorescence in the red wavelength region also affects the effective lifetime. The normal skin is characterized by a higher short-lived autofluorescence and a lower long-lived PpIX fluorescence, resulting in a relatively short effective lifetime, whereas the opposite relation holds for the lesion.

With the introduction of ALA-induced PpIX for fluorescence investigations, the technique has been clinically accepted. Due to its strong fluorescence, simple endoscopically adapted imaging systems have been constructed. A commonly used approach is to go back to the early techniques, using a normal white light endoscope with the possibility to switch to a UV or near UV light source for fluorescence investigations. An optical filter is used to block the scattered excitation light, and thus only the fluorescence can be seen.

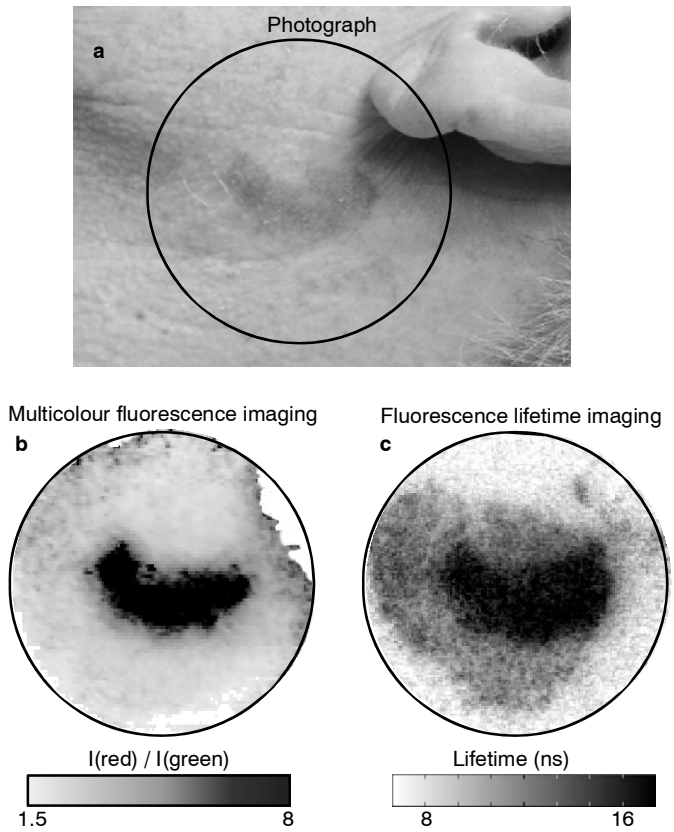

Figure 6-6 A basal cell carcinoma (25×12 mm), located below the ear of an 84-year-old man in connection with ALA-PDT. (a) A photograph of the lesion. (b) An image obtained with the multi-colour fluorescence imaging system. The investigated area is indicated by a circle in the photograph. The lesions is clearly outlined, having a high red-to-green fluorescence ratio. (c) A fluorescence lifetime image of the same area. The lesion is characterized by a longer effective lifetime. The area where ALA was applied (lesion and immediate adjacent skin) has a longer lifetime than the normal skin without ALA.

6.6 Evaluation of fluorescence spectra

The data obtained from the fluorescence investigations are, of course, dependent on the type of equipment used. A single detector seeing only the red fluorescence emission can be used to investigate the accumulation of a photosensitizer. The detected signal can then be used as a measure on the concentration of the sensitizer. Several factors might, however, influence the signal, resulting in erratic interpretations, *e.g.*, variations in measurement geometry and excitation light

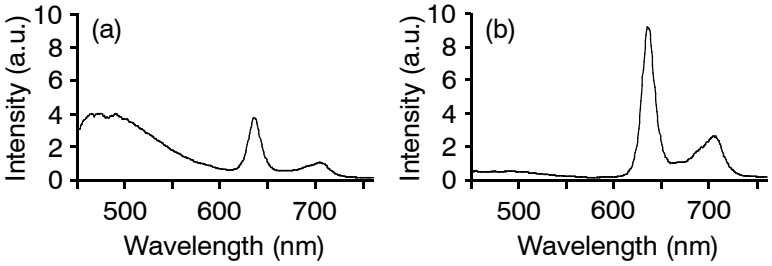

Figure 6-7 Fluorescence spectra recorded in (a) the normal skin and (b) a superficial basal cell carcinoma (Paper XII). The measurements were performed 6 hours after topical application of ALA. The lesion has a higher PpIX fluorescence (635 and 705 nm) and a lower autofluorescence (around 500 nm) than the normal skin.

intensity, the presence of absorbers such as haemoglobin, *etc.* To minimize the influence of the tissue optical properties, a double-ratio approach has been developed.[284,285] A ratio between the fluorescence intensities in two bands (660-750 nm and 550-600 nm) was formed for two excitation wavelengths (405 and 435 nm), for which the tissue optical properties are similar. By dividing the two ratios with each other, the influence of absorption and scattering was more or less cancelled out. This method has been shown to accurately quantify the photosensitizer concentration, also in pigmented lesions.

Another approach to avoid artefacts in the data, is to record the full spectrum. Figure 6-7 shows fluorescence spectra recorded in a basal cell carcinoma and in the surrounding normal skin six hours after topical application of ALA, using the OMA system described previously. The PpIX fluorescence show up as two peaks at about 635 nm and 705 nm. At these wavelengths, there is also a certain contribution from the tissue autofluorescence that must be taken into account in order to estimate the concentration. This contribution can be estimated by an exponential curve. Using a single fibre for both excitation and collection, variations in the tissue absorption will result in an overall attenuation of the intensity, without major influence on the spectral shape. Occasionally, imprints of the haemoglobin absorption peaks can be seen in the recorded spectra, which might appear as illusive emission peaks.[286] The problem of quantifying the *in vivo* concentration of the photosensitizer remains, though. A solution could, again, be to incorporate two excitation wavelengths.

A technique that has been extensively used in Lund for tissue characterization following the administration of fluorescent tumour markers, is to form fluorescence ratios. This technique was briefly described in section 6.5.2. One

important aspect of ratios is that the resulting value is independent of variations in the system, such as fluctuations in the excitation light, the illumination geometry, *etc.*, since these variations affect all wavelengths similarly. By forming the ratio between the fluorescence from the fluorescent tumour marker and the autofluorescence a "contrast enhancement" between normal and diseased tissue is obtained.[287] This is the combined result of an increased concentration of the fluorescent tumour marker and a decreased autofluorescence intensity in diseased tissue, as compared to the surrounding healthy tissue. The ratio can, *e.g.*, be used to guide the physician to the optimal site to take a biopsy for histopathological examination. When used in an imaging system, the ratio can be presented in a pseudo-colour image and mixed with an ordinary white light image to mark suspicious areas. This approach is specially useful for fluorescence investigations after administration of low-dose ALA, since this does not lead to any general photosensitization. It is, however, not the ideal solution for routine screening purposes since the administration of an exogenous drug is essentially an invasive process, which can result in concomitant side effects. It is also associated with a substantial cost.

For a good excitation of porphyrins, a wavelength around 405 nm should be used. This is, on the other hand, not an optimal wavelength for investigations of the autofluorescence, since most of the tissue fluorophores have their main excitation wavelength at shorter wavelengths, below 360 nm (see Table 6-1). Thus, the nitrogen laser (337 nm) offers a better excitation wavelength for investigations without any fluorescent tumour markes. Also in these studies, the formation of ratios can be used for evaluation. For instance, by dividing the intensities recorded at two wavelengths, equally absorbed by haemoglobin, a "blood-free" criterion for the characterization of atherosclerotic plaque can be obtained.[256]

Several other techniques have been proposed for the evaluation of fluorescence spectra. One statistical approach is to use stepwise multivariate linear regression (MVLR). This method relies on the shape of the normalized spectra. On a training set, the intensities at a number of wavelengths are multiplied with different weights to obtain a score +1 for normal and -1 for diseased tissue. The weights are then applied to the data set. This kind of analysis has been successfully applied, *e.g.*, to differentiate between normal mucosa and adenomas in the colon.[288-290] Principal component analysis (PCA) has also been used in the evaluation of fluorescence and near-infrared reflection spectra.[291-293] The idea of PCA is to reduce the data into a smaller set of linear combinations of the original variables that account for most of the variance of the original data set. PCA may not, however, provide direct insight to the morphologic and biochemical basis of the spectra. Instead, the spectral information is condensed into a few manageable components, with minimal loss of information. Moreover, this approach does not require any a priori

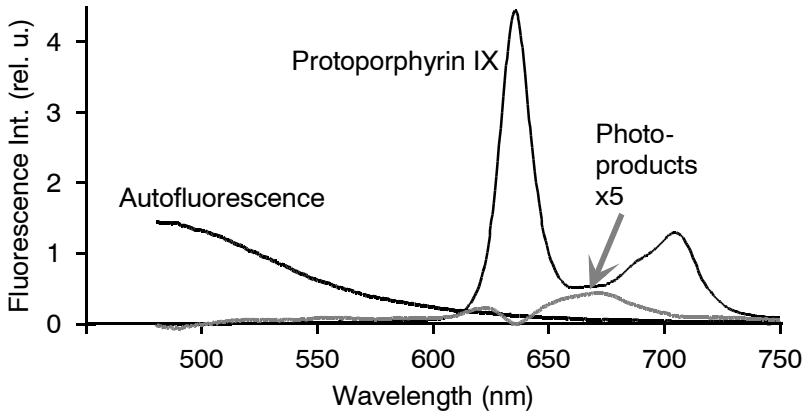

Figure 6-8 The three fluorescence contributions used for fluorescence investigations of basal cell carcinomas in connection with ALA-PDT (From Paper XIII).

knowledge on the signals. Various pre-processing techniques, such as normalization with respect to the peak-intensity, mean-scaling, and a combination of the two, have been evaluated in combination with PCA.[291,292] Mean-scaling means that an average of all spectra recorded in one patient is subtracted from each individual spectrum in the same patient. The statistical evaluation is then performed on these difference spectra. With this technique it is important to investigate approximately the same number of suspicious and normal tissue areas. The combination of normalization and mean-scaling has also been used with good result for fluorescence investigations of the oesophagus.[294,295] In these papers, the method has been termed differential normalized fluorescence (DNF).

As PCA does not require any a priori knowledge, the largest variances might be due to differences not related to the pathological condition of the tissue, but rather to variations between different patients, and different measurement sites. In partial least squares (PLS) analysis, a PCA algorithm is used to describe the maximum variance of both the measured data and the known diagnosis. This procedure is performed on a learning set, and can then be applied to other data.

A technique similar to PCA was used in Paper XIII to investigate the accumulation of PpIX in basal cell carcinomas following topical application of ALA. In PCA the principal components are determined from mathematical operations to describe the variance of the data with decreasing significance. In Paper XIII, the contributions were chosen by making the assumption that the recorded spectrum consisted of three different contributions; the autofluorescence, the PpIX fluorescence, and the fluorescence emission from the

photoproducts appearing as a result of the photodynamic reactions in the tissue (Figure 6-8). The average spectra associated with these three contributions were calculated from the measurements performed in the centre of the lesion at different occasions, as described in the paper. Linear combinations of these "principal components" were then fitted, together with an offset value, to the spectra recorded in the lesion and in the normal skin.

6.7 Summary

Fluorescence diagnostics attracts increased interest both on a research level, and in the clinics. Several point-monitoring and imaging systems have been developed, and some have also turned into commercial products. Some of these systems rely on the tissue autofluorescence, while others are combined with the administration of fluorescent tumour markers. The former approach is more suited for screening purposes, since the use of fluorescing compounds can be associated with side effects, and are usually quite expensive. The use of fluorescent tumour markers with no or little photosensitivity effects, such as ALA-induced PpIX, has increased the clinical acceptance since rather simple instrumentation can be used, a UV lamp and a filter for the detection. Since the detection is based only on fluorescence intensity, there is a risk for misinterpretation, due to variations in the tissue optical properties and the relatively low selectivity in the PpIX buildup. In order to make a better classification of the tissue, imaging systems based on spectral or temporal variations of the fluorescence can be used. Most prototypes for fluorescence imaging systems presented so far are expensive and complex. A constant development of light sources and detectors will most likely make the construction of systems better suited for the clinical situation.

7. Laser-Doppler flowmetry

Laser-Doppler flowmetry is a non-invasive technique, based on quasi elastic scattering, that can be employed for continuous measurements of the tissue blood flow. A local, abnormal increase in the superficial perfusion indicates an increased activity caused by for example an inflammatory response. Studies on the microvascular blood perfusion *in vivo* can provide information on the response to various stimuli, such as mechanical or electrical skin stimuli, changes in temperature, *etc*.[296,297] The laser-Doppler technique can also be used to study responses to various agents[298-300] and the immediate response and healing time following various treatments[301,302] (Paper XIV). Various diseases, such as diabetes and arteriosclerosis also affects the microcirculation. Point-monitoring systems have been developed for clinical use. Due to the significant spatial variations in the microcirculation, the average perfusion over a larger area has to be sampled to give a representative measurement. Furthermore, point-monitoring systems are usually based on contact measurements, which also might influence the perfusion. Finally, laser-Doppler flowmetry cannot be used for absolute measurements and thus only variations, either temporal or spatial, can be measured.[303] To better meet the needs, a non-contact imaging system would be advantageous. Such a system, clinically adapted, has been developed,[304] and is commercially available (Lisca Development AB, Linköping, Sweden). This system has, *e.g.*, been used to monitor the perfusion in skin flaps in plastic surgery,[305] and to map the myocardial perfusion in connection with coronary by-pass surgery.[306] It has also been used to study the perfusion in port-wine stains following laser treatment,[302] and to evaluate the response of PDT.[301]

We have used this LDI system to investigate the healing time following ALA-PDT and cryosurgery in the treatment of basal cell carcinomas (Paper XIV). The system, thoroughly described elsewhere,[304] uses laser light with a wavelength of 633 nm (from a helium-neon or diode laser). The probe beam is step-wise scanned over the tissue by means of two computer-controlled scanning mirrors. At each measurement site (up to 64×64), the beam is halted for 50 ms, and the measurement is performed. The probe depth of the measurement has been estimated to a couple of hundred micrometers.[307] A photo diode, mounted next to the scanning mirrors, is used to record a fraction of the diffusely backscattered light. When the light is scattered by moving blood cells, a fraction of the kinetic energy is transferred to the photons. This leads to a change in frequency of the scattered light, which is known as the Doppler shift. The change in frequency is very small, only about 10^{-11} times the frequency of the incident light.[303] It can be shown that the frequency shift at a single scattering event is

$$\Delta f = \frac{1}{2\pi}\left(\mathbf{k}_s - \mathbf{k}_i\right)\cdot \mathbf{v}\,, \tag{7.1}$$

where $\mathbf{k}_s$ and $\mathbf{k}_i$ are the wave vectors of the scattered and the incident light, respectively, and $\mathbf{v}$ is the velocity vector of the scattering blood cell. Since both the blood cells and photons are moving in all directions, a distribution of frequency shifts will be obtained, which can be used to calculate the velocity distribution of the blood cells.[304] Furthermore, the amplitude of the frequency-shifted signal is related to the concentration of blood cells. The perfusion is then calculated as the product of the concentration of moving particles and their average velocity. The spatial variations of the perfusion is then presented as a pseudo-colour image on the computer monitor. The resulting images can be statistically evaluated in a commercially available computer program (LDISOFT 1.0, Lisca Development AB, Linköping, Sweden).

From the measurements performed in connection with the two treatment modalities, the perfusion was evaluated before and immediately after the treatment, and during a follow-up period of 1-2 years. At each occasion, the ratio in the perfusion of the lesion and of the surrounding normal skin was calculated. By forming ratios, the influences on the evaluation caused by variations in perfusion due to temperature, stress, and other irrelevant factors are minimized. Before treatment, the perfusion was on average 3 (SD = 2) times higher in the lesion as compared to the normal skin. Both treatment modalities induced an immediate increase in the superficial blood flow. During the follow-up period, the ratio approached unity for successfully treated lesions. Normal perfusion was reached two months after PDT, compared to approximately one year after cryosurgery. For recurrent tumour growth, the perfusion remained elevated. Thus, it can be concluded that LDI can be used as an objective tool at the follow-up visits to aid the physician in evaluating the treatment response.

Acknowledgements

This work could not have been accomplished without the help and support from a large number of people, including colleagues and the staff of the Division of Atomic Physics and at the Lund University Medical Laser Centre. The friendly atmosphere and the scientific environment have been inspiring, and I am truly grateful for the possibility to work in the border zone between physics and medicine.

First of all, I would like to thank my supervisor Dr. Stefan Andersson-Engels. His broad knowledge of physics and medicine, and his ability to always put the right questions have stimulated much discussion, from which we both have obtained a better understanding. I am also grateful to Professor Sune Svanberg, whose enthusiasm encouraged me to start this work, and who has been a constant source of ideas and inspiration, and to Dr. Katarina Svanberg, who has contributed with the medical expertise and the essential clinical perspective to the work.

Further, I would like to thank the members of the medical group at the Division of Atomic Physics for good collaboration and friendship. I would especially like to thank Roger Berg, Jonas Johansson, Annika Enejder, Ingrid Wang, and Charlotta Eker for the work we have performed together in the laboratory and at various clinics. I especially appreciate and that Ingrid put up with my increasing invasion of our joint office space, and the discussions we have had when struggling with our theses.

A special thank to Antonio Pifferi, Politecnico di Milano, Italy, for friendship and the good collaboration in the dark laboratories in the basement, during his post-doc period in Lund. I also enjoyed the further collaboration with him and the rest of the group from Milano.

I am also grateful to Åke Bergquist, whose help with electronics and commuting has been invaluable, Anders Persson, the person to ask when lasers or computers do not work, and Ulf Gustafsson, who always has an helping hand, especially when heavy equipment needs to be moved.

Finally, I would like to thank my family and friends for the support that you have given me. My parents have always encouraged me in my work, for which I am very grateful. Most of all, I would like to thank my wife, Carola, for the love and motivation you have given me, especially during the hardest of times.

Summary of papers

Papers I-IV are describing a time-resolved technique to determine the optical properties of tissue over a large spectral region in a single measurement. Femtosecond pulses from a near-infrared high-power laser were used to generate very short white light pulses. A streak camera was used in combination with a spectrometer to achieve time- and wavelength resolved detection of the diffusely scattered light. In Paper I, this technique was used on a tissue phantom to detect an inclusion with different absorbing and scattering properties. In Papers II-III, the optical properties of breast tissue *in vivo* and *in vitro* are studied. From the *in vitro* studies, differences between normal tissue and tumours are investigated. In Paper IV, the same technique is used to determine the *in vivo* absorption spectrum of a photosensitizer. Differences in the scattering and absorption spectra between tumour and normal muscle tissue in rat are being examined.

Paper V reports on an investigation using laser-induced fluorescence from the female genital tract, especially the cervix. The investigation was performed using two excitation wavelengths (337 and 405 nm). Most of the patients were given an oral dose of ALA prior to the investigation.

Paper VI describes the construction of a new, compact OMA-system, which is intended to be used for laser-induced fluorescence spectroscopy, complemented with white light diffuse reflectance measurements. Two different excitation wavelengths (337 and 405 nm) can be employed. The system can be used for both time-integrated and time-resolved fluorescence spectroscopy. A flexible software allows the use of user-defined interfaces. The size of the system is of the order of a carry-on luggage.

Paper VII presents probably the first use of a diode laser system at 635 nm for ALA-PDT. This laser was used to treat various skin lesions. The therapeutic efficacy was, as expected, comparable to that of a dye-laser system, pumped by a frequency-doubled Nd:YAG-laser. In connection with the treatment, two fluorescence imaging systems were used. One system displayed false-colour images of the fluorescence lifetimes, while the other was based on image processing of fluorescence images simultaneously acquired in different wavelength bands.

Paper VIII reports on a comparison between fluorescence lifetime imaging and multi-colour fluorescence imaging of basal cell carcinomas following topical application of ALA.

Paper IX describes the use of a diode laser system, emitting light at 652 nm, in the treatment of skin lesions following topical application of ALA. The computer controlled diode laser allowed the use of various amplitude modulation schemes of the light. Three modes were tested and compared; continuous wave, pulsed (alternating dark and light periods of 100 ms), and a mode called TSO by the manufacturer (pre-determined intensity variations in the order of 0-30 Hz). No significant differences were found between the to former modes, while the statistical material was too small in the third group.

Paper X presents a study on pain experienced during ALA-PDT. The treatment was carried out at two different wavelengths, 635 and 652 nm. The shorter wavelength matches the absorption peak of PpIX, and more sensations of pain is experienced by the patients. The clinical outcome is also better at this wavelength. A simple, but effective, way of reducing the pain is by spraying the treated area with water.

Papers XI-XIV present the results obtained in a prospective, randomized Phase III clinical trial comparing ALA-PDT with cryosurgery in the treatment of basal cell carcinomas. In total, 88 patients were included in the study. The clinical outcome, with regard to recurrence rate and tolerability, *i.e.*, the time of healing, the pain in connection with the treatment, and the final cosmetic result, is presented in Paper XI. A comparable efficacy of the two treatment modalities was found, with a tendency of a small advantage for cryosurgery. A significantly shorter healing time and a better cosmetic outcome was, however, in favour for ALA-PDT. Laser-induced fluorescence measurements were performed in connection with the ALA-PDT measurements. The pharmacokinetics of the ALA-induced PpIX synthesis was studied in 15 patients. The result of this study is presented in Paper XII. In Paper XIII, the fluorescence pre ALA, pre PDT, and post PDT was investigated in all patients in the ALA-PDT-arm of the clinical trial. The average fluorescence spectra of the endogenous tissue fluorophores, PpIX, and the photoproducts are derived. Linear combinations of these spectra are fitted to the data, and the average weights are determined. The fluorescence information was not found to give any significant indication on the resulting treatment efficacy. Laser-Doppler perfusion imaging was used to evaluate the healing time after the treatment, as reported in Paper XIV. Prior to the treatment, an elevated superficial perfusion was found in the lesions, as compared to the adjacent normal tissue. During a follow-up period of 13 to 24 months, the perfusion-ratio between the lesion and normal skin decreased towards unity. The healing process was found to be significantly faster following ALA-PDT. The ratio could also be used as an aid to evaluate the treatment response, since residual or recurrent tumour growth could be seen as increase in this ratio.

The author has contributed the work reported in the papers as follows:

Experimental and clinical work for Papers I-V, VII-IX, and X-XIV.

Evaluation of all data for Papers V, XII, and XIII, and parts of the data for Papers II-IV, VI, IX-XI, and XIV.

Preparation of figures for Papers II-V, VII-X, and XII-XIV.

Writing of major parts of the manuscript for Papers II-V, VII, IX, X, XII, XIII, and parts of Papers VIII and XIV.

The author made major contributions to the design, specification of the system presented in Paper VI. Moreover, the author acted as co-supervisor for the Master's thesis project, within which the system was assembled and the software was developed

References

1. N.R. Finsen, *Phototherapy*, (Edward Arnold, London, England, 1901).
2. M.D. Daniell and J.S. Hill, A history of photodynamic therapy, *Aust. N. Z. J. Surg.* **61**, 340-348 (1991).
3. M. Cutler, Transilluminating as an aid in the diagnosis of breast lesions, *Surg. Gynecol. Obstet.* **48**, 721-728 (1929).
4. E. Viherkoski, Lasers in medicine, *Ann. Chir. Gynaecol.* **79**, 176-181 (1990).
5. F.P. Bolin, L.E. Preuss, R.C. Taylor and R.J. Ference, Refractive index of some mammalian tissue using a fiber optic cladding method, *Appl. Opt.* **28**, 2297-2303 (1989).
6. S.A. Prahl, Tabulated molar extinction coefficient for hemoglobin in water, http://omlc.ogi.edu/spectra/hemoglobin/summary.html, Accessed March 3, 1999, (1998).
7. G.M. Hale and M.R. Querry, Optical constants of water in the 200-nm to 200-µm wavelength region, *Appl. Opt.* **12**, 555-563 (1973).
8. S.L. Jacques, C.A. Alter and S.A. Prahl, Angular dependence of HeNe laser light scattering by human dermis, *Lasers Life Sci.* **1**, 309-333 (1987).
9. G. Yoon, A.J. Welch, M. Motamedi and M.J.C. van Gemert, Development and application of three-dimensional light distribution model for laser irradiated tissue, *IEEE J. Quant. Electr.* **QE-23**, 1721-1733 (1987).
10. M.R. Arnfield, J. Tulip and M.S. McPhee, Optical propagation in tissue with anisotropic scattering, *IEEE Trans. Biomed. Eng.* **35**, 372-381 (1988).
11. L.G. Henyey and J.L. Greenstein, Diffuse radiation in the galaxy, *Astrophys. J.* **93**, 70-83 (1941).
12. W.-F. Cheong, Summary of optical properties, in *Optical-thermal response of laser-irradiated tissue,* eds. A.J. Welch and M.J.C. van Gemert, pp. 275-303 (Plenum Press, New York, 1999).
13. W.M. Star, J.P.A. Marijnissen and M.J.C. van Gemert, Light dosimetry in optical phantoms and in tissue: 1 Multiple flux and transport theory, *Phys. Med. Biol.* **33**, 437-454 (1988).
14. J.H. Joseph, W.J. Wiscombe and J.A. Weinman, The delta-Eddington approximation for radiative flux transfer, *J. Atmos. Sci* **33**, 2452-2459 (1976).
15. W.M. Star, Diffusion theory of light transport, in *Optical-Thermal Response of Laser-Irradiated Tissue,* eds. A.J. Welch and M.J.C. van Gemert, pp. 131-206 (Plenum Press, New York, 1995).
16. V. Venugopalan, J.S. You and B.J. Tromberg, Radiative transport in the diffusion approximation: An extension for highly absorbing media and small source-detector separations, *Phys. Rev. E* **58**, 2395-2407 (1998).
17. A. Ishimaru, *Wave propagation and scattering in random media*, (Academic Press, New York, NY, 1978).
18. K.M. Case and P.F. Zweifel, *Linear transport theory*, (Addison-Wesley Publishing Co., Reading, MA, 1967).
19. M.S. Patterson, B. Chance and B.C. Wilson, Time resolved reflectance and transmittance for the non-invasive measurement of optical properties, *Appl. Opt.* **28**, 2331-2336 (1989).
20. F. Liu, K.M. Yoo and R.R. Alfano, Should the photon flux or the photon density be used to describe the temporal profiles of scattered ultrashort laser pulses in random media?, *Opt. Lett.* **18**, 432-434 (1993).
21. J.-M. Kaltenbach and M. Kaschke, Frequency- and time-domain modelling of light transport in random media, in *Medical Optical Tomography: Functional Imaging and Monitoring,* eds. G.J. Müller, B. Chance, R.R. Alfano, S.R. Arridge, J. Beuthan, E. Gratton, M. Kaschke, B.R. Masters, S. Svanberg and P. van der Zee, (SPIE Optical Engineering Press, Bellingham, Washington, USA, 1993).
22. S. Chandrasekar, Stochastic problems in physics and astronomy, *Reviews of Modern Physics* **15**, 1-89 (1943).
23. T.J. Farrell, M.S. Patterson and B. Wilson, A diffusion theory model of spatially resolved, steady-state diffuse reflectance for noninvasive determination of tissue optical properties *in vivo*, *Med. Phys.* **19**, 879-888 (1992).

24. M. Keijzer, W.M. Star and P.R.M. Storchi, Optical diffusion in layered media, *Appl. Opt.* **27**, 1820-1824 (1988).
25. R.C. Haskell, L.O. Svaasand, T.-T. Tsay, T.-C. Feng, M.S. McAdams and B.J. Tromberg, Boundary conditions for the diffusion equation in radiative transfer, *J. Opt. Soc. Am. A* **11**, 2727-2741 (1994).
26. J.R. Lakowicz, G. Laczo, I. Gryczynski, H. Szmacinski, W. Wiczk and M.L. Johnson, Frequency-domain fluorescence spectroscopy; principles, biochemical applications and future developments, *Ber. Bunsenges. Phys. Chem.* **93**, 316-327 (1989).
27. M.S. Patterson, J.D. Moulton, B.C. Wilson and B. Chance, Applications of time-resolved light scattering measurements to photodynamic therapy dosimetry, in *Photodynamic Therapy: Mechanisms II*, Proc. SPIE vol. **1203**, 62-75 (1990).
28. M.S. Patterson, J.D. Moulton, B.C. Wilson, K.W. Berndt and J.R. Lakowicz, Frequency-domain reflectance for the determination of the scattering and absorption properties of tissue, *Appl. Opt.* **30**, 4474-4476 (1991).
29. J. Fishkin, E. Gratton, M.J. vandeVen and W.W. Mantulin, Diffusion of intensity modulated near-infrared light in turbid media, in *Time-Resolved Spectroscopy and Imaging of Tissue*, ed. B. Chance, Proc. SPIE vol. **1431**, 122-135 (1991).
30. J.B. Fishkin and E. Gratton, Propagation of photon-density waves in strongly scattering media containing an absorbing semiinfinite plane bounded by a straight edge, *J. Opt. Soc. Am. A* **10**, 127-140 (1993).
31. S. Fantini, M.A. Franceschini and E. Gratton, Semi-infinite-geometry boundary problem for light migration in highly scattering media: a frequency-domain study in the diffusion approximation, *J. Opt. Soc. Am. B* **11**, 2128-2138 (1994).
32. J.B. Fishkin and E. Gratton, Propagation of photon density waves in strongly scattering media containing an absorbing semi-infinite plane bounded by a straight edge, *J. Opt. Soc. Am. A* **10**, 127-140 (1993).
33. M.A. O'Leary, D.A. Boas, B. Chance and A.G. Yodh, Refraction of diffuse photon density waves, *Phys. Rev. Lett.* **69**, 2658-2661 (1992).
34. A. Knüttel, J.M. Schmitt and J.R. Knutson, Spatial localization of absorbing bodies by interfering diffusive photon-density waves, *Appl. Opt.* **32**, 381-389 (1993).
35. J.M. Schmitt, A. Knüttel and J.R. Knutson, Interference of diffusive lightwaves, *J. Opt. Soc. Am.* **9**, 1832-1843 (1992).
36. B. Chance, K. Kang, L. He, J. Weng and E. Sevick, Highly sensitive object location in tissue models with linear in-phase and anti-phase multi-element optical arrays in one and two dimensions, *Proc. Natl. Acad. Sci. USA* **90**, 3423-3427 (1995).
37. C. Lindquist, A. Pifferi, R. Berg, S. Andersson-Engels and S. Svanberg, Reconstruction of diffuse photon-density wave interference in turbid media from time-resolved transmittance measurements, *Appl. Phys. Lett.* **69**, 1674-1676 (1996).
38. L. Wang and S.L. Jacques, Monte Carlo modeling of light transport in multi-layered tissues in standard C, (Laser Biology Research Laboratory, M. D. Anderson Cancer Center, University of Texas, Houston, Texas 1992).
39. S.T. Flock, B.C. Wilson, M.S. Patterson and D.R. Wyman, Monte Carlo modeling of light propagation in highly scattering tissues - I: Model predictions and comparison with diffusion theory, *IEEE Trans. Biomed. Eng.* **36**, 1162-1168 (1989).
40. R.A.J. Groenhuis, H.A. Ferwerda and J.J. ten Bosch, Scattering and absorption of turbid materials determined from reflection measurements. 1: Theory, *Appl. Opt.* **22**, 2456-2462 (1983).
41. M.S. Patterson, E. Schwartz and B.C. Wilson, Quantitative reflectance spectrophotometry for the noninvasive measurement of photosensitizer concentration in tissue during photodynamic therapy, Proc. SPIE vol. **1065**, 115-122 (1989).
42. M.G. Nichols, E.L. Hull and T.H. Foster, Design and testing of a white-light, steady-state diffuse reflectance spectrometer for determination of optical properties of highly scattering systems, *Appl. Opt.* **36**, 93-104 (1997).
43. T.H. Foster, D.F. Hartley, M.G. Nichols and R. Hilf, Fluence rate effects in photodynamic therapy of multicell tumor spheroids, *Cancer Res.* **53**, 1249-1254 (1993).

44. R.M.P. Doornbos, R. Lang, M.C. Aalders, F.W. Cross and H.J.C.M. Sterenborg, The determination of *in vivo* human tissue optical properties and absolute chromophore concentrations using spatially resolved steady state diffuse reflectance spectroscopy, *Physics in Medicine and Biology,* (1999). (In press).
45. T.J. Farrell, B.C. Wilson and M.S. Patterson, The use of a neural network to determine tissue optical properties from spatially resolved diffuse reflectance measurements, *Phys. Med. Biol.* **37**, 2281 (1992).
46. J.S. Dam, P.E. Andersen, T. Dalgaard and P.E. Fabricius, Determination of tissue optical properties from diffuse reflectance profiles by multivariate calibration, *Appl. Opt.* **37**, 772-778 (1998).
47. J.S. Wyatt, M. Cope, D.T. Delpy, S. Wray and E.O.R. Reynolds, Quantification of cerebral oxygenation and haemodynamics in sick newborn infants by near infrared spectrophotometry, *Lancet* 1063-1066 (1986).
48. D.T. Delpy, M. Cope, P. van der Zee, S. Arridge, S. Wray and J. Wyatt, Estimation of optical pathlength through tissue from direct time of flight measurement, *Phys. Med. Biol.* **33**, 1433-1442 (1988).
49. S.J. Madsen, B.C. Wilson, M.S. Patterson, Y.D. Park, S.L. Jacques and Y. Hefetz, Experimental tests of a simple diffusion model for the estimation of scattering and absorption coefficients of turbid media from time-resolved diffuse reflectance measure, *Appl. Opt.* **31**, 3509-3517 (1992).
50. A. Pifferi, R. Berg, P. Taroni and S. Andersson-Engels, Fitting of time-resolved reflectance curves with a Monte Carlo model, in *Advances in optical imaging and photon migration*, eds. R.R. Alfano and J.G. Fujimoto, Proc. Optical Society of America vol. **2**, 311-314 (1996).
51. A. Pifferi, P. Taroni, G. Valentini and S. Andersson-Engels, Real-time method for fitting time-resolved reflectance and transmittance measurements with a Monte Carlo model, *Appl. Opt.* **37**, 2774-2780 (1998).
52. R.F. Bonner, R. Nossal, S. Havlin and G.H. Weiss, Model for photon migration in turbid biological media, *J. Opt. Soc. Am. A* **4**, 423-432 (1987).
53. W. Cui, N. Wang and B. Chance, Study of photon migration depths with time-resolved spectroscopy, *Opt. Lett.* **16**, 1632-1634 (1991).
54. S. Feng, F.-A. Zeng and B. Chance, Perturbation theory of photon migration in the presence of a single defect, in *Advances in Optical Imaging and Photon Migration*, ed. R.R. Alfano, Proc. OSA vol. **21**, 217-228 (1994).
55. S. Feng, F. Zeng and B. Chance, Photon migration in the presence of a single defect: a perturbation analysis, *Appl. Opt.* **34**, 3826-3837 (1995).
56. M.S. Patterson, S. Andersson-Engels, B.C. Wilson and E.K. Osei, Absorption spectroscopy in tissue-simulating materials: a theoretical and experimental study of photon paths, *Appl. Opt.* **34**, 22-30 (1995).
57. S. Andersson-Engels, R. Berg, A. Persson and S. Svanberg, Multispectral tissue characterization with time-resolved detection of diffusely scattered white light, *Opt. Lett.* **18**, 1697-1699 (1993).
58. O. Jarlman, R. Berg, S. Andersson-Engels, S. Svanberg and H. Pettersson, Time-resolved white light transillumination for optical imaging, *Acta Radiol.* **38**, 185-189 (1997).
59. R. Cubeddu, A. Pifferi, P. Taroni, A. Torricelli and G. Valentini, Experimental test of theoretical models for time-resolved reflectance, *Med. Phys.* **23**, 1625-1633 (1996).
60. J. Johansson, R. Berg, A. Pifferi, S. Svanberg and L.O. Björn, Time-resolved studies of light propagation in *Crassula* and *Phaseolus* leaves, *Photochem. Photobiol.* **69**, 242-247 (1999).
61. J. Carlsson, P. Hellentin, L. Malmqvist, A. Persson, W. Persson and C.-G. Wahlström, Time-resolved studies of light propagation in paper, *Appl. Opt.* **34**, 1528-1535 (1995).
62. R. Berg, O. Jarlman and S. Svanberg, Medical transillumination imaging using short-pulse diode lasers, *Appl. Opt.* **32**, 574-579 (1993).
63. V. Ntziachristos, X.H. Ma, A.G. Yodh and B. Chance, Multichannel photon counting instrument for spatially resolved near infrared spectroscopy, *Rev. Sci. Instrum.* **10**, 193-201 (1999).
64. V. Ntziachristos, X.H. Ma and B. Chance, Time-correlated single photon counting imager for simultaneous magnetic resonance and near-infrared mammography, *Rev. Sci. Instrum.* **69**, 4221-4233 (1998).

65. J.C. Hebden, R.A. Kruger and K.S. Wong, Time resolved imaging through a highly scattering medium, *Appl. Opt.* **30**, 788-794 (1991).
66. K.M. Yoo, B.B. Das and R.R. Alfano, Imaging of a translucent object hidden in highly scattering medium from the early portion of the diffuse component of a transmitted ultrafast laser pulse, *Opt. Lett.* **17**, 958-960 (1992).
67. G. Mitic, J. Kölzer, J. Otto, E. Plies, G. Sölkner and W. Zinth, Time-gated transillumination of biological tissues and tissuelike phantoms, *Appl. Opt.* **33**, 6699-6710 (1994).
68. J.C. Hebden, Line scan acquisition for time-resolved imaging through scattering media, *Opt. Eng.* **32**, 626-633 (1993).
69. B.J. Tromberg, L.O. Svaasand, T.-T. Tsay and R.C. Haskell, Properties of photon density waves in multiple-scattering media, *Appl. Opt.* **32**, 607-616 (1993).
70. R.W. Boyd, *Nonlinear Optics*, (Academic Press, Inc., San Diego, CA, 1992).
71. R.G. Brewer, Frequency shifts in self-focused light, *Phys. Rev. Lett.* **19**, 8-10 (1967).
72. F. Shimizu, Frequency broadening in liquids by a short light pulse, *Phys. Rev. Lett.* **19**, 1097-1100 (1967).
73. A.C. Cheung, D.M. Rank, R.Y. Chiao and C.H. Townes, Phase modulation of Q-switched laser beams in small-scale filaments, *Phys. Rev. Lett.* **20**, 786-789 (1968).
74. R.R. Alfano and S.L. Shapiro, Observation of self-phase modulation and small-scale filaments in crystals and glasses, *Phys. Rev. Lett.* **24**, 592-594 (1970).
75. R.R. Alfano, ed., *The supercontinuum laser source*, (Springer-Verlag, New York, 1989).
76. S. Svanberg, J. Larsson, A. Persson and C.G. Wahlström, Lund high-power laser facility - systems and first results, *Physica Scripta* **49**, 187-197 (1994).
77. W.J. Jones and B.P. Stoicheff, Inverse Raman spectra: Induced absorption at optical frequencies, *Phys. Rev. Lett.* **13**, 657-659 (1964).
78. *Cancer incidence in Sweden 1996*, Official Statistics of Sweden, (The National Board of Health and Welfare, Sweden, 1998).
79. O. Jarlman, Diagnostic transillumination of the breast, Dissertation thesis, Lund University Hospital, Department of Diagnostic Radiology, Lund, Sweden (1991).
80. M. Swift, D. Morell, R.B. Massey and C.L. Chase, Incidence of cancer in 161 families affected by ataxia-telangiectasia, *N. Engl. J. Med.* **325**, 1831-1836 (1991).
81. R. Nowak, Discovery of AT gene sparks biomedical research bonanza, *Science* **268**, 1700-1701 (1995).
82. K. Savitsky, A. Barshira, S. Gilad, G. Rotman, Y. Ziv, L. Vanagaite, D.A. Tagle, S. Smith, T. Uziel, S. Sfez, M. Ashkenazi, I. Pecker, M. Frydman, R. Harnik, S.R. Patanjali, A. Simmons, G.A. Clines, A. Sartiel, R.A. Gatti, L. Chessa, O. Sanal, M.F. Lavin, N.G.J. Jaspers, A. Malcolm, R. Taylor, C.F. Arlett, T. Miki, S.M. Weissman, M. Lovett, F.S. Collins and Y. Shiloh, A single ataxia-telangiectasia gene with a product similar to PI-3 kinase, *Science* **268**, 1749-1753 (1995).
83. J. Cuzick, R. Holland, V. Barth, R. Davies, M. Faupel, I. Fentiman, H.J. Frischbier, J.L. LaMarque, M. Merson, V. Sacchini, D. Vanel and U. Veronesi, Electropotential measurements as a new diagnostic modality for breast cancer, *Lancet* **351**, 359-363 (1998).
84. B. Ohlsson, J. Gundersen and D.M. Nilsson, Diaphanography: a method for evaluation of the female breast, *World J. Surg.* **4**, 701-707 (1980).
85. R.J. Bartrum and H.C. Crow, Transillumination lightscanning to diagnose breast cancer: A feasibility study, *Am. J. Rad.* **142**, 409-414 (1984).
86. E.N. Carlsen, Transmission spectroscopy: An improvement in light scanning, *RNM Images* **13**, 22-25 (1983).
87. H. Key, P.C. Jackson and N.T. Wells, New approaches to transillumination imaging, *J. Biomed. Eng.* **10**, 113-119 (1988).
88. B. Drexler, J.L. Davis and G. Schofield, Diaphanography in the diagnosis of breast cancer, *Radiology* **157**, 41-44 (1985).
89. B. Monsees, J.M. Destouet and W.G. Totty, Light scanning versus mammography in breast cancer detection, *Radiology* **163**, 463-465 (1987).
90. J.H. Hoogenraad, M.B. van der Mark, S.B. Colak, G.W. 't Hooft and E.S. van der Linden, First results from the Philips Optical Mammoscope, in *Photon Propagation in Tissues III*, eds. D.A. Benaron, B. Chance and M. Ferrari, Proc. SPIE vol. **3194**, 184-190 (1998).

91. J.M. Maarek, G. Jarry, J. Crowe, M.-H. Bui and D. Laurent, Simulation of laser tomoscopy in a heterogeneous biological medium, *Med. Biol. Eng. Comput.* **24**, 407-414 (1986).
92. R. Berg, Time-resolved studies of light propagation in tissue, Master's thesis, Lund Institute of Technology, Lund, Sweden (1989).
93. S. Andersson-Engels, R. Berg, O. Jarlman and S. Svanberg, Time-resolved transillumination for medical diagnostics, *Opt. Lett.* **15**, 1179-1181 (1990).
94. K.M. Yoo and R.R. Alfano, Time-resolved coherent and incoherent components of forward light scattering in random media, *Opt. Lett.* **15**, 320-322 (1990).
95. S. Andersson-Engels, R. Berg and S. Svanberg, Effects of optical constants on time-gated transillumination of tissue and tissue-like media, *J. Photochem. Photobiol. B* **16**, 155-167 (1992).
96. J.C. Hebden, Time-resolved imaging of opaque and transparent spheres embedded in a highly scattering medium, *Appl. Opt.* **32**, 3837-3841 (1993).
97. V.G. Peters, D.R. Wyman, M.S. Patterson and G.L. Frank, Optical properties of normal and diseased human breast tissues in the visible and near infrared, *Phys. Med. Biol.* **35**, 1317-1334 (1990).
98. R. Cubeddu, A. Pifferi, P. Taroni, A. Torricelli and G. Valentini, Imaging of optical inhomogeneities in highly diffusive media: Discrimination between scattering and absorption contributions, *Appl. Phys. Lett.* **69**, 4162-4164 (1996).
99. S.R. Arridge and J.C. Hebden, Optical imaging in medicine: II. Modelling and reconstruction, *Phys. Med. Biol.* **42**, 841-853 (1997).
100. K. Wells, J.C. Hebden, F.E. Schmidt and D. Delpy, UCL multichannel time-resolved system for optical tomography, in *Optical Tomography and Spectroscopy of Tissue: Theory, Instrumentation, Model, and Human Studies II*, eds. B. Chance and R.R. Alfano, Proc. SPIE vol. **2979**, 599-607 (1997).
101. J.C. Hebden, Biomedical optics research group, research topics, http://www.medphys.ucl.ac.uk/research/borg/research.htm, (1999).
102. R. Grable, What is CTLM? Computed tomography laser mammography, http://www.imds.com/CTLM.htm, Accessed March 15, 1999, (1999).
103. E. Gratton, W.W. Mantulin, M.J. vandeVen, J. Fishkin, M.B. Maris and B. Chance, A novel approach to laser tomography, *Bioimaging* **1**, 40-46 (1993).
104. S.J. Madsen, E.R. Anderson, R.C. Haskell and B.J. Tromberg, Portable, high-bandwidth frequency-domain photon migration instrument for tissue spectroscopy, *Opt. Lett.* **19**, 1934-1936 (1994).
105. J.B. Fishkin, O. Coquoz, E.R. Anderson, M. Brenner and B.J. Tromberg, Frequency-domain photon migration measurements of normal and malignant tissue optical properties in a human subject, *Appl. Opt.* **36**, 10-20 (1997).
106. O. Coquoz, J.B. Fishkin, T.H. Pham and B.J. Tromberg, Quantitative measurements of tissue optical properties using phase and amplitude of photon density waves, *J. Opt. Soc. Am. A* (1998).
107. B.J. Tromberg, O. Coquoz, J.B. Fishkin, T. Pham, E.R. Anderson, J. Butler, M. Cahn, J.D. Gross, V. Venugopalan and D. Pham, Non-invasive measurements of breast tissue optical properties using frequency-domain photon migration, *Philos. Trans. R. Soc. Lond. B Biol. Sci.* **352**, 661-668 (1997).
108. C. Eker, N. Shah, T. Pham, J. Fishkin and B. Tromberg, Non-invasive determination of blood, water, and fat content in human breast tissue using frequency-domain photon migration spectroscopy, Manuscript in preparation (1998).
109. M. Kaschke, H. Jess, G. Gaida, J.-M. Kaltenbach and W. Wrobel, Transillumination imaging of tissue by phase modulation techniques, in *Advances in Optical Imaging and Photon Migration*, ed. R.R. Alfano, Proc. OSA vol. **21**, 88-92 (1994).
110. S. Fantini, M.A. Franceschini, G. Gaida and M. Kaschke, Frequency-domain optical mammography: the correction of tissue thickness variations within the scanned region, in *Photon Propagation in Tissues*, eds. B. Chance, D.T. Delpy and G.J. Müller, Proc. SPIE vol. **2626**, 228-236 (1995).
111. B. Chance, M. Cope, E. Gratton, N. Ramanujam and B. Tromberg, Phase measurements of light absorption and scatter in human tissue, *Rev. Sci. Instrum.* **69**, 3457-3481 (1998).
112. R. Berg, S. Andersson-Engels and S. Svanberg, Time-resolved transillumination imaging, in *Medical Optical Tomography: Functional Imaging and Monitoring,* eds. G.J. Müller, B. Chance, R.R.

Alfano, S.R. Arridge, J. Beuthan, E. Gratton, M. Kaschke, B.R. Masters, S. Svanberg and P. van der Zee, pp. 397-424 (SPIE Optical Engineering Press, Bellingham, Washington, USA, 1993).
113. J.C. Hebden, S.R. Arridge and D.T. Delpy, Optical imaging in medicine: I. Experimental techniques, *Phys. Med. Biol.* **42**, 825-840 (1997).
114. T.J. Dougherty, C.J. Gomer, B.W. Henderson, G. Jori, D. Kessel, M. Korbelik, J. Moan and Q. Peng, Photodynamic therapy, *J. Natl. Cancer Inst.* **90**, 889-905 (1998).
115. R. Bonnett and M. Berenbaum, Porphyrins as photosensitizers, eds. G. Bock and S. Harnett, pp. 40-59 (John Wiley & Sons Ltd, Chichester, UK, 1989).
116. J.S. Pangka, A.R. Morgan and D. Dolphin, Diels-Adler reactions of protoporphyrin IX dimethyl ester with electron-deficient alkynes, *J. Org. Chem.* **51**, 1094-1100 (1986).
117. D. Kessel, *In vitro* photosensitization with a benzoporphyrin derivative, *Photochem. Photobiol.* **49**, 579-582 (1989).
118. A.M. Richter, S. Cerruti-Sola, E.D. Sternberg, D. Dolphin and J.G. Levy, Biodistribution of tritiated benzoporphyrin derivative (^{3}H-BPD-MA), a new potent photosensitizer, in normal and tumor-bearing mice, *J. Photochem. Photobiol. B* **5**, 231-244 (1990).
119. G. Kostenich, A. Orenstein, L. Roitman, Z. Malik and B. Ehrenberg, In vivo photodynamic therapy with the new near-IR absorbing water soluble photosensitizer lutetium texaphyrin and a high intensity pulsed light delivery system, *J. Photochem. Photobiol. B* **39**, 36-42 (1997).
120. J.M. Fernandez, M.D. Bilgin and L.I. Grossweiner, Singlet oxygen generation by photodynamic agents, *J. Photochem. Photobiol. B* **37**, 131-140 (1997).
121. S. Andersson-Engels and B.C. Wilson, *In vivo* fluorescence in clinical oncology: fundamental and practical issues, *J. Cell Pharmacol.* **3**, 48-61 (1992).
122. T.G. Papazoglou, Malignant and atherosclerotic plaque diagnosis - is laser induced fluorescence spectroscopy the ultimate solution?, *J. Photochem. Photobiol. B* **28**, 3-11 (1995).
123. N.I. Berlin, A. Neuberger and J.J. Scott, The metabolism of δ-aminolaevulic acid. 1. Normal pathways, studied with the aid of ^{15}N, *Biochem. J.* **64**, 80-90 (1956).
124. N.I. Berlin, A. Neuberger and J.J. Scott, The metabolism of δ-aminolaevulic acid. 2. Normal pathways, studied with the aid of ^{14}C, *Biochem. J.* **64**, 90-100 (1956).
125. Z. Malik and H. Lugaci, Destruction of erythroleukaemic cells by photoinactivation of endogenous porphyrins, *Br. J. Cancer* **56**, 589-595 (1987).
126. Q. Peng, J.F. Evensen, C. Rimington and J. Moan, A comparison of different photosensitizing dyes with respect to uptake C3H-tumors and tissues of mice, *Cancer Lett.* **36**, 1-10 (1987).
127. J.C. Kennedy, R.H. Pottier and D.C. Pross, Photodynamic therapy with endogenous protoporphyrin IX: Basic principles and present clinical experience, *J. Photochem. Photobiol. B* **6**, 143-148 (1990).
128. J.C. Kennedy and R. Pottier, Endogenous protoporphyrin IX, a clinically useful photosensitizer for photodynamic therapy, *J. Photochem. Photobiol. B* **14**, 275-292 (1992).
129. L. Leibovici, N.I.L.I. Schoenfeld, H.A. Yehoshua, R. Mamet, R. Rakowski, A. Shindel and A. Atsmon, Activity of porphobilinogen deaminase in peripheral blood mononuclear cells of patients with metastatic cancer, *Cancer* **62**, 2297-2300 (1988).
130. M. Kondo, N. Hirota, T. Takaoka and M. Kajiwara, Heme-biosynthetic enzyme activities and porphyrin accumulation in normal liver and hepatoma cell lines of rat, *Cell Biol. Toxicol.* **9**, 95-105 (1993).
131. P. Hinnen, F.W.M. de Rooij, M.L.F. van Velthuysen, A. Edixhoven, R. van Hillegersberg, H.W. Tilanus, J.H.P. Wilson and P.D. Siersema, Biochemical basis of 5-aminolaevulinic acid-induced protoporphyrin IX accumulation: a study in patients with (pre)malignant lesions of the oesophagus, *Br. J. Cancer* **78**, 679-682 (1998).
132. H.A. Dailey and A. Smith, Differential interaction of porphyrins used in photoradiation therapy with ferrochelatase, *Biochem. J.* **223**, 441-445 (1984).
133. M.M.H. El-Sharabasy, A.M. El-Waseef, M.M. Hafez and S.A. Salim, Porphyrin metabolism in some malignant diseases, *Br. J. Cancer* **65**, 409-412 (1992).
134. R. van Hillegersberg, J.W.O. van den Berg, W.J. Kort, O.T. Terpstra and J.H.P. Wilson, Selective accumulation of endogenously produced porphyrins in a liver metastasis model in rats, *Gastroenterology* **103**, 647-651 (1992).

135. J. Regula, A.J. MacRobert, A. Gorchein, G.A. Buonaccorsi, S.M. Thorpe, G.M. Spencer, A.R. Hatfield and S.G. Bown, Photosensitisation and photodynamic therapy of oesophageal, duodenal and colorectal tumours using 5 aminolaevulinic acid induced protoporphyrin IX - a pilot study, *Gut* **36**, 67-75 (1995).
136. H. Heyerdahl, I. Wang, D.L. Liu, R. Berg, S. Andersson-Engels, Q. Peng, J. Moan, S. Svanberg and K. Svanberg, Pharmacokinetic studies on 5-aminolevulinic acid-induced protoporphyrin IX accumulation in tumours and normal tissues, *Cancer Lett.* **112**, 225-231 (1997).
137. Q. Peng, T. Warloe, K. Berg, J. Moan, M. Kongshaug, K.-E. Giercksky and J.M. Nesland, 5-aminolevulinic acid-based photodynamic therapy: clinical research and future challenges, *Cancer* **79**, 2282-2308 (1997).
138. W.D. Tope, E.V. Ross, N. Kollias, A. Martin, R. Gillies and R.R. Anderson, Protoporphyrin IX fluorescence induced in basal cell carcinoma by oral δ-aminolevulinic acid, *Photochem. Photobiol.* **67**, 249-255 (1998).
139. A. Orenstein, G. Kostenich and Z. Malik, The kinetics of protoporphyrin fluorescence during ALA-PDT in human malignant skin tumors, *Cancer Lett.* **120**, 229-234 (1997).
140. J.D. Spikes, The historical development of ideas on applications of photosensitised reactions in health sciences, in *Primary Photoprocesses in Biology and Medicine,* eds. R.V. Bergasson, G. Jori, E.J. Land and T.G. Truscott, pp. 209-227 (Plenum Press, New York, 1985).
141. J.M. Epstein, Phototherapy and photochemotherapy, *N. Engl. J. Med.* **32**, 1149-1151 (1990).
142. J.F. Cauvin, *Des bienfaits de l'insolation*, (, Paris, 1815).
143. T.B. Fitzpatrick and M.A. Pathak, Historical aspects of methoxsalen and other furocoumarins, *J. Invest. Dermatol.* **23**, 229-231 (1959).
144. O. Raab, Über die Wirkung fluoreszierenden Stoffe auf Infusoria, *Z. Biol.* **39**, 524-546 (1900).
145. H. von Tappeiner, Über die Wirkung Fluorescierenden Stoffe auf Infusiorien nach Versuchen von O. Raab, *Munch. Med. Wochenschr.* **47**, 5-5 (1900).
146. H. von Tappeiner and A. Jodlbauer, *Die sensibiliserende Wirkung fluorescierender Substanzer. Gasammette Untersuchungen über die photodynamische Erscheinung*, (FCW Vogel, Leipzig, 1907).
147. H. von Tappeiner and A. Jesionek, Therapeutische Versuche mit fluorescierenden Stoffen, *Munch. Med. Wochenschr.* **47**, 2042-2044 (1903).
148. W. Hausmann, Über die sensibilisierende Wirkung tierischer Farbstoffe und ihre physiologische Bedeutung, *Biochem. Z.* **14**, 275-278 (1908).
149. F. Meyer-Betz, Untersuchungen über die biologische (photodynamische) Wirkung des Hämatoporphyrins und andere Derivate des Blut- und Gallenfarbstoffs, *Dtsch. Arch. Klin. Med.* **112**, 476-450 (1913).
150. A. Policard, Etudes sur les aspects offerts par des tumeur experimentales examinée à la lumière de Woods, *CR. Soc. Biol.* **91**, 1423-1423 (1924).
151. H. Auler and G. Banzer, Untersuchungen über die Rolle der Porphyrin bei Geschwulstkranken Menschen und Tieren, *Z. Krebsforsch.* **53**, 65-68 (1942).
152. F.H.J. Figge, G.S. Weiland and L.O.J. Manganiello, Cancer detection and therapy: Affinity of neoplastic, embryonic and traumatised tissues for porphyrins and metalloporphyrins, *Proc. Soc. Exp. Med. Biol.* **68**, 640-641 (1948).
153. D.S. Rasmussen-Taxdal, G.E. Ward and F.H.J. Figge, Fluorescence of human lymphatic and cancer tissues following high doses of intraveneous haematoporphyrin, *Cancer* **8**, 78-81 (1955).
154. R.L. Lipson, E.J. Baldes and M.J. Gray, Hematoporphyrin derivative for detection and management of cancer, *Cancer* **20**, 2255-2257 (1967).
155. I. Diamond, S.G. Granelli, A.F. McDonagh, S.F. Nielsen, C.B. Wilson and R. Jaenicke, Photodynamic therapy of malignant tumours, *Lancet* **ii**, 1175-1177 (1972).
156. T.J. Dougherty, G.B. Grindey, R. Fiel, K.R. Weishaupt and D.G. Boyle, Photoradiation therapy II. Cure of animal tumors with haematoporphyrin and light, *J. Natl. Cancer Inst.* **55**, 115-119 (1975).
157. J.F. Kelly, M.E. Snell and M.C. Berenbaum, Photodynamic destruction of human bladder carcinoma, *Br. J. Cancer* **31**, 237-244 (1975).
158. T.J. Dougherty, J.E. Kaufman, A. Goldfarb, K.R. Weishaupt, D. Boyle and A. Mittleman, Photoradiation therapy for the treatment of malignant tumors, *Cancer Res.* **38**, 2628-2635 (1978).

159. F. Urbach, P.D. Forbes, R.E. Davies and D. Berger, Cutaneous photobiology: past, present and future, *J. Invest. Dermatol.* **67**, 209-224 (1976).
160. J. Moan and K. Berg, The photodegradation of porphyrins in cells can be used to estimate the lifetime of singlet oxygen, *Photochem. Photobiol.* **53**, 549-553 (1991).
161. G.S. Cox and D.G. Whitten, Mechanisms for the photooxidation of protoporphyrin IX in solution, *J. Am. Chem. Soc.* **104**, 516-521 (1982).
162. K. König, H. Wabnitz and W. Dietel, Variation in the fluorescence decay properties of haematoporphyrin derative during its conversion to photoproducts, *J. Photochem. Photobiol. B* **8**, 103-111 (1990).
163. K. König, H. Schneckenburger, A. Rück and R. Steiner, *In vivo* photoproduct formation during PDT with ALA-induced endogenous porphyrins, *J. Photochem. Photobiol. B* **18**, 287-290 (1993).
164. R. Rotomskis, S. Bagdonas and G. Streckyte, Spectroscopic studies of photobleaching and photoproproduct formation of porphyrins used in tumour therapy, *J. Photochem. Photobiol. B* **33**, 61-67 (1996).
165. J. Moan and D. Kessel, Photoproducts formed from Photofrin II in cells, *J. Photochem. Photobiol. B* **1**, 429-436 (1988).
166. E.F. Gudgin Dickson and R. Pottier, On the role of protoporphyrin IX photoproducts in photodynamic therapy, *J. Photochem. Photobiol. B* **29**, 91-93 (1995).
167. P. Charlesworth and T.G. Truscott, The use of 5-aminolevulinic acid (ALA) in photodynamic therapy (PDT), *J. Photochem. Photobiol. B* **18**, 99-100 (1993).
168. K. Svanberg, T. Andersson, D. Killander, I. Wang, U. Stenram, S. Andersson-Engels, R. Berg, J. Johansson and S. Svanberg, Photodynamic therapy of non-melanoma malignant tumours of the skin using topical δ-amino levulinic acid sensitization and laser irradiation, *Br. J. Dermatol.* **130**, 743-751 (1994).
169. I. Wang, B. Bauer, S. Andersson-Engels, S. Svanberg and K. Svanberg, Photodynamic therapy utilising topical δ-aminolevulinic acid in non-melanoma skin malignancies of the eyelid and the periocular skin, *Acta Ophthalmologica Scandinavica,* (1998). (In press).
170. D.L. Liu, I. Wang, S. Andersson-Engels, C.H. Håkansson, U. Stenram and K. Svanberg, Intra-operative laser-induced photodynamic therapy in the treatment of experimental hepatic tumours, *Eur. J. Gastroenterol. Hepatol.* **7**, 1073-1080 (1995).
171. A.M.K. Nilsson, R. Berg and S. Andersson-Engels, Measurements of the optical properties of tissue in conjunction with photodynamic therapy, *Appl. Opt.* **34**, 4609-4619 (1995).
172. K. Svanberg, D.L. Liu, I. Wang, S. Andersson-Engels, U. Stenram and S. Svanberg, Photodynamic therapy using intravenous δ-aminolaevulinic acid-induced protoporphyrin IX sensitisation in experimental hepatic tumours in rats, *Br. J. Cancer* **74**, 1526-1533 (1996).
173. D.M. Fiedler, G. Schnitzhofer, H. Walt, D. Dobler-Girdziunaite and B. Krammer, Photodynamic cytotoxicity enhancement by pulsed diode laser irradiation, To appear (1999).
174. A. Busetti, M. Soncin and G. Jori, A novel diode laser system delivering structured light for photodynamic therapy, Manuscript in preparation (1998).
175. L.D. Lilge, G. Pang, J. Jonkman and B.C. Wilson, Feasibility study of PDT light sources based on lasing action in strongly scattering media, in *Optical Methods for Tumor Treatment and Detection: Mechanisms and Techniques in Photodynamic Therapy VI*, ed. T.J. Dougherty, Proc. SPIE vol. **2927**, 130-135 (1997).
176. T. Udagawa, K. Takaoka, K. Inoue, N. Hanafus, S. Fukutomi, S. Mimura, Y. Tenjin and H. Kato, Development of a new solid state tunable laser for photodynamic therapy, in *7th Biennial Congress of the International Photodynamic Association*, ed. T. Patrice, RC12 (1998).
177. S. Fijan, H. Hönigsmann and B. Ortel, Photodynamic therapy of epithelial skin tumours using delta-aminolaevulinic acid and desferrioxamine, *Br. J. Dermatol.* **133**, 282-288 (1995).
178. P. Wolf, E. Rieger and H. Kerl, Topical photodynamic therapy with endogenous porphyrins after application of 5-aminolevulinic acid. An alternative treatment modality for solar keratoses, superficial squamous cell carcinomas, and basal cell carcinomas?, *J. Am. Acad. Dermatol.* **28**, 17-21 (1993).
179. A.M. Wennberg, L.E. Lindholm, M. lpsten and O. Larkö, Treatment of superficial basal cell carcinomas using topically applied delta-aminolaevulinic acid and a filtered xenon lamp, *Arch. Dermatol. Res.* **288**, 561-564 (1996).

180. C.A. Morton, R.M. Mackie, C. Whitehurst, J.V. Moore and J.H. McColl, Photodynamic therapy for basal cell carcinoma: effect of tumor thickness and duration of photosensitizer application on response, *Arch. Dermatol.* **134**, 248-249 (1998).
181. C. Whitehurst, K. Byrne and J.V. Moore, Development of an alternative light source to lasers for photodynamic therapy: 1. Comparative in vitro dose response characteristics, *Lasers Med. Sci.* **8**, 259-267 (1993).
182. C.A. Morton, C. Whitehurst, H. Moseley, J.V. Moore and R.M. Mackie, Development of an alternative light source to lasers for photodynamic therapy: 3. Clinical evaluation in the treatment of pre-malignant non-melanoma skin cancer, *Lasers Med. Sci.* **10**, 165-171 (1995).
183. T. Warloe, Photodynamic therapy of human malignant tumors, Dissertation thesis, University of Oslo, Oslo, Norway (1995).
184. J. Moan, V. Iani and L.W. Ma, Choice of the proper wavelength for photochemotherapy, in *Photochemotherapy: Photodynamic Therapy and Other Modalities*, eds. B. Ehrenberg, G. Jori and J. Moan, Proc. SPIE vol. **2625**, 544-549 (1996).
185. M.R. Stringer, Problems associated with the use of broad-band illumination sources for photodynamic therapy, *Phys. Med. Biol.* **40**, 1733-1735 (1995).
186. S.M. Waldow and T.J. Dougherty, Interaction of hyperthermia and photoradiation therapy, *Radiat. Res.* **97**, 380-385 (1984).
187. S. Kimel, L.O. Svaasand, M. Hammer-Wilson, V. Gottfried, S. Cheng, E. Svaasand and M.W. Berns, Demonstration of synergistic effects of hyperthermia and photodynamic therapy using the chich chorioallantoic membrane model, *Lasers Surg. Med.* **12**, 432-440 (1992).
188. L.O. Svaasand, Photodynamic and photohyperthermic response of malignant tumors, *Med. Phys.* **12**, 455-461 (1985).
189. B.C. Wilson, Light sources for photodynamic therapy, *Photodynamics News* **1**, 6-8 (1998).
190. A.C. Lytle, B.K. Dalton, D.R. Doiron, R.W. Keck, S.H. Selman and M.E. Wagoner, Light emitting diode source for photodynamic therapy, in *Optical Methods for Tumor Treatment and Detection: Mechanisms and Techniques in Photodynamic Therapy II*, ed. T.J. Dougherty, Proc. SPIE vol. **1881**, 180-188 (1993).
191. J.C. Chen, Next-generation light delivery system for multitreatmentextended-duration photodynamic therapy (MED-PDT), in *Optical Methods for Tumor Treatment and Detection: Mechanisms and Techniques in Photodynamic Therapy VI*, ed. T.J. Dougherty, Proc. SPIE vol. **2972**, 161-167 (1997).
192. L.I. Grossweiner, PDT light dosimetry revisited, *J. Photochem. Photobiol. B* **38**, 258-268 (1997).
193. L.O. Svaasand, B.J. Tromberg, P. Wyss, M.-T. Wyss-Desserich, Y. Tadir and M.W. Berns, Light and drug distribution with topically administered photosensitizers, *Lasers Med. Sci.* **11**, 261-265 (1996).
194. L.O. Svaasand, P. Wyss, M.T. Wyss, Y. Tadir, B.J. Tromberg and M.W. Berns, Dosimetry model for photodynamic therapy with topically administered photosensitizers, *Lasers Surg. Med.* **18**, 139-149 (1996).
195. R. Cubeddu, G. Canti, M. Musolino, A. Pifferi, P. Taroni and G. Valentini, Absorption-spectrum of hematoporphyrin derivative in-vivo in a murine tumor-model, *Photochem. Photobiol.* **60**, 582-585 (1994).
196. W.M. Star, J. Versteeg, W. van Putten and H. Marijnissen, Wavelength dependence of hematoporphyrin derivative photodynamic treatment effects on rat ears, *Photochem. Photobiol.* **52**, 547-554 (1990).
197. T.J. Farrell, M.C. Olivo, M.S. Patterson, H. Wrona and B.C. Wilson, Investigation of the dependence of tissue necrosis on irradiation wavelength and time post injection using a photodynamic threshold dose model, in *Photodynamic Therapy and Biomedical Lasers,* eds. P. Spinelli, M. Dal Fante and R. Marchesini, pp. 830-834 (Elsevier, Amsterdam, the Netherlands, 1992).
198. G.H.M. Gijsbers, D. Breederveld, M.J.C. van Gemert, T.A. Boon, J. Langelaar and R.P.H. Rettschnick, In vivo fluorescence excitation and emission spectra of hematoporphyrin-derivative, *Lasers Life Sci.* **1**, 29-48 (1986).
199. C.J. Gomer, D.R. Doiron, N. Rucker, N.J. Razum and S.W. Fountain, Action spectrum (620-640 nm) for hematoporphyrin derivative induced cell killing, *Photochem. Photobiol.* **39**, 365-368 (1984).

200. J. Griffiths, J. Cruse-Sawyer, S.R. Wood, J. Schofield, S.B. Brown and B. Dixon, On the photodynamic therapy action spectrum of zinc phthalocyanine tetrasulphonic acid *in vivo*, *J. Photochem. Photobiol. B* **24**, 195-199 (1994).
201. R. Cubeddu, G. Canti, M. Musolino, A. Pifferi, P. Taroni and G. Valentini, In vivo absorption spectrum of disulphonated aluminium phthalocyanine in a murine tumour model, *J. Photochem. Photobiol. B* **34**, 229-235 (1996).
202. M. Ambroz, A.J. MacRobert, J. Morgan, G. Rumbles, M.S.C. Foley and D. Phillips, Time-resolved fluorescence spectroscopy and intracellular imaging of disulphonated aluminium phthalocyanine, *J. Photochem. Photobiol.* **22**, 105-117 (1994).
203. J. Moan, K. Berg, J.C. Bommer and A. Western, Action spectra of phthalocyanines with respect to photosensitization of cells, *Photochem. Photobiol.* **56**, 171-175 (1992).
204. R.A. Weersink, J.E. Hayward, K.R. Diamond and M.S. Patterson, Accuracy of noninvasive *in vivo* measurements of photosensitizer uptake based on a diffusion model of reflectance spectroscopy, *Photochem. Photobiol.* **66**, 326-335 (1997).
205. R.B. Veenhuizen and F.A. Stewart, The importance of fluence rate in photodynamic therapy: is there a parallel with ionizing radiation dose-rate effects?, *Radiother. Oncol.* **37**, 131-135 (1995).
206. T.H. Foster, R.S. Murant, R.G. Bryant, R.S. Knox, S.L. Gibson and R. Hilf, Oxygen consumption and diffusion effects in photodynamic therapy, *Radiat. Res.* **126**, 296-303 (1991).
207. I.P.J. van Geel, H. Oppelaar, J.P.A. Marijnissen and F.A. Stewart, Influence of fractionation and fluence rate in photodynamic therapy with Photofrin or mTHPC, *Radiat. Res.* **145**, 602-609 (1996).
208. S.A. Blant, A. Woodtli, G. Wagnières, C. Fontolliet, H. van den Bergh and P. Monnier, In vivo fluence rate effect in photodynamic therapy of early cancers with tetra(m-hydroxyphenyl)chlorin, *Photochem. Photobiol.* **64**, 963-968 (1996).
209. T.M. Sitnik and B.W. Henderson, The effect of fluence rate on tumor and normal tissue responses to photodynamic therapy, *Photochem. Photobiol.* **67**, 462-466 (1998).
210. T.M. Sitnik, J.A. Hampton and B.W. Henderson, Reduction of tumour oxygenation during and after photodynamic therapy in vivo: effects of fluence rate, *Br. J. Cancer* **77**, 1386-1394 (1998).
211. Q. Chen, M. Chopp, M.O. Dereski, B.C. Wilson, M.S. Patterson, A. Schreiber and F.W. Hetzel, The effect of light fluence rate in photodynamic therapy of normal rat brain, *Radiat. Res.* **132**, 120-123 (1992).
212. D.J. Robinson, H.S. de Bruijn, N. van der Veen, M.R. Stringer, S.B. Brown and W.M. Star, Fluorescence photobleaching of ALA-induced protoporphyrin IX during photodynamic therapy of normal hairless mouse skin: The effect of light dose and irradiance and the resulting biological effect, *Photochem. Photobiol.* **67**, 140-149 (1998).
213. D.J. Robinson, H.S. de Bruijn, N. van der Veen, M.R. Stringer, S.B. Brown and W.M. Star, Protoporphyrin IX fluorescence photobleaching during ALA-mediated photodynamic therapy of UVB-induced tumors in hairless mouse skin, *Photochem. Photobiol.* **69**, 61-70 (1999).
214. B.W. Pogue, L. Lilge, M.S. Patterson, B.C. Wilson and T. Hasan, Absorbed photodynamic dose from pulsed versus continuous wave light examined with tissue-simulating dosimeters, *Appl. Opt.* **36**, 7257-7269 (1997).
215. M. LaPlant, J. Parker, B. Stewart, M. Waner and R.C. Straight, Comparison of the optical transmission properties of pulsed and continuous wave light in biological tissue, *Lasers Surg. Med.* **7**, 336-338 (1987).
216. P.C. Rausch, F. Rolfs, M.R. Winkler, A. Kottysch, A. Schauer and W. Steiner, Pulsed versus continuous wave excitation mechanisms in photodynamic therapy of differently graded squamous cell carcinomas in tumor-implanted nude mice, *Eur. Arch. Otorhinolaryngol.* **250**, 82-87 (1993).
217. T. Okunaka, H. Kato, C. Konaka, H. Sakai, H. Kawabe and K. Aizawa, A comparison between argon-dye and excimer-dye laser for photodynamic effect in transplanted mouse-tumor, *Jpn. J. Cancer Res.* **83**, 226-231 (1992).
218. P.A. Cowled, J.R. Grace and I.J. Forbes, Comparison of the efficacy of pulsed and continuous-wave red laser light in induction of photocytotoxicity by haematoporphyrin derivative, *Photochem. Photobiol.* **39**, 115-117 (1984).

219. M.J. Shikowitz, Comparison of pulsed and continuous wave light in photodynamic therapy of papillomas: An experimental study, *Laryngoscope* **102**, 300-310 (1992).
220. A.H. Kaye, G. Morstyn and D. Brownbill, Adjuvant high-dose photoradiation therapy in the treatment of cerebral glioma: a phase 1-2 study, *J. Neurosurg.* **67**, 500-505 (1987).
221. M. Panjehpour, F. Bergein, F. Overholt, R.C. DeNovo, M.G. Petersen and R.E. Sneed, Comparative study between pulsed and continuous wave lasers for Photofrin photodynamic therapy, *Lasers Surg. Med.* **13**, 296-304 (1993).
222. A. Ferrario, N. Rucker, S.W. Ryter, D.R. Doiron and C.J. Gomer, Direct comparison of in-vitro and in-vivo Photofrin-II mediated photosensitization using a pulsed KTP pumped dye laser and a continuous wave argon ion pumped dye laser, *Lasers Surg. Med.* **11**, 404-410 (1991).
223. A.J. Pope, J.R.W. Masters and A.J. MacRobert, The photodynamic effect of a pulsed dye laser on human bladder carcinoma cells in vitro, *Urol. Res.* **18**, 267-270 (1990).
224. D.A. Bellnier, C.-W. Lin, J.A. Parrish and P.C. Mock, Hematoporphyrin derivative and pulse laser photoradiation, in *Porphyrin localization and treatment of tumours,* eds. D.R. Doiron and C.J. Gomer, pp. 533-540 (Alan R. Liss, Inc., New York, NY, 1984).
225. H.J.C.M. Sterenborg and M.J.C. van Gemert, Photodynamic therapy with pulsed light sources: a theoretical analysis, *Phys. Med. Biol.* **41**, 835-849 (1996).
226. T.H. Foster and L. Gao, Dosimetry in photodynamic therapy: oxygen and the critical importance of capillary density, *Radiat. Res.* **130**, 379-383 (1992).
227. J.F. Evensen and J. Moan, Photodynamic therapy of C3H tumours in mice: Effect of drug/light dose fractionation and Misonidazole., *Lasers Med. Sci.* **3**, 1-6 (1988).
228. J. Moan and T. Christensen, Photodynamic inactivation of cancer cells in vitro. Effect of irradiation temperature and dose fractionation, *Cancer Lett.* **6**, 331-335 (1979).
229. K. Berg, K. Madslien and J. Moan, Retention and phototoxicity of tetra(4-sulfonatophenyl)porphine in cultivated human cells. The effect of fractionation of light, *Photochem. Photobiol.* **56**, 177-183 (1992).
230. H. Messmann, P. Mlkvy, G. Buonaccorsi, C.L. Davies, A. MacRobert and S.G. Bown, Enhancement of photodynamic therapy with 5-aminolaevulinic acid-induced porphyrin photosensitisation in normal rat colon by threshold and light fractionation studies, *Br. J. Cancer* **72**, 589-594 (1995).
231. A. Curnow, B.W. McIlroy, M.J. Postle-Hacon, A.J. MacRobert and S.G. Bown, Light dose fractionation to enhance photodynamic therapy using 5-aminolevulinic acid in the normal rat colon, *Photochem. Photobiol.* **69**, 71-76 (1999).
232. H. Anholt and J. Moan, Fractionated treatment of CaD2 tumors in mice sensitized with aluminium phthalocyanine tetrasulfonate, *Cancer Lett.* **61**, 263-267 (1992).
233. S. Müller, H. Walt, D. Dobler-Girdziunaite, D. Fiedler and U. Haller, Enhanced photodynamic effects using fractionated laser light, *J. Photochem. Photobiol.* **42**, 67-70 (1998).
234. B.C. Wilson, M.S. Patterson, S.T. Flock and D.R. Wyman, Tissue optical properties in relation to light propagation models and in vivo dosimetry, in *Photon migration in tissue,* ed. B. Chance, pp. 24-42 (Plenum, New York, 1989).
235. S. Svanberg, S. Andersson-Engels, R. Berg, J. Johansson and K. Svanberg, Interaktivt system för fotodynamisk eller fototermisk behandling av tumörer utnyttjande multipla interstitiella fibrer, Swedish patent application, (1995).
236. N. Ohlsson and O. Rylow, Development of a multifibre system for interstitial photodynamic therapy of malignant tumours, Master's thesis, Lund Institute of Technology, Lund, Sweden (1998).
237. A.E. Profio, Review of fluorescence diagnosis using porphyrins, Proc. SPIE vol. **907**, 150-156 (1988).
238. A.E. Profio, Fluorescence diagnosis and dosimetry using porphyrins, in *Photodynamic Therapy of Neoplastic Disease,* ed. D. Kessel, pp. 77-89 (CRC Press, Boca Raton, FL, 1990).
239. A.E. Profio, Endoscopic fluorescence detection of early lung cancer, in *Optical Methods for Tumor Treatment and Early Diagnosis: Mechanisms and Techniques*, ed. T.J. Dougherty, Proc. SPIE vol. **1426**, 44-46 (1991).

240. I.J. Bigio and J.R. Mourant, Ultraviolet and visible spectroscopies for tissue diagnostics: fluorescence spectroscopy and elastic-scattering spectroscopy, *Phys. Med. Biol.* **42**, 803-814 (1997).
241. S. Andersson-Engels, C. af Klinteberg, K. Svanberg and S. Svanberg, In vivo fluorescence imaging for tissue diagnostics, *Phys. Med. Biol.* **42**, 815-824 (1997).
242. G.A. Wagnières, W.M. Star and B.C. Wilson, *In vivo* fluorescence spectroscopy and imaging for oncological applications, *Photochem. Photobiol.* **68**, 603-632 (1998).
243. G.G. Stokes, Über die Änderung der Brechbarkeit des Lichtes, *Phil. Transact.* **107**, 11-11 (1852).
244. H. Stübel, Die Fluoreszenz tierischer Gewebe in ultravioletten Licht, *Pflügers Arch.* **142**, 1-1 (1911).
245. R.P. Rava, R. Richards-Kortum, M. Fitzmaurice, R.M. Cothren, R.E. Petras, M.V. Sivak, H. Levin and M.S. Feld, Early detection of dysplasia in colon and bladder tissue using laser induced fluorescence, in *Optical Methods for Tumor Treatment and Early Diagnosis: Mechanisms and Techniques*, ed. T.J. Dougherty, Proc. SPIE vol. **1426**, 68-78 (1991).
246. R. Richards-Kortum, R.P. Rava, R.E. Petras, M. Fitzmaurice, M.V. Sivak and M.S. Feld, Spectroscopic diagnosis of colonic dysplasia, *Photochem. Photobiol.* **53**, 777-786 (1991).
247. A. Mahadevan, M.F. Mitchell, E. Silva, S. Thomsen and R. Richards-Kortum, Study of the fluorescence properties of normal and neoplastic human cervical tissue, *Lasers Surg. Med.* **13**, 647-655 (1993).
248. S. Andersson-Engels, L. Baert, R. Berg, M.A. D'Hallewin, J. Johansson, U. Stenram, K. Svanberg and S. Svanberg, Fluorescence characteristics of human atherosclerotic plaque and malignant tumors, in *Optical Methods for Tumor Treatment and Early Diagnosis: Mechanisms and Techniques*, ed. T.J. Dougherty, Proc. SPIE vol. **1426**, 31-43 (1991).
249. D.H. Blankenhorn and H. Braunstein, Carotenoids in man III. The microscopic pattern of fluorescence in atheromas, and its relation to their growth, *J. Clin. Invest.* **37**, 160-165 (1958).
250. B. Chance and L. Thorell, Localization and kinetics of reduced pyridine nucleotide in living cells by microfluorometry, *J. Biol. Chem.* **234**, 3044-3050 (1959).
251. I. Berlman, *Handbook of fluorescence spectra of aromatic molecules, 2nd Edition*, (Academic Press, New York, NY, 1971).
252. D.M. Kirschenbaum, ed., *Atlas of protein spectra in the ultraviolet and visible regions*, vol. **II**, (IFI/Plenum Press, New York, NY, 1974).
253. M.R. Hubmann, M.J.P. Leiner and R.J. Schaur, Ultraviolet fluorescence of human sera: I. Sources of characteristic differences in the ultraviolet fluorescence spectra of sera from normal and cancer-bearing humans, *Clin. Chem.* **36**, 1880-1883 (1990).
254. B. Chance, P. Cohen, F. Jöbsis and B. Schoener, Intracellular oxidation-reduction states in vivo, *Science* **137**, 499-508 (1962).
255. W. Lohmann, J. Mussmann, C. Lohmann and W. Künzel, Native fluorescence of the cervix uteri as a marker for dysplasia and invasive carcinoma, *Eur. J. Obstet. Gynecol. Reprod. Biol.* **31**, 249-253 (1989).
256. S. Andersson-Engels, J. Johansson, U. Stenram, K. Svanberg and S. Svanberg, Malignant tumor and atherosclerotic plaque diagnosis using laser-induced fluorescence, *IEEE J. Quant. Electr.* **26**, 2207-2217 (1990).
257. R.C. Benson, R.A. Meyer, M.E. Zaruba and G.M. McKhann, Cellular autofluorescence - is it due to flavins?, *J. Histochem. Cytochem.* **27**, 44-48 (1979).
258. R.R. Alfano, D.B. Tata, J. Cordero, P. Tomashefsky, F.W. Longo and M.A. Alfano, Laser induced fluorescence spectroscopy from native cancerous and normal tissue, *IEEE J. Quant. Electr.* **QE-20**, 1507-1511 (1984).
259. Y. Yang, Y. Ye, F. Li, Y. Li and P. Ma, Characteristic autofluorescence for cancer diagnosis and its origin, *Lasers Surg. Med.* **7**, 528-532 (1987).
260. W. Lohmann and E. Paul, Native fluorescence of unstained cryosections of the skin with melanomas and naevi, *Naturwissenschaften* **76**, 424-426 (1989).
261. L. Baert, R. Berg, B. van Damme, M.A. D'Hallewin, J. Johansson, K. Svanberg and S. Svanberg, Clinical fluorescence diagnosis of human bladder carcinoma following low-dose Photofrin injection, *Urology* **41**, 322-330 (1993).
262. S. Svanberg, *Atomic and molecular spectroscopy*, (Springer Verlag, Heidelberg, Germany, 1992).

263. S. Andersson-Engels, Å. Elner, J. Johansson, S.-E. Karlsson, L.G. Salford, L.-G. Strömblad, K. Svanberg and S. Svanberg, Clinical recording of laser-induced fluorescence spectra for evaluation of tumour demarcation feasibility in selected clinical specialities, *Lasers Med. Sci.* **6**, 415-424 (1991).
264. J. Johansson, Fluorescence spectroscopy for medical and environmental diagnostics, Dissertation thesis, Lund Institute of Technology, Lund, Sweden (1993).
265. R. Berg, Laser-based cancer diagnostics and therapy - Tissue optics considerations, Dissertation thesis, Lund Institute of Technology, Lund, Sweden (1995).
266. I. Wang, Photodynamic therapy and laser-based diagnostic studies of malignant tumours, Dissertation thesis, Lund University, Lund, Sweden (1999).
267. W. Alian, S. Andersson-Engels, K. Svanberg and S. Svanberg, Laser-induced fluorescence studies of *meso*-tetra(hydroxyphenyl)chlorin in malignant and normal tissues in rat, *Br. J. Cancer* **70**, 880-885 (1994).
268. M. Andreasson and O. Sandström, The design and implementation of a compact fluoresensor for medical diagnostics, Master's thesis, Lund Institute of Technology, Lund, Sweden (1998).
269. R.L. Lipson, E.J. Baldes and A.M. Olsen, Hematoporphyrin derivative: A new aid for endoscopic detection of malignant disease, *J. Thorac. Cardiovasc. Surg.* **42**, 623-629 (1961).
270. R.L. Lipson, J.H. Pratt, E.J. Baldes and M.B. Dockerty, Hematoporphyrin derivative for detection of cervical cancer, *Obstet. Gynecol.* **24**, 78-84 (1964).
271. A.E. Profio and D.R. Doiron, A feasibility study of the use of fluorescence bronchoscopy for localization of small lung tumours, *Phys. Med. Biol.* **22**, 949-957 (1977).
272. D.R. Doiron, E. Profio, R.G. Vincent and T.J. Dougherty, Fluorescence bronchoscopy for detection of lung cancer, *Chest* **76**, 27-32 (1979).
273. A.E. Profio, D.R. Doiron, O.J. Balchum and G.C. Huth, Fluorescence bronchoscopy for localization of carcinoma *in situ*, *Med. Phys.* **10**, 35-39 (1983).
274. T. Hirano, M. Ishizuka, K. Suzuki, K. Ishida, S. Suzuki, S. Miyaki, A. Honma, M. Suzuki, K. Aizawa, H. Kato and Y. Hayata, Photodynamic cancer diagnosis and treatment system consisting of pulse lasers and an endoscopic spectro-image analyzer, *Lasers Life Sci.* **3**, 1-18 (1989).
275. S. Montán, K. Svanberg and S. Svanberg, Multi-color imaging and contrast enhancement in cancer tumor localization using laser-induced fluorescence in hematoporphyrin derivative (HpD)-bearing tissue, *Opt. Lett.* **10**, 56-58 (1985).
276. S. Andersson-Engels, J. Johansson and S. Svanberg, Multicolor fluorescence imaging system for fluorescence diagnostics, in *Bioimaging and Two-Dimensional Spectroscopy*, ed. L.C. Smith, Proc. SPIE vol. **1205**, 179-189 (1990).
277. S. Andersson-Engels, J. Johansson, K. Svanberg and S. Svanberg, Fluorescence imaging and point measurements of tissue: Applications to the demarcation of malignant tumors and atherosclerotic lesions from normal tissue, *Photochem. Photobiol.* **53**, 807-814 (1991).
278. K. Svanberg, I. Wang, S. Colleen, I. Idvall, C. Ingvar, R. Rydell, D. Jocham, H. Diddens, S. Bown, G. Gregory, S. Montán, S. Andersson-Engels and S. Svanberg, Clinical multi-colour fluorescence imaging of malignant tumours - initial experience, *Acta Radiol.* **39**, 2-9 (1998).
279. Z. Malik, M. Dishi and Y. Garini, Fourier transform multipixel spectroscopy and spectral imaging of protoporphyrin in single melanoma cells, *Photochem. Photobiol.* **63**, 608-614 (1996).
280. R. Cubeddu, F. Docchio, W.Q. Liu, R. Ramponi and P. Taroni, A system for time-resolved laser fluorescence spectroscopy with multiple picosecond gating, *Rev. Sci. Instrum.* **59**, 2254-2259 (1988).
281. R. Cubeddu, G. Canti, P. Taroni and G. Valentini, Tumour visualization in a murine model by time-delayed fluorescence of sulphonated aluminium phthalocyanine, *Lasers Med. Sci.* **12**, 200-208 (1997).
282. R. Cubeddu, G. Canti, A. Pifferi, P. Taroni and G. Valentini, Fluorescence lifetime imaging of experimental tumors in hematoporphyrin derivative-sensitized mice, *Photochem. Photobiol.* **66**, 229-236 (1997).
283. R. Cubeddu, A. Pifferi, P. Taroni, G. Valentini, G. Canti, C. Lindquist, S. Andersson-Engels, S. Svanberg, I. Wang and K. Svanberg, Multispectral and lifetime imaging for the detection of skin tumors, in *Biomedical Optical Spectroscopy and Diagnostics / Therapeutic Laser Applications*, eds. E.M.

Sevick-Muraca, J.A. Izatt and M.N. Ediger, Proc. OSA Trends in Optics and Photonics vol. **22**, 106-109 (1998).
284. M. Sinaasappel and H.J.C.M. Sterenborg, Quantification of the hematoporphyrin derivative by fluorescence measurement using dual-wavelength excitation and dual-wavelength detection, *Appl. Opt.* **32**, 541-548 (1993).
285. H.J.C.M. Sterenborg, M. Motamedi, R.F. Wagner, M.L. Duvic, S. Thomsen and S.L. Jacques, In vivo fluorescence spectroscopy and imaging of human skin tumors, *Lasers Med. Sci.* **9**, 191-201 (1994).
286. C.H. Liu, G.C. Tang, A. Pradhan, W.L. Sha and R.R. Alfano, Effects of self-absorption by hemoglobins on the fluorescence spectra from normal and cancerous tissues, *Lasers Life Sci.* **3**, 167-176 (1990).
287. S. Andersson-Engels, J. Johansson, K. Svanberg and S. Svanberg, Laser-induced fluorescence in medical diagnostics, in *Photodynamic Therapy: Mechanisms II*, ed. T.J. Dougherty, Proc. SPIE vol. **1203**, 76-96 (1990).
288. C.R. Kapadia, F.W. Cutruzzola, K.M. O'Brien, M.L. Stetz, R. Enriquez and L.I. Deckelbaum, Laser-induced fluorescence spectroscopy of human colonic mucosa: Detection of adenomatous transformation, *Gastroenterology* **99**, 150-157 (1990).
289. K.T. Schomacker, J.K. Frisoli, C.C. Compton, T.J. Flotte, J.M. Richter, N.S. Nishioka and T.F. Deutsch, Ultraviolet laser-induced fluorescence of colonic tissue: Basic biology and diagnostic potential, *Lasers Surg. Med.* **12**, 63-78 (1992).
290. C. Eker, S. Montán, E. Jaramillo, K. Koizumi, C. Rubio, S. Andersson-Engels, K. Svanberg, S. Svanberg and P. Slezak, Clinical spectral characterization of colonic mucosal lesions using autofluorescence and δ-aminolevulinic acid sensitization, *Gut* **44**, 511-518 (1999).
291. N. Ramanujam, M.F. Mitchell, A. Mahadevan, S. Thomsen, A. Malpica, T. Wright, N. Atkinson and R. Richards-Kortum, Development of a multivariate statistical algorithm to analyze human cervical tissue fluorescence spectra acquired in vivo, *Lasers Surg. Med.* **19**, 46-62 (1996).
292. N. Ramanujam, M.F. Mitchell, A. Mahadevan, S. Thomsen, A. Malpica, T. Wright, N. Atkinson and R. Richards-Kortum, Spectroscopic diagnosis of cervical intraepithelial neoplasia (CIN) in vivo using laser-induced fluorescence spectra at multiple excitation wavelengths, *Lasers Surg. Med.* **19**, 63-74 (1996).
293. A.M.K. Nilsson, D. Heinrich, J. Olajos and S. Andersson-Engels, Near infrared diffuse reflection and laser-induced fluorescence spectroscopy for myocardial tissue characterisation, *Spectrochim. Acta* **53**, 1901-1912 (1997).
294. T. Vo-Dinh, M. Panjehpour, B. Overholt, C. Farris, P. Buckley III and R. Sneed, In vivo cancer diagnostis of the oesophagus using differential normalized fluorescence indices, *Lasers Surg. Med.* **16**, 41-47 (1995).
295. T. Vo-Dinh, M. Panjehpour and B.F. Overholt, Laser-induced fluorescence for esophageal cancer and dysplasia diagnosis, in *Advances in Optical Biopsy and Optical Mammography*, ed. R.R. Alfano, pp. 116-122 (The New York Academy of Sciences, New York, NY, 1998).
296. C. Anderson, T. Andersson and K. Wårdell, Changes in skin circulation after insertion of a microdialysis probe visualized by laser Doppler perfusion imaging, *J. Invest. Dermatol.* **102**, 807-811 (1994).
297. K. Wårdell, H.K. Naver, G.E. Nilsson and B.G. Wallin, The cutaneous vascular axon reflex in humans characterized by laser Doppler perfusion imaging, *J. Physiol.* **460**, 185-199 (1993).
298. A.K. Andreasson, S. Simonsen, R. Bjørnerheim and K. Kvernebo, Attenuated microvascular perfusion and reactivity in cardiac transplant recipients treated with cyclosporine, *Int. J. Microcirc. Clin. Exp.* **15**, 117-124 (1995).
299. S. Bertuglia, A. Colantuoni, M. Arnold and H. Witte, Dynamic coherence analysis of vasomotion and flow motion in skeletal muscle microcirculation, *Microvasc. Res.* **52**, 235-244 (1996).
300. S. Bertuglia and A. Colantuoni, Venular oscillatory flow during hemorrhagic shock and NO inhibition in hamster cheek pouch microcirculation, *Microvasc. Res.* **54**, 233-242 (1997).
301. I. Wang, S. Andersson-Engels, G.E. Nilsson, K. Wårdell and K. Svanberg, Superficial blood flow following photodynamic therapy of malignant skin tumours measured by laser Doppler perfusion imaging, *Br. J. Dermatol.* **136**, 184-189 (1997).

302. A.M. Troilius and B. Ljunggren, Evaluation of port wine stains by laser Doppler perfusion imaging and reflectance photometry before and after pulsed dye laser treatment, *Arch. Derm. Venereol.* **76**, 291-294 (1996).
303. P.Å. Öberg, Laser-Doppler flowmetry, *Crit. Rev. Biomed. Eng.* **18**, 125-163 (1990).
304. K. Wårdell, A. Jakobsson and G.E. Nilsson, Laser Doppler perfusion imaging by dynamic light scattering, *IEEE Trans. Biomed. Eng.* **40**, 309-316 (1993).
305. W. Eichhorn, T. Auer, E.D. Voy and K. Hoffmann, Laser-Doppler imaging of axial and random pattern flaps in the maxillo-facial area. A preliminary report., *J. Craniomaxillofac. Surg.* **22**, 301-306 (1994).
306. K. Wårdell, U. Hermansson, H.C. von Ahn and G.E. Nilsson, Laser Doppler perfusion imaging in coronary by-pass surgery, *14th International Annual Conference of IEEE in Engineering in Medicine and Biology*, Paris, France, 1992.
307. A. Jakobsson and G.E. Nilsson, Prediction of sampling depth and photon pathlength in laser Doppler flowmetry, *Med. Biol. Eng. Comput.* **31**, 301-307 (1993).